

# The XMM-Newton SSC survey of the Galactic Plane\*

A. Nebot Gómez-Morán<sup>1</sup>, C. Motch<sup>1</sup>, X. Barcons<sup>2</sup>, F. J. Carrera<sup>2</sup>, M. T. Ceballos<sup>2</sup>, M. Cropper<sup>3</sup>, N. Grossi<sup>1</sup>, P. Guillout<sup>1</sup>, O. Hérent<sup>1</sup>, S. Mateos<sup>2</sup>, L. Michel<sup>1</sup>, J. P. Osborne<sup>4</sup>, M. Pakull<sup>1</sup>, F.-X. Pineau<sup>1</sup>, J. P. Pye<sup>4</sup>, T. P. Roberts<sup>5</sup>, S. R. Rosen<sup>4</sup>, A. D. Schwope<sup>6</sup>, M. G. Watson<sup>4</sup>, N. Webb<sup>7</sup>

<sup>1</sup> Observatoire Astronomique de Strasbourg, Université de Strasbourg, CNRS, UMR 7550, 11 rue de l'Université, 67000 Strasbourg, France.

e-mail: ada.nebot@astro.unistra.fr

<sup>2</sup> Instituto de Física de Cantabria (CSIC-UC), Avenida de los Castros, 39005 Santander, Spain.

<sup>3</sup> Mullard Space Science Laboratory, University College London, Holmbury St Mary, Dorking Surrey RH5 6NT.

<sup>4</sup> Space Research Centre, Department of Physics & Astronomy, University of Leicester, Leicester LE1 7RH, UK.

<sup>5</sup> Department of Physics, Durham University, South Road, Durham, DH1 3LE, UK.

<sup>6</sup> Leibniz-Institut für Astrophysik Potsdam (AIP), An der Sternwarte 16, 14482, Potsdam, Germany.

<sup>7</sup> Institut de Recherche en Astrophysique et Planétologie (IRAP), Université de Toulouse, UPS, 9 Avenue du colonel Roche, 31028 Toulouse Cedex 4, France.

## ABSTRACT

Many different classes of X-ray sources contribute to the Galactic landscape at high energies. Although the nature of the most luminous X-ray emitters is now fairly well understood, the population of low-to-medium X-ray luminosity ( $L_X = 10^{27-34}$  erg s $^{-1}$ ) sources remains much less studied, our knowledge being mostly based on the observation of local members. The advent of wide field and high sensitivity X-ray telescopes such as XMM-Newton now offers the opportunity to observe this low-to-medium  $L_X$  population at large distances. We report on the results of a Galactic plane survey conducted by the XMM-Newton Survey Science Centre (SSC). Beyond its astrophysical goals, this survey aims at gathering a representative sample of identified X-ray sources at low latitude that can be used later on to statistically identify the rest of the serendipitous sources discovered in the Milky Way. The survey is based on 26 XMM-Newton observations, obtained at  $|b| < 20$  deg, distributed over a large range in Galactic longitudes and covering a summed area of 4 deg $^2$ . The flux limit of our survey is  $2 \times 10^{-15}$  erg cm $^{-2}$ s $^{-1}$  in the soft (0.5–2 keV) band and  $1 \times 10^{-14}$  erg cm $^{-2}$ s $^{-1}$  in the hard (2–12 keV) band. We detect a total of 1319 individual X-ray sources. Using optical follow-up observations supplemented by cross-correlation with a large range of multi-wavelength archival catalogues we identify 316 X-ray sources. This constitutes the largest group of spectroscopically identified low latitude X-ray sources at this flux level. The majority of the identified X-ray sources are active coronae with spectral types in the range A–M at maximum distances of  $\sim 1$  kpc. The number of identified active stars increases towards late spectral types, reaching a maximum at K. Using infrared colours we classify 18% of the stars as giants. The observed distributions of  $F_X/F_V$ , X-ray and infrared colours indicates that our sample is dominated by a young (100 Myr) to intermediate (600 Myr) age population with a small contribution of close main sequence or evolved binaries. We find other interesting objects such as cataclysmic variables ( $d \sim 0.6 - 2$  kpc), low luminosity high mass stars (likely belonging to the class of  $\gamma$ -Cas-like systems,  $d \sim 1.5 - 7$  kpc), T Tauri and Herbig-Ae stars. A handful of extragalactic sources located in the highest Galactic latitude fields could be optically identified. For the 20 fields observed with the EPIC pn camera, we have constructed log N(>S) – log S curves in the soft and hard bands. In the soft band, the majority of the sources are positively identified with active coronae and the fraction of stars increases by about one order of magnitude from  $b = 60^\circ$  to  $b = 0^\circ$  at an X-ray flux of  $2 \times 10^{-14}$  erg cm $^{-2}$ s $^{-1}$ . The hard band is dominated by extragalactic sources, but there is a small contribution from a hard Galactic population formed by CVs, HMXB candidates or  $\gamma$ -Cas-like systems and by some active coronae that are also detected in the soft band. At  $b = 0^\circ$  the surface density of hard sources brighter than  $1 \times 10^{-13}$  erg cm $^{-2}$ s $^{-1}$  steeply increases by one order of magnitude from  $l = 20^\circ$  to the Galactic centre region ( $l = 0.9^\circ$ ).

**Key words.** X-rays: binaries - X-rays: stars - surveys - binaries: close

## 1. Introduction

\* Based on observations obtained with XMM-Newton, an ESA science mission with instruments and contributions directly funded by ESA Member States and NASA. Based on observations carried out at the European Southern Observatory, La Silla and Paranal, Chile under program Nos 69.D-0143, 70.D-0227, 71.D-0296, 71.D-0552. Based on observations obtained at the Canada-France-Hawaii Telescope (CFHT) which is operated by the National Research Council of Canada, the Institut National des Sciences de l'Univers of the Centre National de la Recherche Scientifique of France, and the University of Hawaii. Based on observations obtained at the Observatoire de Haute Provence which is operated by the Centre National de la Recherche Scientifique of France.

Non-solar X-ray emission was discovered in the early 1960s using collimating instruments. The low spatial resolution and high background inherent in these detectors only allowed the observations of bright, mostly Galactic X-ray sources. The launch of focusing X-ray telescopes in the '80s has paved the way for the study of fainter high energy sources and opened the high energy window to virtually all types of astrophysical objects from comets to the most remote AGNs.

The first imaging Galactic X-ray survey was conducted by the Einstein satellite (Giacconi et al. 1979; Hertz & Grindlay 1984). A decade later, the ROSAT (Trümper 1982) all-sky sur-

vey and pointed observations mapped the entire soft ( $<2$  keV) X-ray content of the Galaxy (see e.g. Motch et al. 1997; Morley et al. 2001) and allowed the discovery of many new species of soft X-ray sources. The ASCA (Tanaka et al. 1994) Galactic Plane Survey (Sugizaki et al. 2001) was the first to explore the hard ( $> 2$  keV) X-ray content of the Galaxy at X-ray fluxes much lower than achievable with collimating instruments.

The launch of the XMM-Newton (Jansen et al. 2001) and Chandra (Weisskopf et al. 2002) X-ray observatories has opened the possibility to carry out large surveys by analysing the properties of the X-ray sources serendipitously detected around the observation's main target. Although based on a field by field approach, these surveys benefit from the high quality of the parameters, position, spectral indices, etc.. derived for each source and a several-fold improved sensitivity, achievable thanks to the large collecting area of the telescopes. In particular, the much improved position accuracy of the detected X-ray sources facilitates their identification at other wavelengths, thus opening the way for detailed source characterisation. The ChamPlane project, based on Chandra observations, has been described in Grindlay et al. (2005). It will eventually cover about 8 deg $^2$  down to limiting fluxes a few times fainter than can be achieved with XMM-Newton. Recent results on the Galactic centre area have been reported in van den Berg et al. (2012); Hong et al. (2012); Hong (2012). XMM-Newton has conducted a shallow low latitude X-ray survey of relatively large area (Hands et al. 2004). Optical identifications and properties of its brightest sources carried out in the framework of the XMM-Newton Survey Science Centre (SSC, Watson et al. 2001), have been discussed in Motch et al. (2010). Finally, the nature of the overall low latitude XMM-Newton source population has recently been investigated by Warwick et al. (2011) and Motch & Pakull (2012) using cross-correlations with large optical and X-ray catalogues.

Many different classes of unresolved sources contribute to the X-ray content of the Galaxy: early and late-type stars, interacting binaries such as cataclysmic variables (CVs), RS CVns, white dwarfs, neutron stars or black holes with low (LMXB) or high mass companion stars (HMXB), isolated neutron stars and possibly isolated black holes (for a review, see Motch 2006).

At low X-ray luminosities, between  $10^{27}$  and  $10^{31}$  erg s $^{-1}$ , and soft energies ( $kT < 2$  keV) the X-ray sky is dominated by relatively nearby active stellar coronae (see e.g. Motch et al. 1997, and references therein). In contrast, at high X-ray luminosities,  $> 10^{35}$  erg s $^{-1}$ , the make-up of the Galaxy is dominated by HMXBs and LMXBs (Grimm et al. 2002; Gilfanov 2004). However, at intermediate X-ray luminosities, the nature of the hard ( $> 2$  keV) X-ray sources is still poorly understood. Although CVs and stellar coronae are expected to contribute significantly to this population (Sazonov et al. 2006; Hong 2012), other interesting objects such as magnetic OB stars (Gagné et al. 2011), single and binary Wolf Rayet stars (Skinner et al. 2010; Kogure 2009),  $\gamma$ -Cas like objects (Motch et al. 2007; Lopes de Oliveira et al. 2010) and X-ray transient binaries in quiescent state have also been identified in this luminosity range.

The scientific interest of optically identified Galactic X-ray surveys cannot be overemphasised. The low to medium X-ray luminosity point source population may only be resolved in our Galaxy and to some extent in the Magellanic Clouds due to the currently available combination of spatial resolution and sensitivity delivered by the most efficient X-ray observatories in operation such as Chandra and XMM-Newton. In addition, the optical identification process, which is a mandatory step when

studying the detailed nature of these X-ray populations can only be performed on a large number of sources in our Galaxy due to the still relatively large X-ray error circles. Similar to other wavelength ranges, flux limited X-ray surveys allow us to gather large and homogeneous samples of different species of high energy sources such as stars or AGN (see e.g. Guillout et al. 1999; Barcons et al. 2002), while they have proved to be instrumental for discovering rare or elusive X-ray emitters such as isolated neutron stars (see e.g. Pires et al. 2009, for results based on XMM-Newton data).

So far, observations provide very few constraints on evolutionary theories of low and high mass X-ray binaries. For instance, we do not detect the long-lived wind accreting low X-ray luminosity stages preceding or following the bright phase during which they become conspicuous. The common envelope spiral-in creation channel for low-mass X-ray binaries predicts the existence of pre-LMXBs which could radiate as much as  $\sim 10^{32}$  erg s $^{-1}$  in hard X-rays through accretion of stellar wind onto the neutron star or its magnetosphere (see e.g. Tauris & van den Heuvel 2006). Up to  $10^{4-5}$  of these objects could be currently present in the Galaxy (Willems & Kolb 2003). Likewise, evolution theories of high mass X-ray binary foresee that about  $10^6$  wind accreting binaries made of a main sequence star and of a neutron star or a black hole populate the Galaxy (Pfahl et al. 2002).

The relative census of the different species of Galactic X-ray sources strongly depends on the Galactic structure considered. Not unexpectedly, massive X-ray emitting stars, either in accreting binaries or alone, concentrate in the Galactic disc (see e.g. the concentration of INTEGRAL HMXBs in the Norma arm Walter et al. 2004), while a large population of CVs and low-mass X-ray binaries seem to gather in the predominantly old Galactic Bulge. Likewise, the very central regions of the Galaxy harbour a heavily concentrated population of low to medium L<sub>X</sub> sources (Muno et al. 2009; Hong et al. 2009) whose exact nature, CVs, stars, remains highly uncertain. X-ray sources are thus useful tracers of their parent stellar populations and their study can shed light on the evolutionary mechanisms of single and binary stars in remote parts of our Galaxy. They may as well help to constrain the past stellar formation rate, in particular the early formation stages during which many massive compact remnants were created.

Solar type stars emit X-rays from magnetically heated coronae. Therefore, their X-ray luminosity strongly depends on differential rotation (Pallavicini et al. 1981). Since magnetic braking efficiently decreases stellar rotation (see e.g. Kawaler 1988; Matt et al. 2012) both X-ray luminosities and thin thermal plasma temperatures (Guedel et al. 1997) strongly decay during pre main sequence and early main sequence stages. Old close binaries in which rotation is maintained by orbital motion are also known to contribute significantly to the X-ray emitting stellar population. One can take advantage of the marked L<sub>X</sub> dependency upon age to discriminate with high efficiency young stars from the background of older populations. In this respect, X-ray selection is more practical than any selection based on weak optical proxy spectral signatures such as, for instance, re-emission in the Ca II H&K lines (see e.g Schrijver 1987) which arises from the stellar chromosphere. Comparing the observed properties of stellar X-ray surveys with population models can provide important constraints on the evolution of Galactic scale height with age (Guillout et al. 1996) and reveal large scale local structures, e.g. the late type component of the Gould Belt. (Guillout et al. 1998).

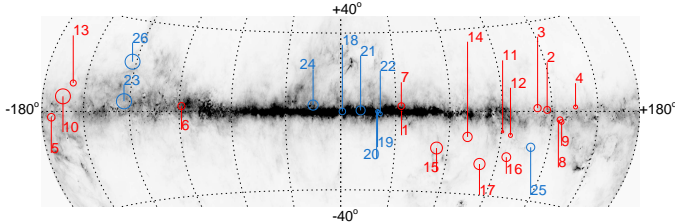


**Fig. 1.** Galactic positions of the XMM-Newton fields overplotted on top of the Galactic extinction map from Schlegel et al. (1998) shown in Aitoff projection running in Galactic longitude from  $-180^\circ$  to  $+180^\circ$ . The optically bright and faint samples (see Section 3) are shown in red and blue respectively. The symbol size is proportional to the number of XMM-Newton sources detected in each field. Numbers indicate the field as listed in Table 1.

In this paper we present results from an optical identification campaign conducted in the Galactic Plane, at low and intermediate Galactic latitudes ( $|b| < 20^\circ$ ) and covering a wide range of Galactic longitudes, by the XMM-Newton Survey Science Centre (Watson et al. 2001). We report the optical identification of over 300 Galactic X-ray sources, most of them being classified on the basis of optical spectroscopy. This constitutes the largest sample of spectroscopically identified X-ray sources at low Galactic latitudes.

Beyond its astrophysical motivations, this project also aims at gathering a large and representative sample of identified low-latitude sources which can be used as a learning sample for identifying and classifying in a statistical manner serendipitous XMM-Newton sources detected in the Milky Way. First attempts to automatically classify XMM-Newton X-ray sources at high Galactic latitudes have been reported in Pineau et al. (2010). SSC surveys covering other Galactic directions have been already presented by Barcons et al. (2002) and Della Ceca et al. (2004), for high Galactic latitude sources at medium and bright fluxes, and by Motch et al. (2010) for low Galactic latitude sources and bright fluxes.

The structure of the paper is as follows. In Section 2.1 we present the XMM-Newton data, followed by the optical observations in Section 3, and optical and infrared catalogue identifications in Section 4. We present the source classification in Section 5 and the stellar population content of the survey in Section 6. We discuss the overall properties and characteristics of the sample in Section 7 and conclude in Section 8.

## 2. XMM-Newton data

### 2.1. Observations and data reduction

The X-ray Multi-Mirror mission (XMM-Newton, Jansen et al. 2001) was launched in December 1999 by the European Space Agency (ESA). The XMM-Newton satellite has three X-ray telescopes and is equipped with a set of CCD detectors, which constitutes the European Photon Imaging Cameras (EPIC). There are two MOS-CCD arrays (MOS camera, Turner et al. 2001), and one pn-CCD (pn camera, Strüder et al. 2001). The two MOS cameras are located behind the two telescopes equipped with gratings which divert about half of the light towards the Reflecting Grating Spectrometers (RGS, den Herder et al. 2001), so only about 40% of the light reaches the MOS cameras. The pn camera is located behind the third telescope, receiving all

the incident light (Strüder et al. 2001). The field of view is about  $30'$ , it covers the energy range from 0.15 to 15 keV, with spectral resolution ( $\frac{E}{\Delta E}$ ) = 20–50 and angular resolution of  $6''$ .

The 26 XMM-Newton fields presented in this work were selected shortly after the launch of the XMM-Newton satellite. They are all at low and intermediate Galactic latitudes ( $|b| < 20^\circ$ ) and cover a wide range in Galactic longitudes (see Fig. 1). Observations were selected so as to be void of extended diffuse emission and represent as much as possible typical Galactic fields. We therefore excluded stellar clusters and star forming regions in general. Very bright target sources were also avoided if possible. Fields are divided in two samples: the *optically bright* and the *optically faint* samples, depending on the limiting magnitude reached by the combination of telescope and instrument used for the optical identification of the X-ray sources (see Section 3). In Table 1 we list the fields, their Galactic coordinates, observation IDs and EPIC pn exposure times. Among the 26 fields, 20 were observed with the three EPIC cameras, while for six we have only MOS detections. Exposure times range from 5 to 57 ks, reaching flux limits of around  $2 \times 10^{-15} \text{ erg cm}^{-2} \text{s}^{-1}$  and  $1 \times 10^{-14} \text{ erg cm}^{-2} \text{s}^{-1}$  in the 0.5–2 keV and in the 2–12 keV energy bands respectively. The area covered by this survey is  $\sim 4 \text{ deg}^2$  ( $\sim 3 \text{ deg}^2$  for the pn camera). This survey is ten times deeper than the ROSAT medium sensitivity survey of the Galactic Plane from Morley et al. (2001) and the ASCA faint X-ray survey from Sugizaki et al. (2001). Although 10 times shallower than the Chandra deep Galactic Plane survey of Ebisawa et al. (2005) and than the ChaMPiNE survey of Grindlay et al. (2005) our survey covers a much larger area. The XMM-Newton SSC survey of the Galactic Plane can be considered a medium sensitivity survey slightly deeper than that of Hands et al. (2004).

The original source list contained a total of 2353 X-ray sources, detected in either the pn or MOS cameras, using the Science Analysis System (SAS)<sup>1</sup> version 5.0 or earlier. In all cases we excluded the target of the observation. All observations were visually screened in order to discard spurious or dubious detections before scheduling sources for optical identification at ground-based telescopes, leaving us with a total of about 1800 "good" sources. Optical spectra were taken using the X-ray source positions derived in this first analysis of the X-ray data. In most cases, optical targets were prioritised using the broadband X-ray flux, starting with the brightest sources. Since then, other improved SAS processing versions became available, and in order to have up-to-date and homogeneous X-ray parameters we cross-matched our source lists with the 2XMMi-DR3 catalogue<sup>2</sup>. To evaluate the success rate of our visual screening we performed the cross-match for all the 2353 X-ray sources and found 1319 sources in the 2XMMi-DR3 within a 20 arcsec radius (1126 with the best XMM-Newton quality, i.e. sum\_flag = 0<sup>3</sup>). Extending the radius to larger values did not yield many more matches. In Fig. 2 we show the distribution of the distance between the original XMM-Newton sources and the 2XMMi-DR3 sources. The majority of the matches are found to be within 3–5''. About 50% of the unrecovered sources in the 2XMMi-DR3 catalogue had been flagged by us as being spurious or dubious based on our visual screening. Unrecovered sources have lower EPIC-pn count rates (0.2–12 keV) than

<sup>1</sup> <http://xmm.esa.int/sas/>

<sup>2</sup> [http://xmmsc-www.star.le.ac.uk/Catalogue/xcat\\_public\\_2XMMi-DR3.html](http://xmmsc-www.star.le.ac.uk/Catalogue/xcat_public_2XMMi-DR3.html)

<sup>3</sup> The summary flag sum\_flag contains information about the flags set automatically and manually for each source, a value equal to zero assures that there are no negative flags for the detection of the source.

**Table 1.** Target fields and source classification.

#	Field	l [°]	b [°]	N <sub>H</sub> <sup>†</sup> [cm <sup>-2</sup> ]	Observation ID	Epic pn exp [ks]	N <sub>tot</sub>	Active Coronae	HMXB	Pre-MS	EG	unID
Optically bright sample, Rlim~17												
1	Ridge 1	33.1	+0.0	$1.4 \times 10^{23}$	0017740401	26	4	1 (25%)	0	0	0	3
2	RX J0002+6246	117.0	+0.5	$4.2 \times 10^{21}$	0016140101	[17]	40	7 (18%)	1	0	0	32
3	LHB-3	111.1	+1.1	$1.3 \times 10^{22}$	0203130201	19	42	13 (31%)	0	0	0	29
4	GRB010220	135.1	+1.4	$4.8 \times 10^{21}$	0128530401	9	23	12 (52%)	0	0	0	11
5	Saturn	187.0	-1.6	$6.2 \times 10^{21}$	0089370501	21	44	6 (14%)	0	0	0	38
6	RXJ0925.7-4758	271.4	+1.9	$1.4 \times 10^{22}$	0111150201	57	42	9 (21%)	0	0	0	33
7	Ridge 2	33.0	+2.0	$1.5 \times 10^{22}$	0017740601	20	39	12 (31%)	0	1	0	26
8	HTCas	125.2	-2.7	$3.9 \times 10^{21}$	01111310101	18	34	6 (18%)	0	0	0	28
9	PSRJ0117+5914	126.3	-3.4	$3.4 \times 10^{21}$	0112200201	6	27	4 (14%)	1	0	0	22
10	Geminga	195.1	+4.3	$3.0 \times 10^{21}$	0111170101	[86]	88	9 (10%)	0	0	0	79
11	SS Cyg	90.7	-7.1	$2.5 \times 10^{21}$	01111310201	[12]	13	5 (38%)	0	0	2	6
12	ARLac	95.6	-8.3	$1.9 \times 10^{21}$	0111370101	[20]	24	5 (22%)	0	0	0	20
13	PSR0656+14	201.1	+8.3	$5.0 \times 10^{20}$	0112200101	[21]	36	6 (17%)	0	0	0	30
14	PSRJ2043+2740	70.6	-9.2	$1.4 \times 10^{21}$	0037990101	[17]	54	10(19%)	0	0	1	43
15	AXJ2019+112	53.6	-13.5	$1.2 \times 10^{21}$	0112960301	12	69	6 (9%)	0	0	1	62
16	3C449	95.4	-15.9	$8.9 \times 10^{20}$	0002970101	18	52	9 (17%)	0	1	3	39
17	3C436	80.2	-18.8	$5.0 \times 10^{20}$	0201230101	29	65	5 (8%)	0	0	1	59
All							696	125	2	2	8	560
								17.9%	0.3%	0.3%	1.1%	80.3%
Optically faint sample, Rlim~21												
18	GC2	0.9	+0.0	$4.0 \times 10^{23}$	0112970201	13	38	15 (39%)	0	0	0	23
19	Ridge 3	20.0	+0.0	$1.1 \times 10^{23}$	0104460301	8	22	11 (54%)	0	1	0	10
20	Ridge 4	20.4	+0.0	$1.1 \times 10^{23}$	0104460401	5	12	2 (17%)	0	0	0	10
21	WR110	10.8	+0.4	$5.5 \times 10^{22}$	0024940201	23	52	21 (40%)	1	1	0	28
22	G21.5-09 offset 2	21.5	-0.9	$5.0 \times 10^{22}$	0122700301	25	24	5 (22%)	0	0	0	19
23	PKS 0745-19-offset	236.4	+3.3	$2.3 \times 10^{21}$	0105870201	36	88	24 (27%)	0	0	18	46
24	GROJ1655-40	345.0	+2.4	$6.1 \times 10^{21}$	0112460201	21	59	15 (25%)	0	0	1	43
25	Z And	109.0	-12.1	$8.9 \times 10^{20}$	0093552701	17	48	13 (27%)	0	0	0	35
26	GRB001025	237.4	+16.3	$3.3 \times 10^{20}$	0128530301	26	87	4 (5%)	0	0	6	77
All							430	110	1	2	25	291
								25.8%	0.2%	0.4%	5.8%	67.7%
Total							1126	235	3	4	33	851

**Notes.** Field, Galactic coordinates, observation ID, EPIC-pn exposure time (EPIC-MOS exposure time in brackets), total number of 2XMMi-DR3 sources detected, number of identified active coronae (AC), High-mass X-ray binaries (HMXB), pre-main sequence stars (pre-MS), extragalactic sources (EG), and unidentified sources (unID). We restricted to sources with sum\_flag = 0. <sup>†</sup>Calculated hydrogen column density. We used the Schlegel et al. (1998) maps to estimate the color excess E(B-V) at each Galactic position. We transformed into optical extinction A<sub>V</sub> using the relation from Savage & Mathis (1979), and we used the empirical relation from Predehl & Schmitt (1995) to calculate N<sub>H</sub>. We note that for very low Galactic latitudes ( $|b| < 5^\circ$ ) values could be wrong, but we use the values for orientative purposes.

those with counterparts (see Fig. 3) and are thus likely to be spurious sources with low detection likelihood (Watson et al. 2009, Section 4.4). Hereinafter we limit our analysis to the 1319 sources with 2XMMi-DR3 counterpart and X-ray parameters are based on 2XMMi-DR3 catalogue values.

## 2.2. Modelled X-ray spectra

Making use of XSPEC<sup>4</sup> we created model X-ray spectra for the following different types of objects:

- i) three different populations of active coronae: a young population of 70 Myr, an intermediate population of 300 Myr, and an old population of 1.9 Gyr. We assumed 2-temperature thermal emission (Guedel et al. 1997), one

component representing the hot plasma (T<sub>1</sub>) and a second hotter component (T<sub>2</sub>). Temperatures used for the coronae are (kT<sub>1</sub>, kT<sub>2</sub>)=(0.2, 0.8), (0.12, 0.55), and (0.09, 0.32) keV, and X-ray emission measure ratios are EM<sub>2</sub>/EM<sub>1</sub> = 1, EM<sub>2</sub>/EM<sub>1</sub> = 1, and EM<sub>2</sub>/EM<sub>1</sub> = 0.6 for the young, intermediate, and old populations respectively.

- ii) for AY Cet, a typical BY Dra binary (Dempsey et al. 1997), with (kT<sub>1</sub>, kT<sub>2</sub>)=(0.2, 1.38) keV and EM<sub>2</sub>/EM<sub>1</sub> = 3.75, and for the RS CVn star WW Dra (Dempsey et al. 1993), with (kT<sub>1</sub>, kT<sub>2</sub>)=(0.2, 2.1) keV and EM<sub>2</sub>/EM<sub>1</sub> = 6.77.
- iii) accreting binaries, assuming two different power laws with photon indices Γ of 0 and 2.
- iv) active galactic nuclei (AGN) assuming a power law with photon index Γ = 1.9.

We used the models *mekal* and *powerlaw*, alongside *phabs* for the photoelectric absorption, for our simulations. They were per-

<sup>4</sup> <http://heasarc.nasa.gov/xanadu/xspec/>

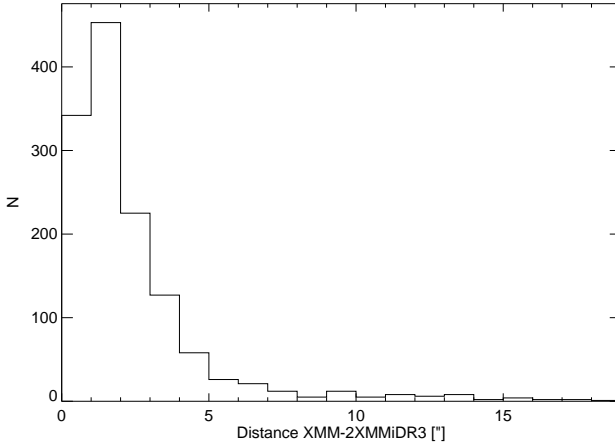


**Fig. 2.** Distance between the original XMM-Newton source positions and the 2XMMi-DR3 counterparts within 20 arcsec. Most of the counterparts are found within 3–5 arcsec.

formed for a wide range of Galactic absorption ( $N_H = 10^{20-23} \text{ cm}^{-2}$ ) and with a step of 0.1 in  $\log(N_H)$ . Simulated hardness ratios<sup>5</sup> (HR) were computed for each model with the aim of comparing with the observed values.

### 3. Optical observations

Photometry was carried out at the Isaac Newton Telescope (INT), at the Canada France Hawaii Telescope (CFHT) and at the 2.2m ESO telescope. INT images were bias subtracted and flat-field corrected using the WFC pipeline, following the instructions described by the Cambridge Astronomy Survey Unit<sup>6</sup>. CFHT images were reduced using the ELIXIR<sup>7</sup> pipeline. ESO images were reduced using the GaBoDS pipeline<sup>8</sup>. Images were used to find the optical counterpart of the X-ray sources, to measure the magnitude of the faintest candidate counterparts, and to prioritise the target selection for spectroscopic identification. Whenever a bright extended optical object was detected in the X-ray error box we considered the source as being extragalactic and did not obtain optical spectra.

Optical spectroscopic observations were carried out between the years 2000 and 2003 with the Very Large Telescope (VLT-UT4) and with the ESO-3.6 m telescope at ESO La Silla/Paranal Observatory, with the William Herschel Telescope (WHT) at the Observatory Roque de los Muchachos (La Palma), and with the 1.9 m telescope at the Observatoire de Haute-Provence (OHP). A large part of the optical data were acquired in the framework of the AXIS project<sup>9</sup>. Telescope, instrument, instrumental setup, wavelength coverage and spectral resolution are listed in Table 2. Depending on the telescope/instrument used for each observed field the limiting magnitude is  $R \sim 17$  or  $R \sim 21$ . Seventeen fields were observed reaching a magnitude limit of  $R \sim 17$ , belonging

<sup>5</sup>  $HR_i = \frac{C_{i+1} - C_i}{C_i + C_{i+1}}$ , being  $C_i$  the count rate in band  $i$ , where  $i = 0.2 - 0.5, 0.5 - 1.0, 1.0 - 2.0, 2.0 - 4.5, 4.5 - 12.0 \text{ keV}$ .

<sup>6</sup> <http://www.ast.cam.ac.uk/~wfcsur>

<sup>7</sup> <http://www.cfht.hawaii.edu/science/CFHTLS/cfhtlsdataflow.html>

<sup>8</sup> <http://www.astro.uni-bonn.de/~heckmill/Software/GABODS.html>

<sup>9</sup> <http://venus.ifca.unican.es/~xray/AXIS/>

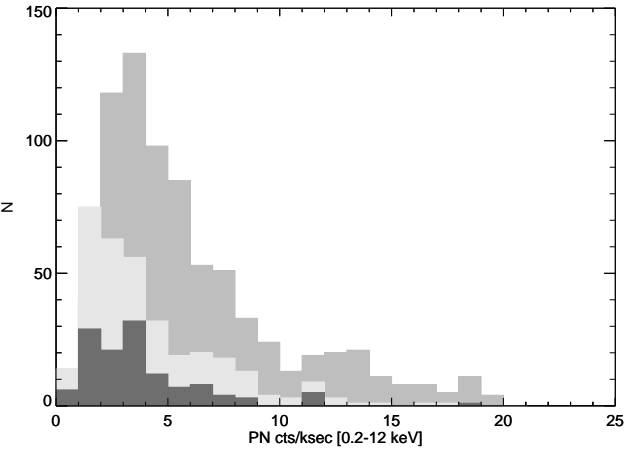


**Fig. 3.** EPIC pn count rate (0.2–12 keV) distribution for the original unscreened XMM-Newton sources with (medium grey) and without (light grey) 2XMMi-DR3 counterpart, highlighting with a dark grey histogram those detections originally flagged as spurious or dubious.

to the optically bright sample. The remaining nine fields were observed with a limiting magnitude  $R \sim 21$  defining the optically faint sample (see Table 1).

Spectra were bias corrected, flat-fielded, and extracted using standard MIDAS<sup>10</sup> procedures. We used arc-lamps to calibrate in wavelength and spectrophotometric standard stars to flux calibrate (see Motch et al. 2010, for details).

Observations were carried out using the original (see Section 2.1) positions of the X-ray sources, available at the time of the observing runs. In the Galactic Plane, optical crowding often prevents a clear identification of X-ray sources. It is therefore very important to have a good knowledge of the X-ray positional errors. The XMM-Newton error circle is the combination of two errors. The first one is the statistical uncertainty on the centroid of the PSF determined by the detection algorithm,  $\sigma_{radec}$  typically  $\sim 1 - 2''$ . The second one is the systematic error introduced by the uncertainty of the satellite's attitude, with values  $\sigma_{systematic} \sim 1''$ . In the less crowded fields, systematic errors were reduced to  $\sim 0.35''$  by matching the XMM-Newton positions with the USNO-B1.0 (Monet et al. 2003) catalogue making use of the SAS task *eposcorr*. Assuming a two-dimensional Gaussian distribution, the 90% confidence-level radius is given by:

$$r_{90} = 2.15 \times \sqrt{\sigma_{radec}^2 + \sigma_{systematic}^2} \quad (1)$$

In many cases the X-ray source position error circle contained more than one optical candidate brighter than our limiting magnitude. We obtained optical spectra of all candidates present in the 90% confidence error circle down to our limiting magnitude, sorting objects by decreasing  $R$  brightness. A source was positively identified when specific spectral signatures such as emission lines were detected.

Spectroscopic classification of stellar spectra was carried out as in Motch et al. (2010). In summary, template spectra from Jacoby et al. (1984); Pickles (1998), STELIB (Le Borgne et al. 2003) and from the NASA/JPL NStars project<sup>11</sup>, degraded to

<sup>10</sup> <http://www.eso.org/sci/software/esomidas>

<sup>11</sup> <http://stellar.phys.appstate.edu/>

**Table 2.** Spectroscopic settings.

Telescope	Instr.	Slit width (")	Spectral range (Å)	Spectral res. (Å)	Grisms
VLT-UT4	FORS2	1.0	3850–7500	15	GRIS_300V
WHT	WYFOS	2.7	3900–7100	6–7	
WHT	ISIS	1.2–2.0	3500–8500	3.0–3.3	
ESO-3.6	EFOSC2	1.5	3185–10940	59	Grism #1
ESO-3.6	EFOSC2	1.5	3860–8070	17.3	Grism #6
ESO-3.6	EFOSC2	1.5	3095–5085	7.1	Grism #14
OHP	CARELEC	1.0–2.0	3760–6840	5–7	133Å/mm

the resolution of our observations (Table 2), were fitted to the observed spectra by adjusting the mean flux and the interstellar absorption. Spectral classification of the sources is given in the online version of the paper and statistics on the identifications are discussed in Section 5.

#### 4. Optical and infrared catalogue identifications

As stated above, source identification can be difficult in the Galactic plane since several optical candidates are often found within the X-ray error circle and spectral signatures obtained at the telescope can be sometimes ambiguous. We therefore helped our optical identification process by cross-correlating X-ray source positions with the following archival catalogues: 2MASS (Cutri et al. 2003), USNO-B1.0 (Monet et al. 2003), GSC 2.3 (Lasker et al. 2008) and SDSS-DR7 (Abazajian et al. 2009) catalogues as in Motch et al. (2010). All these cross-matches are provided through the SSC public XCat-DB interface<sup>12</sup> (Michel et al. 2004).

##### 4.1. Cross-correlation method

The cross-correlation process is described in Pineau et al. (2008) and Pineau et al. (2011). In brief, it is based on the classical ratio between the likelihood of the X-ray and catalogue sources to be at the same position, and the likelihood of being a spurious association. This likelihood ratio (LR) depends on the probability of an X-ray source to have a counterpart in the considered catalogue, probability which depends on the distribution and characteristics of the different populations that enter the sample. To estimate the probability of being an spurious identification the method uses a geometrical approach. The process searches for all possible counterparts within a radius corresponding to a 99.7% ( $3\sigma$ ) completeness, which for a two dimensional Gaussian distribution corresponds to 3.44 times the  $1\sigma$  combined positional error. The combined radius is computed by adding in quadrature the X-ray and the catalogue  $1\sigma$  errors. For each possible counterpart, the probability of it being the true counterpart to the X-ray source ( $P_{id}$ ) is given by the ratio between the total number of observed counterparts and the number of estimated spurious associations. Above a given threshold of this probability we calculate the sample reliability, i.e. the expected fraction of correct identifications among all the matches, from which we derive the number of spurious associations, and sample completeness. The sample completeness is defined as the

**Table 3.** 2XMMi-DR3 matches in infrared/optical catalogues.

Catalogue	$N_{total}^{\dagger}$	$N_{P>90\%}^{\ddagger}$
2MASS	557	258
GSC 2.3	741	301
USNO-B1.0	682	264
SDSS-DR7	149	55
Optical	801	329
IR or Optical	829	350

Notes: <sup>†</sup> Total number of matches. <sup>‡</sup> Number of matches with individual identification probability higher than 90%.

ratio between the number of true associations recovered above that probability threshold and the number of true associations expected in the survey (see left panel Fig. 4). As we increase the cutoff in the individual identification probability we reduce the completeness of the survey, but increase the reliability, reducing the fraction of possible spurious identifications.

##### 4.2. Cross-correlation results

Cross-correlation statistics are given in Table 3. The much lower number of X-ray sources with SDSS-DR7 counterpart is due to the fact that only five fields (LHB 3, PSR J2043+2740, 3C449, Saturn and Z And) are covered by the SDSS-DR7 footprint. Probabilities of being the true counterpart are shown in the right panel of Fig. 4. There are a total of 258 (~ 20%) and 329 (~ 25%) X-ray sources with infrared and optical (in either SDSS-DR7, GSC 2.3 or USNO-B1.0) counterparts respectively above the 90% identification probability. The number of expected spurious matches with individual identification probability above 90% is below 2% and we are recovering about 55% among all true associations between the XMM-Newton and the different catalogues (see left panel in Fig. 4). Hereinafter we will only consider matches with individual identification probability higher than 90%.

##### 4.3. X-ray properties of catalogue counterparts

Stars are soft X-ray emitters, therefore it should be easy to distinguish them from the hard X-ray extragalactic and accretion-powered sources on the basis of their X-ray colours. We analysed the hardness ratio distributions of X-ray sources with bright optical or infrared counterparts and compared it with those of sources with faint or no catalogue counterpart.

A total of 350 X-ray sources have either an infrared or an optical catalogue counterpart above the 90% identification probability, among which seven sources exclusively come from the 2XMMi-DR3/SDSS-DR7 crossmatch. Since the limiting magnitude for the SDSS is much deeper ( $g \sim 23$ ) than that for the GSC 2.3 ( $B \sim 21$ ) and the USNO-B1.0 ( $V \sim 20$ ) we discarded these sources for the following analysis. We limit to sources with the best X-ray quality ( $sum\_flag = 0$ ) and with hardness ratio errors lower than 0.3. The HR distributions of the remaining sources (230) is shown in Fig. 5 and compared to those of X-ray sources without a counterpart or with a probability of identification lower than 90% (474).

As expected, X-ray sources with optical or infrared counterparts have lower (softer) HRs than those without counterpart, consistent with the fact that most soft sources are stars, while hard sources are likely to be extragalactic. For each sources we

<sup>12</sup> <http://xcatdb.u-strasbg.fr/2xmmdr3/>

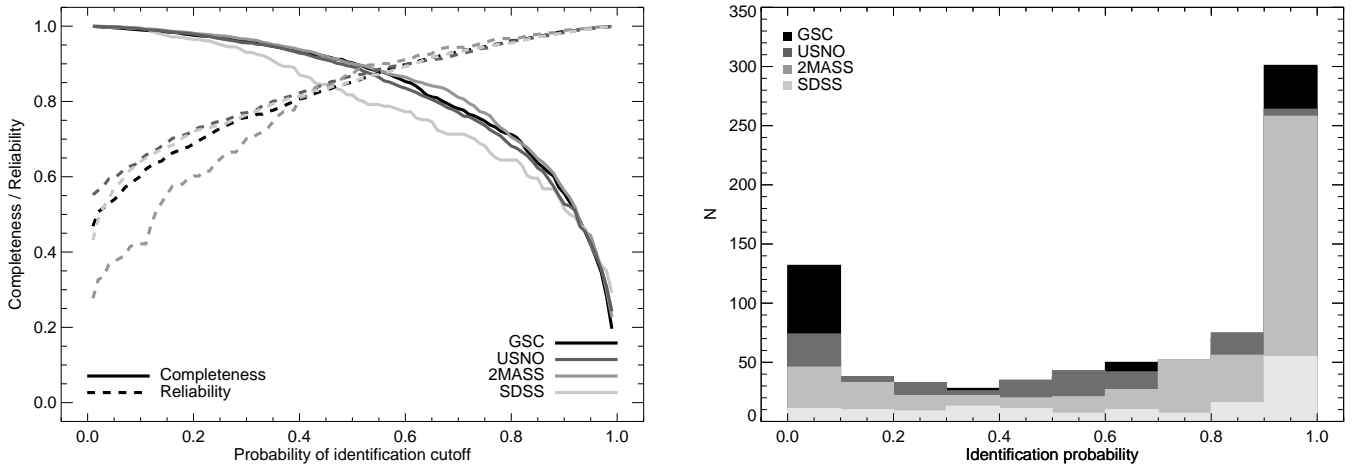


**Fig. 4.** Completeness and reliability of the sample as a function of the threshold in the identification probability (left). Distribution of the probability of being the true counterpart associated with each X-ray source with entry in the 2MASS, USNO-B1.0, GSC 2.3 and SDSS-DR7 catalogues (right).

estimated the total  $N_{\mathrm{H}}$  in the light of sight using the colour excess  $E(B-V)$  calculated from the dust maps from Schlegel et al. (1998) and their IDL code<sup>13</sup>. We compared the distribution in  $N_{\mathrm{H}}$  versus hardness ratio of sources with (without) optical or infrared counterpart to expected values for stars (AGNs) (see Section 2.2) and found similar trends (see Fig. 5).

X-ray-to-optical flux ratios can also provide us with information on the nature of the sources. Whilst extragalactic sources have typical values  $-1 < \log(L_{\mathrm{X}}/L_{\mathrm{R}}) < 1$ , stars have lower X-ray-to-optical flux ratios,  $\log(L_{\mathrm{X}}/L_{\mathrm{R}}) < -1$  (Maccacaro et al. 1988). We thus conclude that the majority of sources without an optical or infrared match have an extragalactic origin or are associated with high  $F_{\mathrm{X}}/F_{\mathrm{opt}}$  galactic hard sources.

There are a few soft sources without counterpart in either catalogue. At the limiting X-ray flux of our survey ( $2 \times 10^{-15} \text{ erg cm}^{-2}\text{s}^{-1}$ ), sources fainter than  $R \sim 20$  ( $R \sim 17$ ), corresponding to the USNO-B1.0 limiting magnitude (restricting to sources with  $P_{\mathrm{id}} > 0.9$ ), will have  $\log(L_{\mathrm{X}}/L_{\mathrm{R}}) > -0.75$  ( $\log(L_{\mathrm{X}}/L_{\mathrm{R}}) > -2$ ), i. e. could be relatively distant late dMe stars too faint to be detected in the optical (see Fig. 7) (Morley et al. 2001), but are also compatible with accreting binaries and with extragalactic objects in the high galactic latitude fields. A few sources with infrared or optical counterpart have higher HR4 value than expected for young active coronae (see Fig. 5). At the chosen cutoff for the individual identification probability, the number of spurious associations is lower than 2%, so we expect a maximum of 5 spurious matches, a value not sufficient to explain the number of sources detected in the HR4 bands. Although in principle such sources could be AGNs with a bright optical or infrared catalogue counterpart, we have classified some of these hard sources as stars on the basis of their optical spectrum (see Section 5).

## 5. Source classification

We classified X-ray sources in three different ways:

- From our spectroscopic observations. In most cases the determination of the spectral type of active coronae was pos-

sible by fitting the observed spectra to template spectra (Section 3).

- From our photometric observations. If the X-ray source position was coinciding with a source resolved in the optical (galaxy) we classified it as an extragalactic candidate.
- From cross-correlation with archival catalogues using XCat-DB developed in Strasbourg (Michel et al. 2004). The list of archival catalogues can be found under <http://xcatdb.u-strasbg.fr/2xmmdr3/catarch>.

Among the total 1319 detected sources we classified 316, with 275 having the best X-ray quality, i.e.  $\text{sum\_flag} = 0$  (see Table 1). We classified 280 X-ray sources on the basis of the optical spectra of their counterparts. In some cases no classification was possible due either to the optical faintness of the object or to the absence of absorption and/or emission lines in the spectra. We classified six X-ray sources as galaxies on the basis of their extension in the optical images. Finally, via cross-correlation with archival catalogues using XCat-DB we classified 30 sources. This SSC interface hosts all candidate identifications derived from the cross-correlation of EPIC source lists with more than 200 archival catalogues, as performed during the SSC pipeline processing (Watson et al. 2009). All X-ray sources with their classification (when possible) will be available via the CDS and the XID result-DB<sup>14</sup>. From the 316 classified sources, 270 have a 2MASS counterpart and 296 an optical counterpart in either the SDSS-DR7, the USNO-B1.0 or the GSC 2.3 catalogues. There are 20 classified sources by our photometric observations with no catalogue counterpart, these sources were too faint in optical to be detected by the USNO-B1.0 and GSC 2.3 surveys and are outside the SDSS-DR7 footprint. The majority of these sources are classified as galaxies.

Optical classification statistics are presented in Table 1, separating the optically bright and faint samples defined in Section 3. The majority of the classified sources are active coronae (AC), representing  $\sim 18\%$  of the sources for the optically bright sample and up to  $\sim 26\%$  for the optically faint sample. The total number of AC for each spectral type is given in Table 4. The fraction of stars at each spectral type increases from 5% for A stars to 29% for K stars and then drops to about 26% for M stars, reflecting

<sup>13</sup> <http://www.astro.princeton.edu/~schlegel/dust/dust.html>. For stars, this value represents an upper limit to the  $N_{\mathrm{H}}$

<sup>14</sup> <http://saada.unistra.fr/xidresult/home>

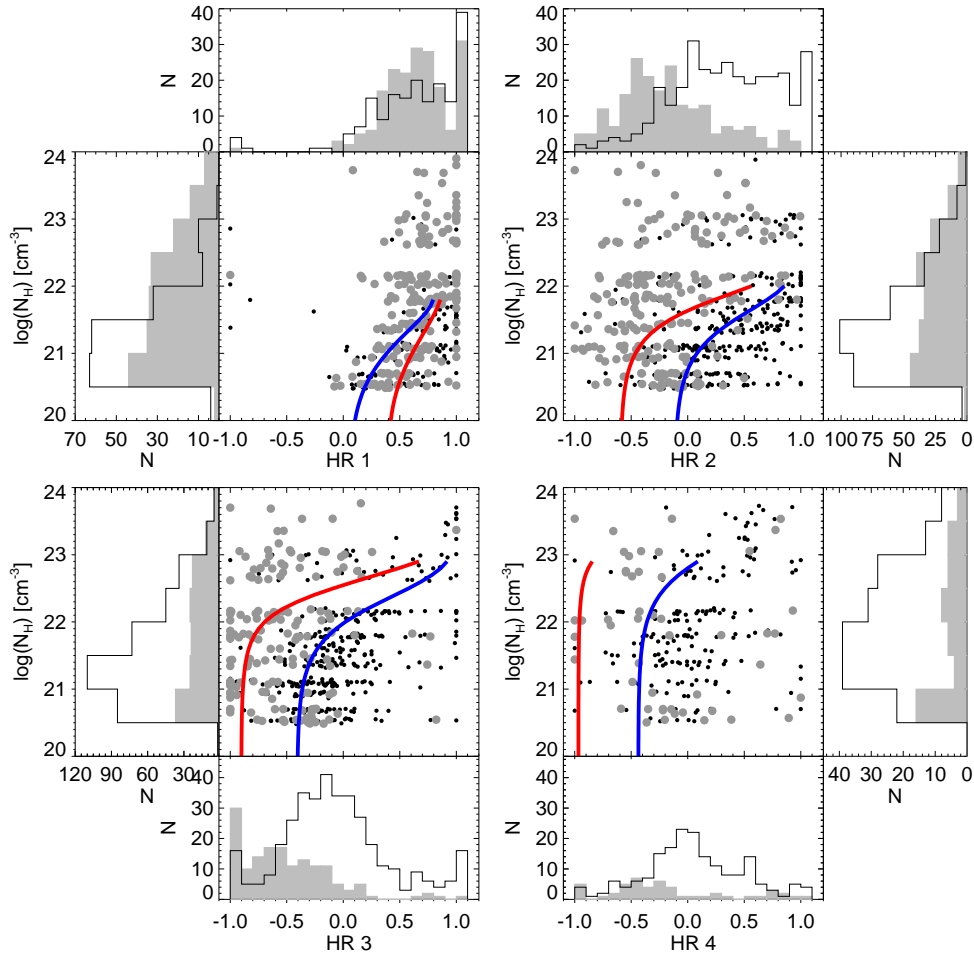


**Fig. 5.** Hardness ratio and Galactic  $N_{\text{H}}$  distribution of X-ray sources with optical or infrared catalogue counterparts with identification probability  $> 0.9$  (large grey dots and grey-filled histograms), and of X-ray sources without catalogue counterpart or with identification probability below 0.9 (small black dots and empty black histograms). We only considered sources with good X-ray quality ( $\text{sum\_flag} = 0$ ) and with errors smaller than 0.3 in X-ray colours. Blue and red lines show the expected position of AGNs ( $\Gamma = 1.9$ ) and stars (70 Myr old population, see Section 2.2 for details) respectively. Most of the objects with no infrared or optical counterpart follow a distribution similar to that of AGNs.

**Table 4.** Spectral types of the identified active coronae.

SpT	Number	Fraction (%)
A	13	5
F	44	16
G	64	24
K	80	29
M	71	26

either a deficit in M stars or an excess of G and K stars. We note that A stars are not expected to be strong X-ray emitters, and that if these sources are not spurious X-ray detections or wrong identifications, then their X-ray emission is likely to be related to a low-mass companion star (De Rosa et al. 2011). A small fraction of the sources are CVs,  $\gamma$ -Cas-like objects, T Tauri and Herbig-Ae stars. In the relatively high galactic latitude fields, due to the lower  $N_{\text{H}}$ , some sources are identified as extragalactic objects. The fraction of identified AGN is larger towards higher Galactic latitudes, as expected. Around 80% of the sources are unclassified

for the optically bright sample, dropping to 60% for the optically faint sample, where we could obtain optical spectra up to a limiting magnitude of about 21 in the R band. Spectral classifications, X-ray parameters and catalogue counterparts are given in Tables 8–33, available in the online version of the paper.

## 6. Stellar population

### 6.1. Pre-main sequence, main sequence and giant stars

While the majority of the Galactic X-ray-emitting stars are expected to be main sequence stars, a fraction of the stellar population will be evolved giants (Guillout et al. 1999). To distinguish between dwarf and giant stars one can use the Balmer lines for stars hotter than about 10 000 K, or Ca II H and K lines, the NaI doublet and Mg Ib lines for cooler stars, since their equivalent widths are highly dependent on surface gravity. Unfortunately, in most cases our spectral resolution was not high enough and/or our wavelength coverage was not sufficiently large so as to use such line diagnostics. We thus based our clas-

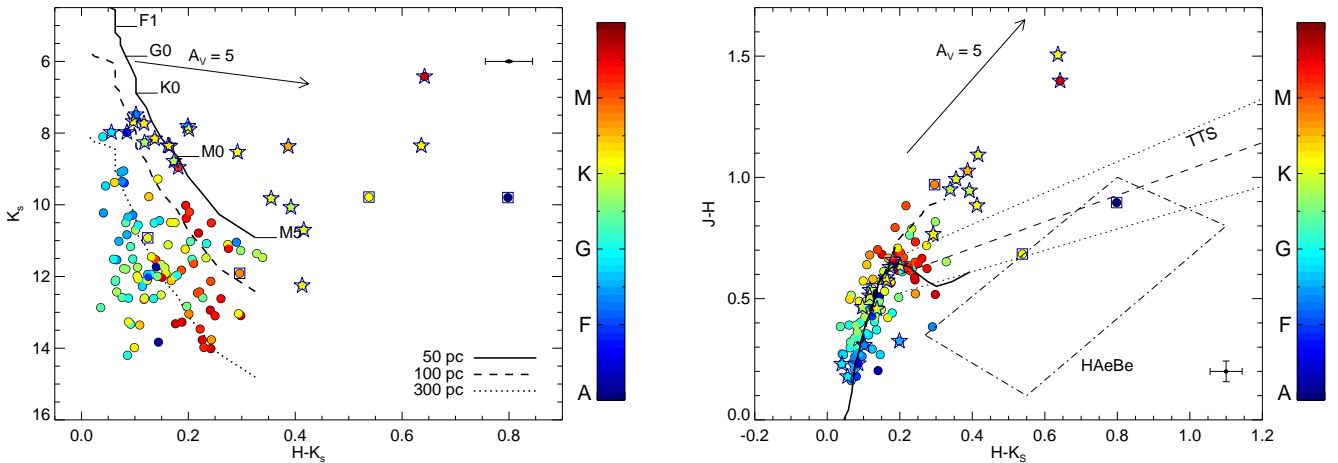


**Fig. 6.** Infrared colour-magnitude diagram (left) and colour-colour diagram (right) for the stellar content of our survey, with spectral type of the stars coded with colour. In the left panel the solid, dashed, and dotted lines show the ZAMS location from Siess et al. (2000) at a distance of 50, 100, and 300 pc respectively. Giant candidates, are over-plotted with a star-symbol. Pre-main sequence stars are shown with squares. We include the reddening vector for an extinction of  $A_V = 5$  magnitudes. In the right panel, the thick black lines show the location of main sequence (solid) and giant (dashed) stars, the thin black dashed line and the thin black dotted lines show the location of classical T Tauri stars (TTS) and associated errors respectively. The black parallelogram shows the location of Herbig AeBe stars (see text for details).

sification in dwarfs or giants on photometric analysis. We constructed infrared colour magnitude diagrams (CMD) in order to be able to distinguish giant stars from dwarf stars. In Fig. 6 we show the locus of the stellar content of our survey (without correcting the magnitudes for extinction). Based on tabulated colours and absolute magnitudes for main sequence stars (Siess et al. 2000) we calculated the expected locus of main sequence stars at limiting distances corresponding to five different intervals, one for each spectral type: 50 pc for M stars, 100 pc for K stars, 150 pc for G stars, 200 pc for F stars, and 300 pc for A stars. This main sequence represents a cut-off limit for dwarf stars. With a maximum apparent magnitude close to 8 in the K<sub>s</sub> band (Cutri et al. 2003), the nearest early M dwarf stars that are detected are going to be at a distance larger than  $\sim 50$  pc, while no A dwarf star can be at a closer distance than about 300 pc. We considered as giant candidate stars those stars that are found above or to the right of the main sequence in all possible combinations of infrared colour-magnitude diagrams. In the left panel of Fig. 6 we show one of the CMDs with the corresponding main sequence cut-off. In the right panel, we show the colour-colour diagram. We include the location of the main sequence and the red giant branch from Bessell & Brett (1988). We indicate the effect of reddening for  $A_V = 5$  transformed into infrared excess using the relations from Mathis (1990). We show the intrinsic colours of classical T Tauri stars in Fig. 6 (Meyer et al. 1997), and of Herbig-AeBe stars (Hernández et al. 2005). We transformed all magnitudes and colours into the 2MASS photometric system using the colour transformation from Carpenter (2001).

Among the 125 stars with determined spectral type detected in the soft band with 2MASS photometry at high probability of identification, we find 98 main sequence stars (78.4%), 23 giant candidates (18.4%), and four pre-main sequence stars (3.2%) (see Table 5). The spectrum of one of the two M giant candidates, 2XMM J184413.9+010026, shows a deficit of NaI at 5897 Å confirming a giant nature of the source. We considered the other M giant candidate, 2XMM J182845.5-111710, to be a dwarf

since the X-ray luminosity is too high (see Section 6.3) and its spectrum shows H $\alpha$  in emission, characteristic of dwarf M stars. There is an excess of yellow giant stars above the overall trend (see Table 5), corresponding to late type G and early K spectral types. This excess was first noticed by Favata et al. (1988) based on the Einstein Medium Sensitivity Survey, and confirmed by the larger number of sources of the Einstein Extended Medium Sensitivity Survey (Sciortino et al. 1995). Later on, Guillout et al. (1999) observed a similar excess based on cross-correlation of ROSAT with Tycho and Hipparcos stars, and associated it with the red clump. The yellow-excess was also noted in the Galactic Plane survey from Morley et al. (2001). As stars evolve off the main sequence, they slow their rotation, decreasing their X-ray luminosity. This age-rotation-luminosity relation implies that single evolved (off main-sequence) stars are not expected to be strong X-ray emitters. On the other hand, in close binaries the rotation of the stars are synchronised with the orbital period. This implies that stars in binary systems do not slow down their spin with age, but on the contrary they preserve their rotation with age, giving rise to X-ray emission through their magnetic activity (Frasca et al. 2006). It is thus very likely that the observed giant stars are evolved binary stars, i. e. RS CVns. We discuss X-ray and infrared properties of these sources in Section 7.1.

## 6.2. Distance

We computed the E(J-K<sub>s</sub>) excess assuming tabulated infrared colours for main-sequence and giant stars from Siess et al. (2000) and Covey et al. (2007) respectively. We calculated the extinction in the K<sub>s</sub> band using the relation  $A_K = 0.67 \times E(J-K_s)$  from Mathis (1990). We corrected our magnitudes for extinction and using the appropriate tabulated absolute magnitudes M<sub>J</sub> for each spectral type and luminosity class, we estimated the distance to the sources. For comparison, we also derived the distances to the sources assuming that all stars were on the main sequence (second panel in Fig. 8). Distances to the sources range

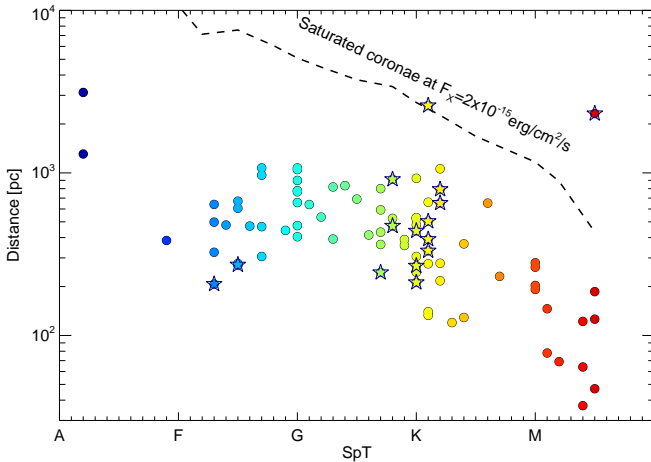


**Fig. 7.** Distance versus spectral type (color-coded symbols) for dwarf and giant (star symbol) stars. The limiting distance associated with the saturation level ( $\log(L_X/L_{bol}) = -3$ ) of dwarf stars at the flux limit of our survey is indicated with a dashed line.

**Table 5.** PMS, MS and giant candidate stars.

SpT	N <sub>pre-MS</sub>	N <sub>MS</sub>	N <sub>Giant</sub>
A	1	4	1
F	0	16	4
G	0	35	4
K	3	20	12
M	0	23	2

from 50 pc to about 1 kpc, with a few sources at larger distances. The distance up to which we can detect stars depends on the spectral type and luminosity class. Assuming saturated coronae,  $\log(L_X/L_{bol}) = -3$ , the X-ray flux limit of our survey gives us an upper distance limit for each spectral type (and luminosity class) up to which stars can be detected. The calculated distances for the stars in our survey are consistent with the maximum distance: while main-sequence F stars can be detected up to several kpc, M stars are detected only up to around 450 pc (see Fig. 7).

### 6.3. X-ray luminosity

We derived X-ray luminosities from the measured fluxes in the soft (0.5–2.0 keV) band. We used the energy-to-flux conversion factor  $1.75 \times 10^{12} \text{ erg cm}^{-2}\text{s}^{-1}/\text{pn counts s}^{-1}$ , corresponding to a thermal plasma with  $kT = 0.5 \text{ keV}$  and absorbed by  $N_H \sim 10^{21} \text{ cm}^{-2}$  most frequent value for the stellar content of our survey (see Fig. 5). Details on the calculation are given in Section 7.3.2. All luminosities from now on will refer to the energy band 0.5–2.0 keV, unless specified otherwise. For giant candidate stars we obtained two values: a first one corresponding to the estimated distance if the source were a main sequence star, and a second one corresponding to the distance derived if it were a giant. The X-ray luminosity distributions are shown in the third and fifth panels of Fig. 8. Assuming all the stars in the sample are dwarf stars, a population of low X-ray luminosity ( $< 10^{28} \text{ erg s}^{-1}$ ) K stars appears at very close distances (dark

grey histograms). There is no observational evidence of an excess of low X-ray luminosity K stars within 70 parsecs to the Sun. It therefore seems more plausible that our sample contains two different evolutionary populations. This is consistent with the idea that not all identified stars are on the main sequence. Assuming that the giant star candidates classified in Section 6.1 are giants yields much more consistent results. X-ray luminosities are in the range  $10^{28} – 10^{31} \text{ erg s}^{-1}$  (see right panel in Fig. 8). The number of detected sources increases with the X-ray luminosity up to  $L_X = 10^{30} \text{ erg s}^{-1}$ . Above that value the number of sources drops. This is a typical characteristic of an X-ray flux limited sample, where we preferentially detect sources with high X-ray luminosities.

We find that, in general, early spectral type stars have higher X-ray luminosities than late spectral type stars, an effect usually attributed to their larger radii (Fleming et al. 1989). A similar trend has been observed by Micela et al. (1988); Barbera et al. (1993); Motch et al. (1997); Guillout et al. (1999) and Zickgraf et al. (2005). Although such a trend has not been observed by Wright et al. (2010), other deep surveys such as that from Covey et al. (2008) show the same behaviour, ruling out the possibility of being an effect associated to nearby stars as suggested by Wright et al. (2010).

X-ray emission is known to decrease with the age of the stars (Jackson et al. 2012, and references therein). Stars slow-down their rotation as they age due to magnetic braking (Kawaler 1988; Matt et al. 2012). This implies that at high X-ray luminosities our survey should be dominated by fast rotators, either young stars or in binary systems, and at low X-ray luminosities the sample should contain an old-to-intermediate age population.

To assess better this statement we compared our X-ray-to-optical flux ratios with those of stars belonging to three different populations, corresponding to three different ages: i) field stars from Schmitt & Liefke (2004) representing an old population with ages older than about 1 Gyr; ii) the Hyades from Stern et al. (1995) as representative of an intermediate age of  $\sim 600$  Myr; and iii) the Pleiades from Micela et al. (1996) representing a young population of about 100 Myr. We restrict the three samples to stars with luminosity class V and consider the same spectral range as covered in our sample, A–M, and divided in two spectral type ranges: F–G and K–M stars (see Fig. 9). The X-ray-to-optical flux ratio  $\log(F_X/F_V)$  distribution of the identified stars in our survey is similar to that of the Pleiades with an extended tail at low values of  $\log(F_X/F_V)$ , i. e. is consistent with a young to intermediate age population, such as the one reported in Koenig et al. (2008). There is a population of F–G stars younger than the Pleiades. In the disk X-ray surveys are dominated by young stars in the flux range covered by our survey (Guillout et al. 1996), which explains the detection of this young population of stars.

### 6.4. Notes on individual sources

Among the identified sources we found CVs, T Tauri stars, Herbig-Ae stars, and  $\gamma$ -Cas-like objects. We discuss here the most relevant features of these objects.

#### 6.4.1. Cataclysmic variables

Cataclysmic variables are semi-detached binary stars consisting of a white dwarf plus a low mass star where the low mass star is filling its Roche lobe and the transferred matter is accreted

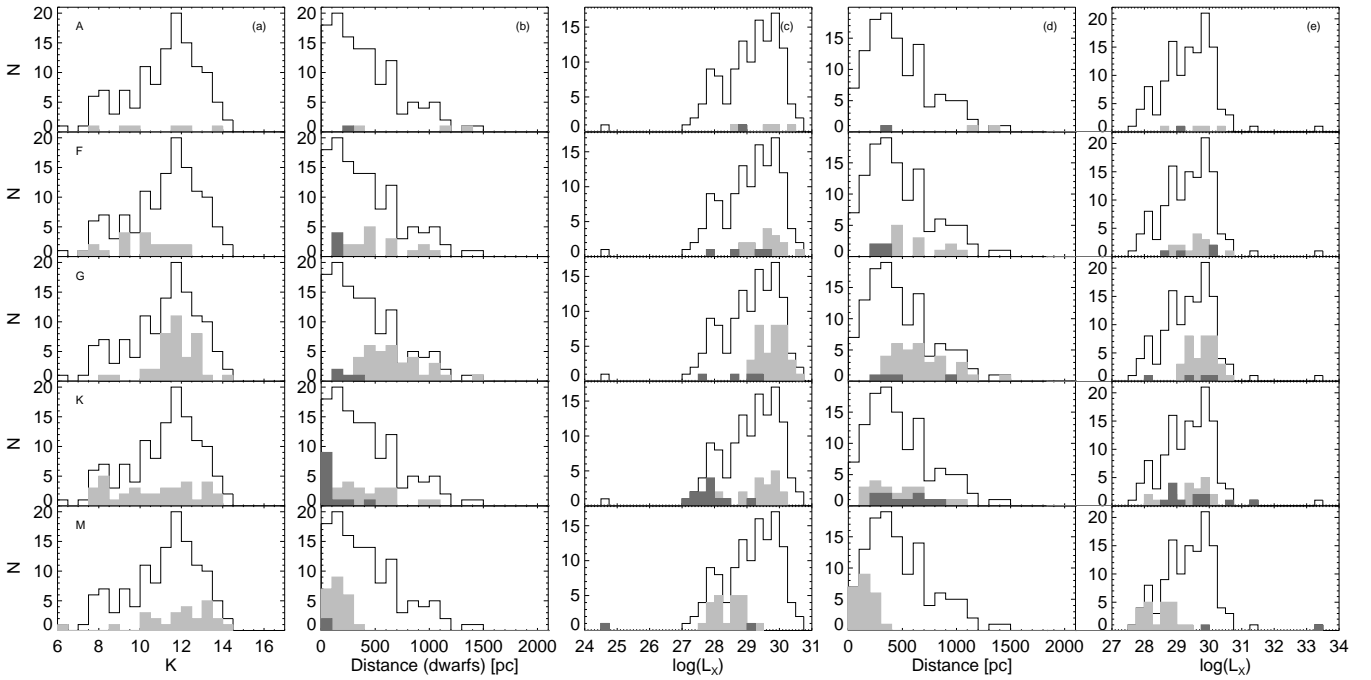


**Fig. 8.** a) Distribution of the K magnitude for all identified active coronae. b) Distribution of distances to the identified active coronae assuming they are all in the main-sequence and associated distribution of X-ray luminosities (c). d) Distribution of distances for main-sequence and giant star candidates and corresponding X-ray luminosities (e). We show distances only up to 2 kpc, since only a few sources, with spectral types A and F, are found at larger distances. We overplot in light grey the distribution for each spectral type, A to M stars from top to bottom on top of the total distribution (white) for comparison. Giant star candidates are shown in dark grey.

**Table 6.** Main properties of the cataclysmic variables.

Name	EW(H $\alpha$ ) [Å]	EW(H $\beta$ ) [Å]	V	D [kpc]
2XMM J074743.5-185654	140	65	20.4	0.6-2.0
2XMM J000134.1+625008	6	2	17.8	< 2

onto the white dwarf (see Warner 1995, for a review). If the white dwarf has a magnetic field, mass transfer can be channelled and accretion will take place on one or both poles of the white dwarf, labelling the CVs as polars or intermediate polars, for lower magnetic fields white dwarfs. They have orbital periods ranging from around 80 minutes and up to about one day (Ritter & Kolb 2003; Gänsicke et al. 2009).

We identified two cataclysmic variables in this study: 2XMM J074743.5-185654, in field PKS 0743-19-off, and 2XMM J000134.1+625008, in field RXJ0002+6246. Both CVs display Balmer emission lines (see Fig. 10), and 2XMM J074743.5-185654 has some He I emission. They both lack the He II line at 4686 Å typical of polars and intermediate polars, indicating both CVs are non-magnetic.

Equivalent widths of H $\alpha$  and H $\beta$  emission lines are given in Table 6. Making use of the empirical EW(H $\beta$ )–absolute magnitude relation from Patterson (1984) we estimate the absolute magnitude of the accretion disk to be M<sub>V</sub> ~ 10.3 for 2XMM J074743.5-185654. From the total Galactic absorption along the line of sight from Schlegel et al. (1998) and using the calibration from Predehl & Schmitt (1995) we derive an upper limit to A<sub>V</sub> of 1.2. We estimate a magnitude of V=20.4 by folding the optical spectrum to the Johnson filter. The distance to the

source is in the range 0.6–2.0 kpc, depending on the assumed A<sub>V</sub>, implying L<sub>X</sub>= $4.8 \times 10^{30}$ – $5.3 \times 10^{31}$  erg s<sup>-1</sup> (0.2–12 keV).

Source 2XMM J000134.1+625008 has a GSC-2.3 counterpart with magnitude V=17.82. Using the empirical relation from Patterson (1984) would imply a very large distance of about 3.8 kpc, incompatible with the small interstellar absorption visible in the slope of the optical spectrum. The spectral energy distribution of 2XMM J074743.5-185654 seems to consist of a blue continuum probably coming from the accretion disk and of a possible late K star continuum in the red. However, our spectrum is too noisy to detect metallic lines from the secondary star. The empirical EW(H $\beta$ )–M<sub>V</sub> relation from Patterson (1984) is based on CVs in which the disk is dominating in the optical and therefore cannot probably be used in this particular case. Assuming a maximum X-ray luminosity of L<sub>X</sub>< $10^{32}$  erg s<sup>-1</sup> for non-magnetic CVs (Pretorius & Knigge 2012), the source must be closer than about 2 kpc.

#### 6.4.2. T Tauri stars

T Tauri stars are low mass ( $M \leq 2M_{\odot}$ ) pre-main sequence stars (Joy 1945). In *Classical T Tauri* stars (cTTs) the central object is accreting from a circumstellar disk, while in *weak line T Tauri* stars (wTTs) there is no longer evidence of accretion (see Bertout 1989; Appenzeller & Mundt 1989, for a definition of the two sub-classes). They can be classified into weak or classical T Tauri on the basis of the equivalent width of the H $\alpha$  emission line (Barrado y Navascués & Martín 2003). T Tauri stars are young objects typically found in star forming regions. Their X-ray energy distribution can be described as thermal emission from an optically thin plasma with temperatures from

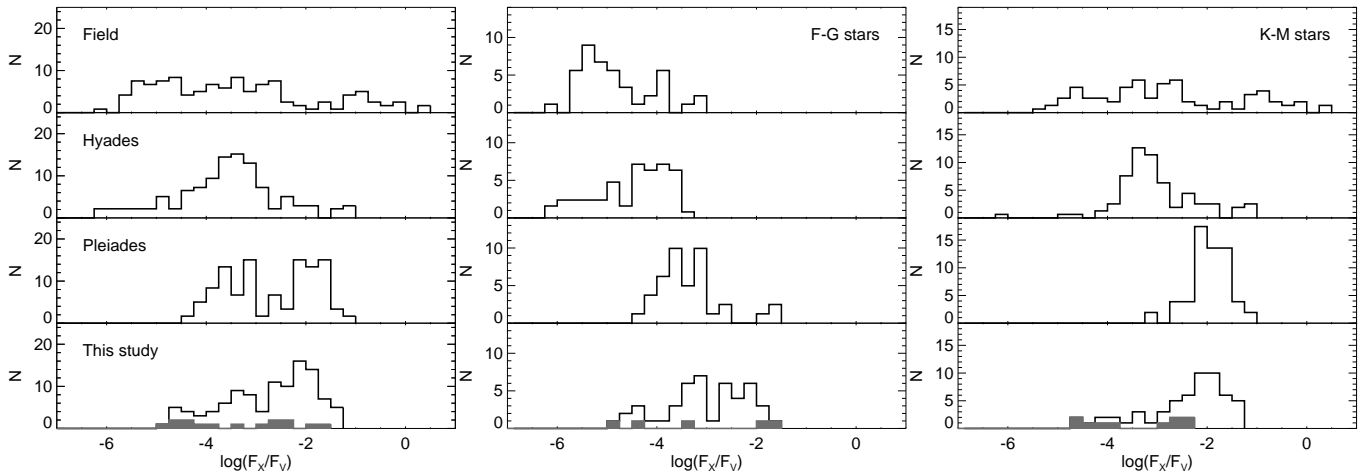


**Fig. 9.** X-ray-to-optical flux ratio ( $\log(F_x/F_v)$ ) distribution of the stellar population of this survey compared to that of: field, Hyades and Pleiades stars representing old, intermediate and young populations respectively. We show the  $\log(F_x/F_v)$  distribution for spectral ranges A–M (left panel), F–G (middle panel), and K–M (right panel). In dark grey we show the location of giant star candidates. For comparison purposes, the total number of field, Hyades and Pleiades stars has been normalised to match the same number as our stellar content.

few to several tens of MK and X-ray luminosities in the range  $\times 10^{28} - 10^{31}$  erg s $^{-1}$  (0.5 - 10 keV), mainly associated with the magnetically heated corona (Güdel & Nazé 2009, and references therein).

Source 2XMM J223122.8+390914, detected in field 3C449, has spectral type K0Ve. Its optical spectrum presents the H $\alpha$  line in emission, with an equivalent width of  $\sim 6 \text{ \AA}$ , pointing to a wTTS nature (Barrado y Navascués & Martín 2003). It has an infrared counterpart in the WISE catalogue (Cutri et al. 2012), WISEP J223122.86+390913.7, which does not reveal any infrared excess with respect to a stellar atmosphere (see Fig. 11). Source 2XMM J223122.8+390914 is located at relatively high Galactic latitude ( $l = 95.3^\circ, b = -16.1^\circ$ ), far from any known star formation region, where T Tauri stars are typically found. Nevertheless, the number of reported isolated T Tauri stars is continuously increasing (Guillout et al. 2010). The existence of T Tauri stars far away from star forming regions containing molecular gas is a matter of lively debate. While kinematic studies suggest some of the stars classified as T Tauri are in fact young main sequence objects (Bertout & Genova 2006), several mechanisms accounting for the apparent dispersal of T Tauri stars have been proposed (Feigelson 1996).

Source 2XMM J184401.2+005455, in field Ridge 2, with spectral type K7Ve, also shows the H $\alpha$  line in emission. The EW of the H $\alpha$  line is  $\sim 25 \text{ \AA}$ , pointing to a cTTS nature for the source (Barrado y Navascués & Martín 2003). The optical images reveal that the source is close to a cloud. The source has a WISE counterpart, WISEP J184401.16+005456.3. The spectral energy distribution (SED), presented in Fig. 11, is consistent with a stellar atmosphere in the optical and NIR, and exhibits an excess in the 22  $\mu\text{m}$  band. For comparison we show the SED based on a stellar model from Castelli & Kurucz (2004) with effective temperature  $T_{\text{eff}} = 4000 \text{ K}$ , and  $\log(g) = 4.5$ . The most likely origin for the IR excess is cold dust emission from a transition disk, where the inner dust disk has dissipated while the disk at larger distance is still integral (e.g. Fang et al. 2009). These two candidate T Tauri stars are at a maximum distance of 300 pc, with maximum X-ray luminosities of  $6.1 \times 10^{28}$  and

$3.8 \times 10^{28}$  erg s $^{-1}$  (in the 0.5 - 2 keV energy band), respectively. Their X-ray to bolometric luminosity ratio,  $\log(L_x/L_{\text{bol}})$ , is below the saturation level.

2MASS infrared photometry revealed an infrared excess ( $(H - K_S) > 0.5$ ) for source 2XMM J180802.0-191505, in field WR110. The source has infrared colours within the T Tauri region from Meyer et al. (1997) (see right panel in Fig. 6), consistent with a classical T Tauri. From its optical spectrum we derived a K1V spectral type. The optical spectrum covers only up to 5000  $\text{\AA}$ , inspection of the H $\alpha$  line was therefore not possible, so we were not able to learn whether accretion is taking place, which would confirm a classical T Tauri nature of the source. No emission from other Balmer lines was detected in the spectrum. After comparison of the WISE source catalogue with the 2MASS point source catalogue, we conclude that the angular resolution of WISE is too low to provide us a reliable photometry of this source in this crowded area. The source was sufficiently bright in X-rays, which allowed us to analyse its X-ray spectrum. The X-ray spectrum is consistent with that of a young star, with a temperature of  $kT = 1.4^{+0.6}_{-0.5} \text{ keV}$ , and the derived  $N_{\text{H}}$  is compatible with the reddening obtained from the optical spectrum,  $A_V = 2.17$ .

The lithium content can be used as a spectral type dependent proxy of the age of the stars. Unfortunately, at our spectral resolution we are not able to measure accurate Li abundances. High resolution spectra would be needed to make a clear statement about the evolutionary state of these stars.

#### 6.4.3. Herbig Ae stars

The optical spectrum of source 2XMM J182658.4-113258 (see Fig. 10), located in field Ridge3, reveals an A0 spectral type star with a very strong and broad H $\alpha$  emission line. The X-ray source has an infrared counterpart, 2MASS 18265832-1132585, with colour  $(H - K_S) = 0.79 \pm 0.06$ , showing a strong near infrared excess with respect to a main-sequence or giant A0 star (see Fig. 6). These two characteristics, H $\alpha$  emission plus infrared excess, are typical of Herbig-Ae (HeAe) stars (Herbig 1960), which are pre-

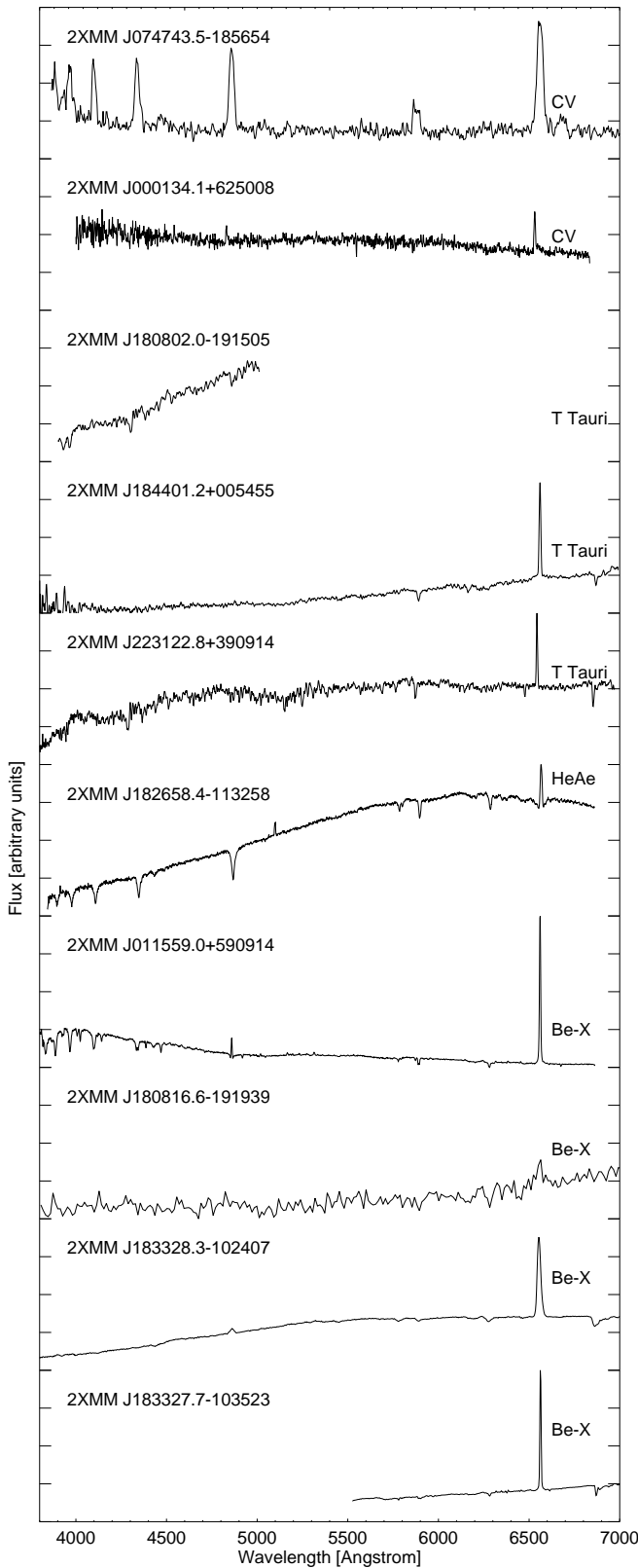


**Fig. 10.** Optical spectra of the two identified CVs, 2XMM J074743.5-185654 and 2XMM J000134.1+625008, the three identified T Tauri stars, 2XMM J180802.0-191505, 2XMM J184401.2+005455, and 2XMM J223122.8+390914, the identified Herbig-Ae star, 2XMM J182658.4-113258, and the four massive X-ray binary candidates, 2XMM J183328.3-102407, 2XMM J011559.0+590914, 2XMM J183327.7-103523, and 2XMM J180816.6-191939, from top to bottom.

main sequence stars of intermediate mass, i.e the high mass counterparts to T Tauri stars. Broad H $\alpha$  emission and infrared excess is associated with dust emission of circumstellar material (Malfait et al. 1998; Meeus et al. 1998, 2001). Nevertheless we note that the K<sub>s</sub> magnitude has a flag indicating bad quality (AAE, where E is standing for a bad PSF fitting), so one should be cautious with the conclusions. The origin of the X-ray emission in HeAe stars is still in debate. A stars are fully radiative stars, therefore not expected to maintain magnetic fields and coronal heating. Possible explanations, proposed earlier by Zinnecker & Preibisch (1994) and Stelzer et al. (2006), are stellar wind instabilities or presence of a T Tauri star companion.

#### 6.4.4. Massive X-ray binary candidates

High mass X-ray binaries (HMXB) consist of a white dwarf (WD), a neutron star (NS) or a black hole and of an early type star dominating the optical emission. Most known HMXBs have a Be star as primary component. Although theoretical population studies predict Be+WD are more frequent than Be+NS (e.g. Raguzova 2001), there are only two candidate HMXBs with a WD known so far (Kahabka et al. 2006; Sturm et al. 2012). Unlike in CVs and LMXBs mass transfer in Be HMXBs occurs through an equatorially condensed decretion disk (Okazaki & Negueruela 2001). They usually have long orbital periods, of the order of days to hundreds of days. Be/X-ray binaries typically have X-ray luminosities in the range  $10^{34} - 10^{38}$  erg s $^{-1}$  (Grimm et al. 2002).

In four cases, we have detected X-ray emission from Be stars at levels significantly above that expected for single Be stars of the same spectral type (Cohen et al. 1997; Cohen 2000). Their optical spectra are shown in Fig. 10.

2XMM J183328.3-102407 (USNO 0750-13549725 C), detected in field G21.5-09 (rev 60), is the brightest star in the cluster NGC 6649. The spectral type of the source is B1-1.5IIIe, and it presents the H $\alpha$  line in emission with an EW of  $\sim 36$  Å. The source is identified with 2MASS 18332830-1024087 with a probability above 99%. We calculated the colour excess E(J-K<sub>s</sub>) with respect to a B1III star, and from its magnitude K<sub>s</sub> = 7.793  $\pm$  0.027 we estimated a distance to the source of about 1.7 kpc, consistent with that to the cluster (Walker & Laney 1987). The colour excess is E(B-V)  $\sim$  1.2 (Turner 1981), and the X-ray luminosity is  $\sim 5 \times 10^{32}$  erg s $^{-1}$  (0.2–12 keV).

2XMM J183327.7-103523, aka SS 397, detected in the field G21.5-09, has a spectral type B0Ve and also shows the H $\alpha$  line in emission, with an EW of  $\sim 34$  Å. It has a 2MASS counterpart, 2MASS 18332777-1035243, with an identification probability above 99% and K magnitude of 8.267  $\pm$  0.026, and an extinction A<sub>V</sub>  $\sim$  5.4. The calculated distance of 1.5 kpc implies an X-ray luminosity of  $\sim 4.4 \times 10^{32}$  erg s $^{-1}$  (0.2–12 keV). The two sources above have already been reported in Motch et al. (2007).

2XMM J011559.0+590914 (TYC 3681-695-1), detected in the field of PSRJ0117+5914, has a counterpart in the 2MASS catalogue, 2MASS 01155905+5909141, with an identification probability above 99%. The estimated spectral type from the optical spectrum is B1-2III/Ve, presenting the H $\alpha$  line in emission with an EW  $\sim 31$  Å. The optical extinction is A<sub>V</sub>  $\sim$  2.3, and the 2MASS magnitude implies a distance to the system in the range of 1.9–3.8 kpc. The X-ray luminosity is between  $1.4 \times 10^{32}$  erg s $^{-1}$  and  $5.8 \times 10^{32}$  erg s $^{-1}$  (0.2–12 keV).

For source 2XMM J180816.6-191939, located in the field of WR110, already reported as a Be/X-ray binary candidate by Motch et al. (2003), we took several spectra, and combined them

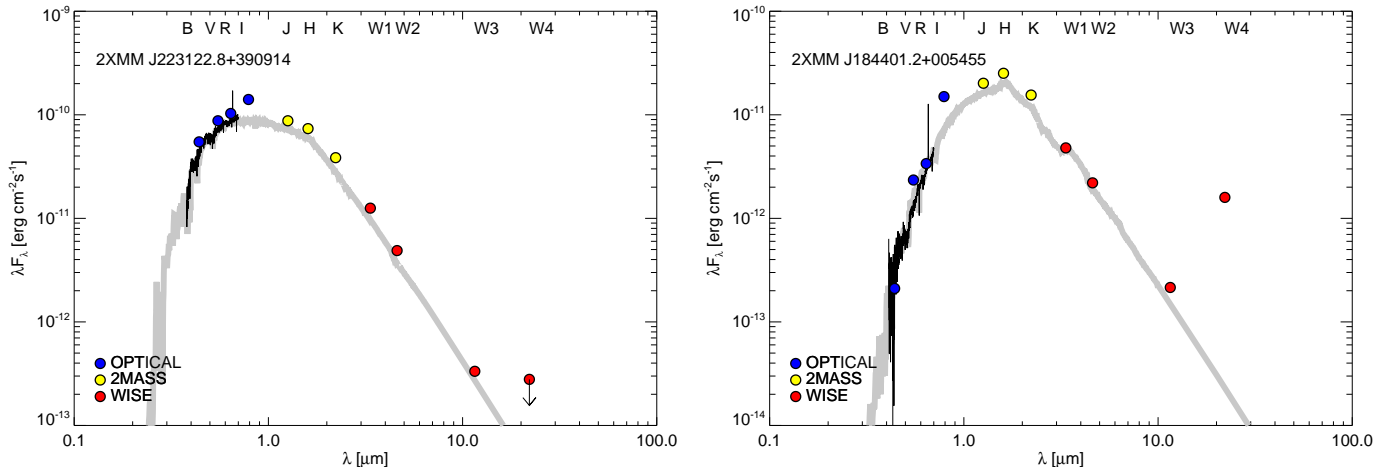


**Fig. 11.** Spectral energy distribution of two T Tauri candidates: 2XMM J223122.8+390914 (left) and 2XMM J184401.2+005455 (right). We compare the SED of the T Tauri stars with stellar atmosphere models (grey) from Castelli & Kurucz (2004) with effective temperatures 5200 K and 4000 K respectively, and  $\log(g) = 4.5$ . The optical spectra obtained at the telescope are shown as a black line, and upper limits on the magnitude are indicated with an arrow.

to improve the signal to noise ratio in order to facilitate the identification. The combined optical spectrum (see Fig. 10), shows the H $\alpha$  line in emission, with an EW of  $\sim 50\text{\AA}$ . The relatively noisy spectrum makes it hard to discern absorption lines that could help to characterise the source and estimate its spectral type, but the absence of the TiO molecular bands rules out a dMe star nature. Although it has a 2MASS counterpart with a low probability of it being the true association ( $P_{\text{id}} \sim 8\%$ ), the presence of emission lines in the optical spectra confirm it as the right association. From the optical spectrum, we derived  $R = 22$  and  $R-I = 2.6$ , indicating a high interstellar absorption. If the counterpart is an intrinsically blue object,  $A_V$  is of the order of 13.8, where  $E(B-V)$  was derived from the spectral fit with a B0V star (Castelli & Kurucz 2004). This value corresponds to  $N_H = 2.47 \times 10^{22} \text{ cm}^{-2}$ , half of the total expected Galactic absorption in that direction. Using the extinction maps from Marshall et al. (2006), with an infrared extinction of  $A_K = 1.23$  we estimated the distance to the source to be between 6 to 7 kpc, ruling out a CV nature. At this distance, we estimate  $M_V$  to be in the range  $-3.3$  to  $-3.7$ , absolute magnitude which is consistent with a B0V star. The X-ray luminosity is in the range  $L_X = 2.4 \times 10^{32} - 3.3 \times 10^{32} \text{ erg s}^{-1}$  (0.2–12 keV).

Luminosities in this section were calculated in the 0.2–12 keV energy band using the corresponding energy-to-flux conversion factor at the estimated galactic absorption and assuming a mekal with  $kT = 8 \text{ keV}$ . All Be stars found in this study have X-ray luminosities  $10^{32} < L_X < 10^{33} \text{ erg s}^{-1}$ , lower than those expected for neutron star accreting HMXBs (Grimm et al. 2002), but higher than those expected for single Be stars (Cohen et al. 1997). The observed X-ray luminosity of our Be stars is at least one order of magnitude below that detected from transient Be/X-ray binaries in quiescence or from members of the class of persistent Be/X-ray pulsars (Reig 2011). The absence of recorded outburst from these Be stars together with their low steady  $L_X$  make it very likely that these sources belong to the new class of  $\gamma$ -Cas-like Be/X-ray systems (Motch et al. 2007; Lopes de Oliveira et al. 2010; Lopes de Oliveira & Motch 2011) in which X-ray emission arises either from the accretion onto a white dwarf or from magnetic interaction between the stellar

photosphere and the inner part of the decretion disc. Marco et al. (2007) have shown that the counterpart of 2XMM J183328.3-102407 is a blue straggler in the 50 Myr old cluster NGC 6649. A similar blue straggler nature has been established for other  $\gamma$ -Cas analogues (see Lopes de Oliveira et al. 2007, and references therein).  $\gamma$ -Cas-like stars seem therefore preferentially created thanks to the high mass transfer occurring during the evolution of a massive close binary. The question remains open, however, whether the outstanding X-ray emission is related to the presence of a compact companion star remain or due to the high angular momentum transferred to the B star.

## 7. Properties and characteristics of the sample

We investigated the X-ray, infrared and optical properties of the sample with the aim of learning about the stellar content of our survey.

### 7.1. Infrared versus X-ray

The different hardness ratio versus  $(H-K_S)$  colour distributions are shown in Fig. 12. Since the colour  $(H-K_S)$  remains within 0 to  $+0.1$  from A to K spectral types and all luminosity classes (see Covey et al. 2007), variations in colour mainly reflect variations in interstellar absorption (Motch & Pakull 2012), or intrinsic emission by circumstellar matter. Assuming intrinsic colour  $(H-K_S = 0)$ , we calculated the expected hardness ratios as a function of the colour excess  $E(H-K_S)$ , through the expression  $N_H = 3.5 \times 10^{22} \times E(H-K_S) \text{ cm}^{-2}$ , for different kinds of objects: i) three different populations of active coronae: a young population of 70 Myr, an intermediate population of 300 Myr, and an old population of 1.9 Gyr, assuming 2-T thermal emission (Guedel et al. 1997); ii) for AY Cet, a typical BY Dra binary (Dempsey et al. 1997), and for the RS CVn star WW Dra (Dempsey et al. 1993); and iii) two power laws with photon indices  $\Gamma$  of 0 and 2 (see Section 2.2).

We limit to sources with X-ray HRs and infrared colours with errors smaller than 0.3. After this cut, we are left with a total of 159 sources, among which 124 are identified as stars,

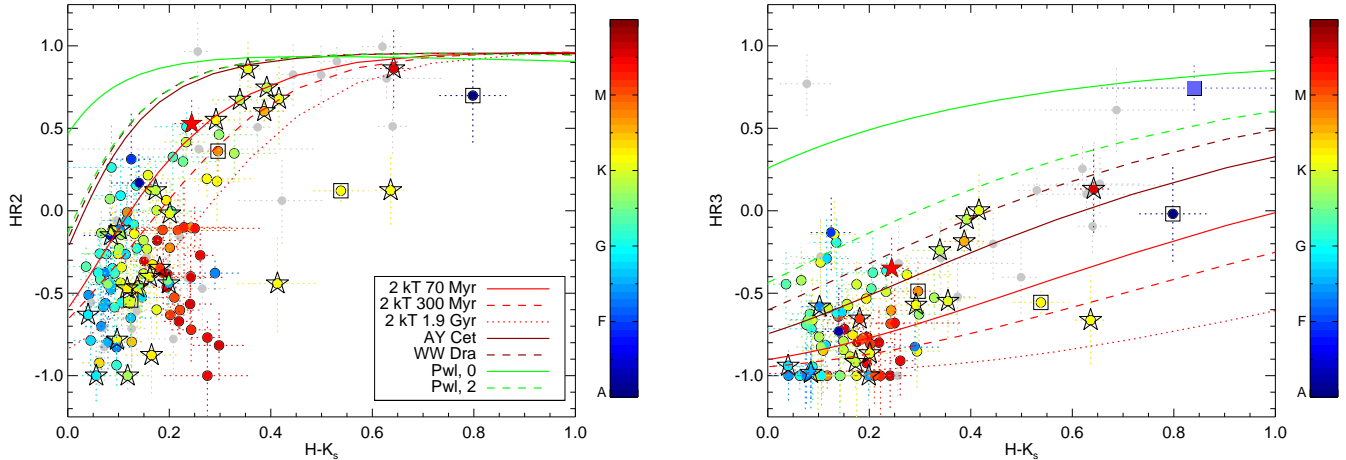


**Fig. 12.** X-ray-infrared colour-colour diagrams. Hardness ratio versus  $(H - K_S)$  for all X-ray sources having a 2MASS counterpart with a probability higher than 90%. Active coronae are represented by filled circles where colour indicates the spectral type, extragalactic objects with blue filled squares. Giant stars are overplotted as stars, pre-main sequence stars are highlighted by an open square and X-ray binaries (CVs, HMXBs) are plotted as a filled star in red. Lines are the expected colours for stars of different ages, main sequence and evolved binaries, and accreting objects (see legend and text). We only plot sources with errors lower than 0.3 in X-ray and infrared colours.

one as a Be/X, two as T Tauri stars, one as HeAe star, two as AGNs, and the remaining 29 are not classified. Most of the stars have colours consistent with the expected values for active coronae younger than 2 Gyr and BY Dra or RS CVn binaries. The majority of the stars with  $HR2 > 0$  have spectral types in the range G–K, with only a minor contribution from earlier and later spectral type stars. There is one M star (2XMM J184413.9+010026) with a very hard HR, classified in the previous section as a giant star candidate on the basis of its infrared colours. The lack of emission lines in its optical spectrum indicates that the star is not a symbiotic binary. Two among the three pre-main sequence stars found in our sample (2XMM J184401.2+005455 and 2XMM J182658.4-113258) and one Be/X-ray binary (2XMM J011559.0+590914) have  $HR2 > 0$  (see left panel in Fig. 12).

Some stars have HRs significantly higher than expected for stars younger than 70 Myr but consistent with expected values for BY Dra or RS CVn binaries. The fraction of stars above the expected HR for 70 Myr old active coronae represents 3% (0%) of the identified stars in the HR2 bands, 37% (8%) in the HR3 bands, and up to 78% (56%) in the harder HR4 bands at a  $1\sigma$  ( $3\sigma$ ) significance, and have infrared colours consistent with main sequence or evolved binary stars.

There are eight sources above the expected value for high accretion rate sources ( $\Gamma = 0$ ) (in either  $HR2 -$ ,  $HR3 -$  or  $HR4 - (H - K_S)$  diagram): the two identified AGNs, three stars, and three unidentified sources, likely to have extragalactic origin. One of the identified stars, 2XMM J174819.7-280727 with spectral type M6V (Raharto et al. 1984) is very close to the HMXB SAX J1748.2-2808 (Sidoli et al. 2006). However, the two sources are well separated and furthermore 2XMM J174819.7-280727 is constantly detected during three observations. This implies that flaring from the M6V star is unlikely to account for the unusually hard X-ray spectrum. The other three identified stars displaying hard X-ray emission are 2XMM J092531.1-474851, and 2XMM J223021.2+392253. They have spectral types K7V, and G5V and 2MASS identifica-

tion probabilities of  $P_{id} = 0.99, 0.96$ , and 0.97 respectively, and thus are not likely to be spurious associations.

## 7.2. X-ray colours

The hardness ratio distributions (X-ray colour-colour diagrams) of X-ray sources are shown in Fig. 13. We again restrict our analysis to sources with HR errors smaller than 0.3 and with the best quality flag. The left (right) panel of Fig. 13,  $HR2 - HR3$  ( $HR3 - HR4$ ) diagram, is populated by 404 (193) sources, 37% (23%) have a bright optical or infrared counterpart (association probability  $> 90\%$ ). The majority of the sources with  $HR2$  errors below 0.3 have  $HR3$  below  $-0.25$ , consistent with a soft X-ray spectrum characteristic of active coronae. Among the sources with bright optical or infrared associations, 70% have been classified as stars using optical spectroscopy, while the extragalactic sources represent 4% of the bright optical/infrared associations. Thirteen spectroscopically identified sources have optical and infrared counterparts with an identification probability lower than 90%. These relatively faint stars have late spectral types (one F, five K, and seven M stars).

As stated in Section 7.1, a number of hard sources with bright optical or infrared counterparts have been classified as active coronae on the basis of their optical spectra (see right panel in Fig. 13). We recall that, at the imposed 90% threshold the number of expected spurious matches is lower than 2%. There are 193 sources in the  $HR3$  versus  $HR4$  diagram (with  $\sigma_{HR_i} < 0.3$ ), hence we expect a maximum of 4 hard sources associated with spurious matches, which is not enough to explain the identified coronae, with bright optical or infrared counterpart, detected in the hard bands.

The majority of the unidentified sources do not have a bright optical or infrared counterpart, and have hardness ratios consistent with those expected for a typical AGN with a power law spectrum of photon index of  $\Gamma = 1.9$  absorbed by the full Galactic line of sight column density (blue region in Fig. 13). A non negligible number of unidentified sources are found to be softer than expected if extragalactic. The nature of these sources

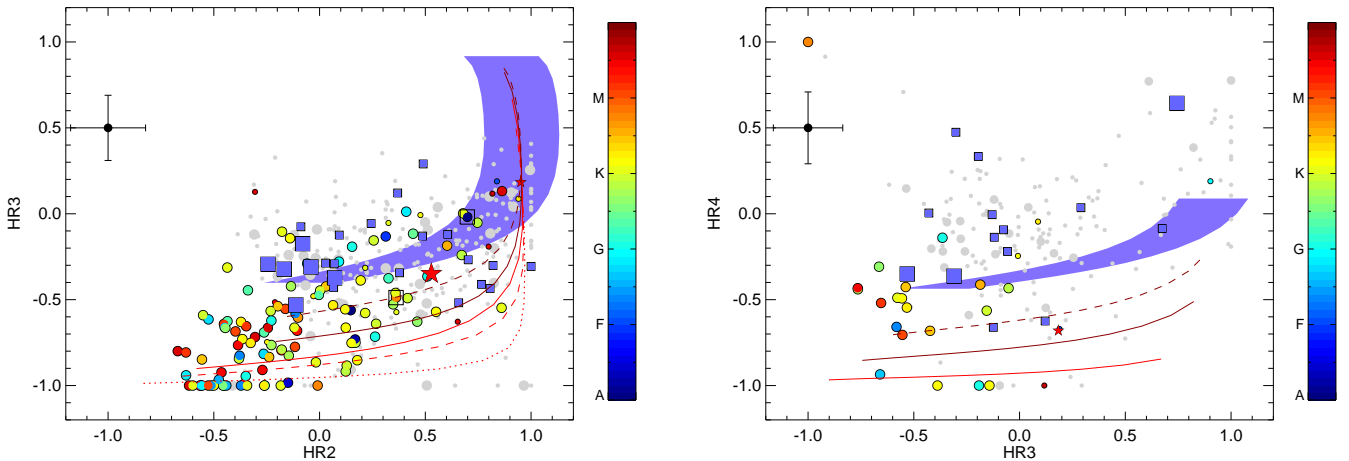


**Fig. 13.** Hardness ratio distribution for all detected X-ray sources (small symbols) and for those with infrared or optical counterpart with a probability higher than 90% (big symbols). Grey are unidentified sources, coloured circles are active coronae with colour indicating their spectral type, blue filled squares are extragalactic objects, open squares highlight the pre-main sequence stars (T Tauri and HeAe), and filled red star are X-ray binaries (CVs and HMXBs). We limit to sources with HR errors smaller than 0.3 and with  $\text{sum\_flag} = 0$ . The mean errors are plotted in the upper left corners. For comparison we show the expected hardness ratio values for a typical AGN (power law with photon index  $\Gamma = 1.9$ ) and for  $10^{20} < N_{\text{H}} < 10^{23} \text{ cm}^{-2}$ , as a shaded area with a width equal to the mean HR2 and HR3 errors in the left and right panels respectively. Lines indicate the position of stars of different ages and main-sequence evolved binaries (see legend in Fig. 12).

is difficult to guess. A fraction among them could be distant dM stars that are too faint to be detected in infrared or optical surveys and fainter than our limit for spectroscopic identification ( $R \sim 21$ ). Assuming a saturated corona ( $\log(L_{\text{X}}/L_{\text{bol}}) = -3$ ), at the limit of our X-ray survey ( $F_{\text{X}} \sim 2 \times 10^{-15} \text{ erg cm}^{-2}\text{s}^{-1}$ ), dM stars can only be detected up to about 450 pc (see Fig. 7).

### 7.3. $\log N(>S) - \log S$ curves

We computed the number of sources per square degree detected above a given flux ( $\log N(>S) - \log S$ ) in two energy bands: soft (0.5–2.0 keV) and hard (2–12 keV). We restricted our analysis to fields observed in full window mode and with the EPIC pn camera. Fields Ridge 3 and Ridge 4 cover nearly the same sky area. We only considered field Ridge 3 in this analysis since it has the longest exposure time. This leaves us with a total of 18 fields.

#### 7.3.1. Effective area of the survey

To estimate the effective area of our survey, we first built sensitivity maps following the method described by Carrera et al. (2007). For each band and field, we created: i) exposure maps, that contain information on exposure times in each detector pixel taking into account the mirror vignetting, the detector efficiency, bad pixels and CCD gaps, and the field of view; and ii) background maps, which hold information on the counts in source free regions. We used the SAS tasks `eexpmmap` and `esplinemmap` respectively. We calculated the count rate in the soft and the hard bands by adding the tabulated count rates in the bands 0.5–1.0 and 1.0–2.0 keV, and 2.0–4.5 and 4.5–12.0 keV respectively. We derived maximum likelihood (ML) values in the soft and hard energy bands making use of the listed individual ML, and using the formula given by Watson et al. (2009) (see their Appendix). We limited our analysis to sources with  $\text{ML} > 8$ , which corresponds to a  $\sim 4\sigma$  detection. We chose a radius

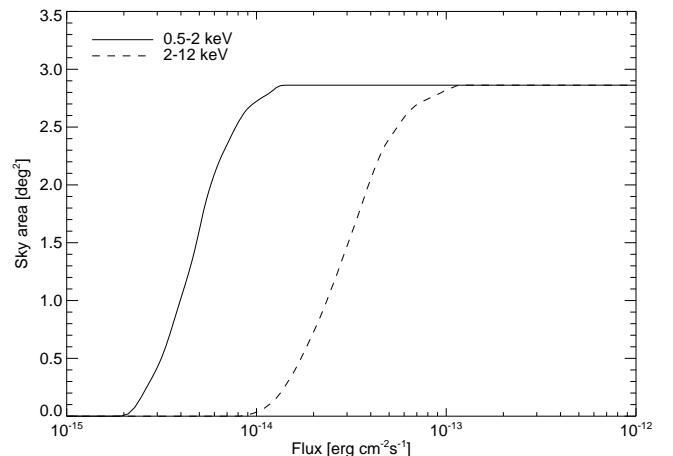


**Fig. 14.** Effective area of the survey in the soft (solid line) and the hard (dashed line) energy bands.

of 5.08 and 5.18 pixels (see Table A.1 from Carrera et al. 2007) for source extraction in the soft and the hard bands respectively. We then generated the sensitivity maps following the different steps listed by Carrera et al. (2007). These sensitivity maps provide us with the minimum count rate that can be detected in each pixel at a given ML. The effective area over which we are sensitive to a given count rate is given by the sum of the number of pixels in the sensitivity map below a given count rate multiplied by the pixel area ( $1\text{pix} = (4'')^2$ ). The total area at a given count rate is then the sum of the areas of each field (see Fig. 14).

With a  $\text{ML} > 8$ , the probability of a spurious detection at this level is  $\sim 0.0003$  per resolution element. The total area of the survey is  $\sim 2.8 \text{ deg}^2$ , and the individual detection cell used by the task `eexpmmap` is  $5 \times 5$  pixels. We thus expect a maximum of 27 spurious detections in each band, corresponding to around

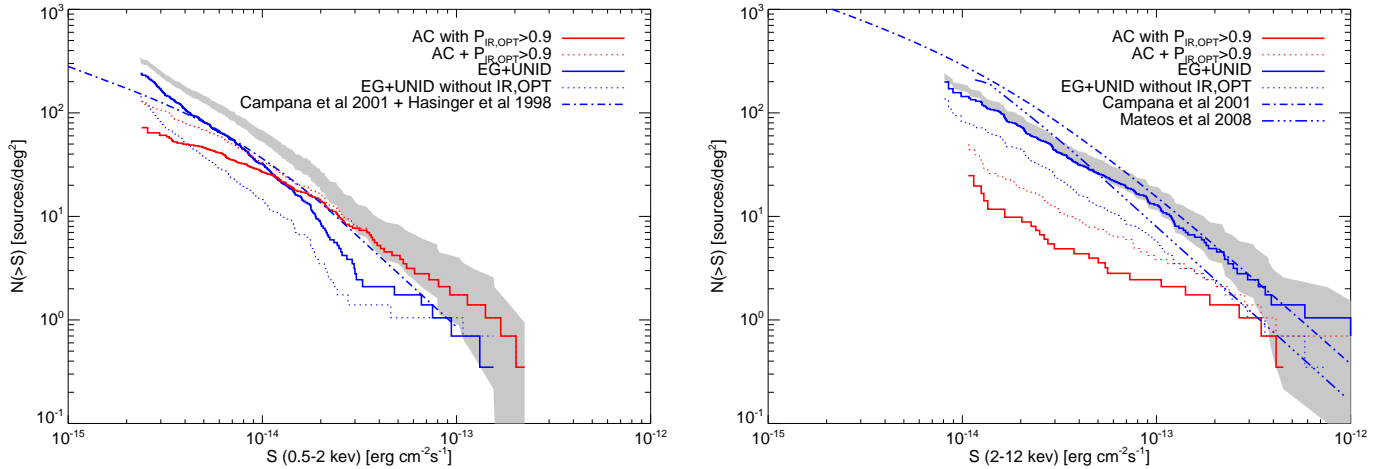


**Fig. 15.**  $\log N(>S) - \log S$  curves in the soft band (0.5–2 keV, left panel) and the hard band (2–12 keV, right panel) for all detected X-ray sources (grey), identified active coronae with  $P_{\text{id}} > 90\%$  (solid red lines) and unidentified plus extragalactic sources (solid blue). Sources either identified as active stars or with  $P_{\text{id}}$  higher than 90% are shown with red dotted lines, and sources either identified as extragalactic or unidentified sources with no infrared and no optical counterpart are shown with blue dotted lines. We show the expected contribution of extragalactic sources from Campana et al. (2001) plus Hasinger et al. (1998) in the soft band, and from Mateos et al. (2008) and Campana et al. (2001) in the hard band.

6% of the sources in the soft band and around 12% of the sources in the hard band.

### 7.3.2. Energy-to-flux conversion factors

To convert count rates into fluxes we calculated energy-to-flux conversion factors using XSPEC. We used the EPIC pn response matrix version 6.7 in full frame mode, for spectra selected from single plus double-pixel events and for on-axis events (epn\_ff20\_sdY9\_v6.7.rmf). We restricted our calculation to the medium filter. For the soft band, since it is dominated by stars, we assumed a thin thermal spectrum, with  $kT = 0.5$  keV absorbed by  $N_H \sim 10^{21} \text{ cm}^{-2}$ , which gives the energy-to-flux conversion factor  $1.75 \times 10^{-12} \text{ erg cm}^{-2} \text{ s}^{-1} / \text{pn counts s}^{-1}$ . We estimate that the difference in soft band energy-to-flux conversion factors introduced by selecting a different filter to the one used during the observations is lower than 2% for the thin filter, while differences up to 23% can be expected for the thick filter. Most of the fields were observed with medium filter, four fields with thin filter (GRB 001025, HT Cas, PKS 0745-19, RX J0925.7-4758), and only one field (Saturn) was observed with thick filter. For the hard band we assumed a power law with photon index equal to 1.7 typical of the AGN population dominating in the hard band. Since the energy-to-flux conversion factors depend on the Galactic absorption, we derived energy-to-flux conversion factors for each field, for the total Galactic absorption along the line of sight, thus assuming that most hard sources are indeed of extragalactic nature. The mean energy-to-flux conversion factor in the hard band is  $\sim 10^{-11} \text{ erg cm}^{-2} \text{ s}^{-1} / \text{pn counts s}^{-1}$ , corresponding to a mean  $N_H$  of  $4.5 \times 10^{22} \text{ cm}^{-2}$ . In the hard band, the choice of a different filter in the computation of the energy-to-flux conversion factors has a smaller impact than in the soft band, with a maximum relative error  $\sim 4\%$  for the thick filter.

### 7.3.3. $\log N(>S) - \log S$

For each source flux we assigned an effective area. We calculated the number of sources above a given flux per unit sky

**Table 7.** Fraction of active coronae.

Galactic latitude	Soft Band [0.5–2 keV]		Hard Band [2–12 keV]		Both Bands	
	$AC^\dagger(\%)$	$opt/ir^\ddagger(\%)$	$AC^\dagger(\%)$	$opt/ir^\ddagger(\%)$	$AC^\dagger(\%)$	$opt/ir^\ddagger(\%)$
$ b  \sim 15^\circ$	15	30	3	26	4	27
$ b  \sim 3^\circ$	34	46	12	18	20	24
$ b  \sim 1^\circ$	39	63	11	23	17	29
$ b  \sim 0^\circ$	58	85	20	31	53	67
All*	$\frac{137}{460}$	$\frac{216}{460}$	$\frac{25}{228}$	$\frac{54}{228}$	$\frac{23}{139}$	$\frac{43}{139}$

Notes:  $^\dagger$  AC are identified active coronae with infrared or optical counterpart with identification probability  $P \geq 90\%$ .  $^\ddagger$  opt/ir are sources that have been either identified as active coronae on the basis of their optical spectra or have an infrared or optical counterpart with  $P \geq 90\%$ , i.e. likely to be Galactic sources. \* number of sources detected in each band.

area,  $N(>S)$ , as the sum of the inverse of the effective areas for sources with fluxes above that value. We excluded a few very faint sources to avoid problems occurring at extreme low effective areas. In Fig. 15 we show the  $\log N(>S) - \log S$  curves in the soft and in the hard energy bands for all the sources in the 18 fields, for spectroscopically identified AC with high identification probability in either optical or infrared catalogues, and for extragalactic plus unidentified sources. In the soft band there is a total of 460 sources, among which 137 are spectroscopically classified as active coronae with an optical and infrared catalogue counterpart with high identification probability. In the hard band there are 228 sources, with 25 sources spectroscopically classified as AC. There are 139 sources in both energy bands, among which 23 are classified as AC. We also show the contribution of two other groups. A first group composed of sources either classified as AC on the basis of their optical spectra (some have  $P_{\text{id}} < 90\%$ ) or with a bright optical and/or infrared catalogue counterpart, which are therefore likely to be stars. The

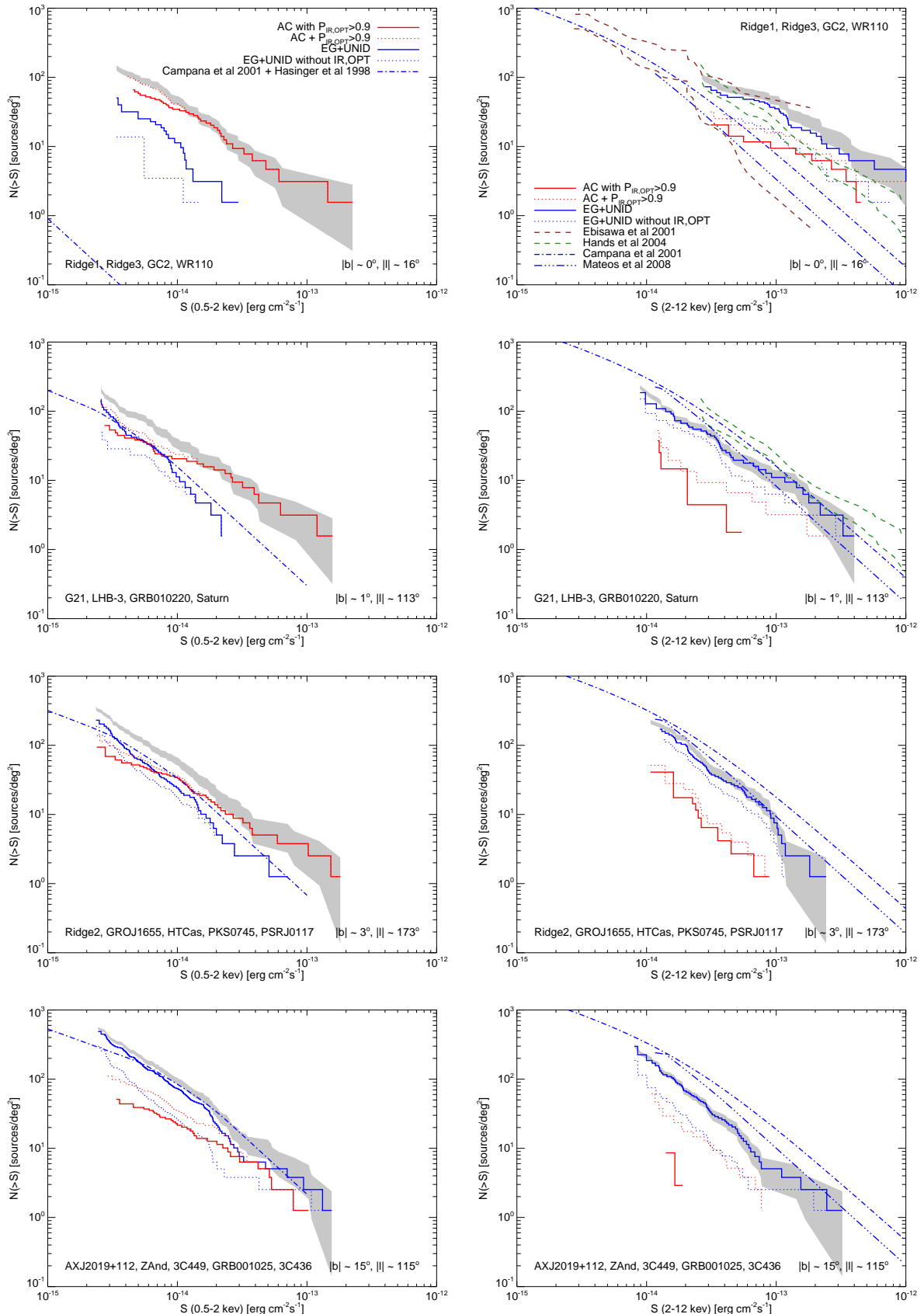


**Fig. 16.**  $\log N(>S)$  –  $\log S$  curves in the soft band (0.5 – 2 keV, left panel) and the hard band (2 – 12 keV, right panel) for all detected X-ray sources (grey), identified active coronae with  $P_{id} > 90\%$  (solid red lines) and unidentified plus extragalactic sources (solid blue lines). Sources either identified as active stars or with  $P_{id} > 90\%$  are shown with red dotted lines, and sources either identified as extragalactic or unidentified sources with no infrared and no optical counterpart are shown with blue dotted lines. We show the expected contribution of extragalactic sources from Campana et al. (2001) plus Hasinger et al. (1998) in the soft band and from Mateos et al. (2008) and Campana et al. (2001) in the hard band. For the lower Galactic latitudes and in the hard band we compare our results with those of Ebisawa et al. (2001) (brown line) and Hands et al. (2004) (green line).

second group is composed of sources either classified as extragalactic objects or without optical nor infrared catalogue counterpart, which are likely to be extragalactic. Stars are dominating the soft band, while extragalactic plus unidentified objects dominate the hard band. With a threshold of 90% in the  $P_{\text{id}}$  we expect the sample to be about 55% complete, so we are missing a large number of the associations, we therefore expect the true fraction of spectroscopically classified sources with counterpart catalogue to be above the one shown in Fig. 15.

The  $\log N(>S) - \log S$  curve in the soft band, after subtraction of the stellar contribution, is steeper than the combined extragalactic contribution from Campana et al. (2001) at low fluxes, based on Chandra Deep Field observations, plus Hasinger et al. (1998) at high fluxes, derived from ROSAT observations in the Lockman Hole<sup>15</sup>. At the faintest fluxes we are subject to Eddington biases, associated with statistical flux variations, likely to introduce a fictitious further steepening of the log  $N(>S) - \log S$ .

Extragalactic  $\log N(>S) - \log S$  curves were corrected for the Galactic absorption in each field and we applied a correction factor to convert fluxes into the appropriate band. The extragalactic  $\log N(>S) - \log S$  from Campana et al. (2001) is based on ASCA and Chandra observations, while the one from Mateos et al. (2008) is based on XMM-Newton observations. Calibration uncertainties between different telescopes/instruments are expected to be lower for the latter, so we expect smaller deviations with our observations than with the former.

In order to understand the contribution of the different populations to the  $\log N(>S) - \log S$  curves we investigated the curves in four different Galactic latitude ranges corresponding to  $|b| \sim 0^\circ, 1^\circ, 3^\circ$ , and  $15^\circ$  (see Fig. 16).

At very low Galactic latitude, the soft band is dominated by stars. The number of stars increases towards lower Galactic latitudes. The fraction of identified stars (classified on the basis of their optical spectra and with  $P_{\text{id}} > 90\%$ ) is 15% at the highest Galactic latitude bin, and increases to 60% at  $|b| \sim 0^\circ$  (see Table 7). On the other hand the number of extragalactic plus unidentified sources increases as we move away from the Galactic Plane. At  $|b| = 15^\circ$  the number of extragalactic plus unidentified sources without optical nor infrared counterpart within the  $3\sigma$  error circle begins to dominate very faint X-ray fluxes ( $< 2 \times 10^{-15} \text{ erg cm}^{-2}\text{s}^{-1}$ ). This is consistent with the fact that  $N_{\text{H}}$  is decreasing with increasing distance to the Galactic Plane, making it easier to detect AGN at soft energies. We are nevertheless aware that at high Galactic latitudes, where  $N_{\text{H}}$  is low, some AGN may be bright enough to give a  $P_{\text{id}} > 90\%$  crossmatch.

The hard band is dominated by extragalactic plus unidentified sources. At high Galactic latitudes hard sources mainly have an extragalactic origin. In the Galactic Plane the number of hard sources is above the expected extragalactic contribution. This excess increases towards the Galactic Centre region. A population of hard spectrum stars is present in all four  $\log N(>S) - \log S$  curves. There are 25 stars detected in the hard band with spectral type known, corresponding to 10% of the detected sources in the hard band. All of them but two are also detected in the soft band. Four hard sources were classified as giant candidates (see Section 6.1): 2XMM 174705.3-280859, 2XMM J180718.4-192454, 2XMM J180736.4-192658, and 2XMM J185139.1+001635. Among the 25 hard active coronae there are two early A stars, two F stars, nine G stars, eight

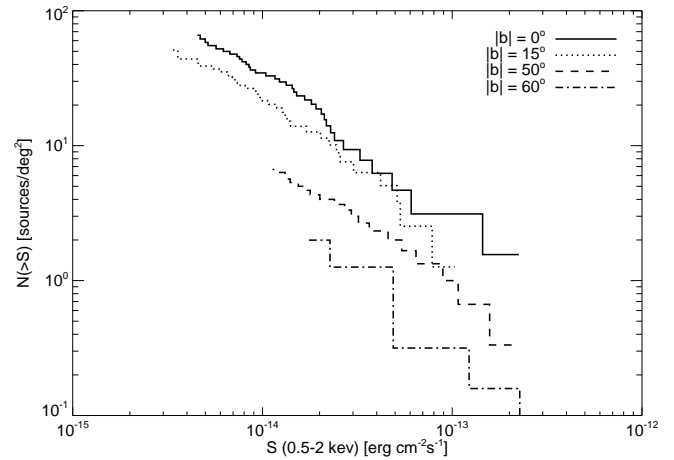


**Fig. 17.**  $\log N(>S) - \log S$  curves in the soft band (0.5–2 keV) for identified active coronae at four Galactic latitudes:  $0^\circ$  and  $15^\circ$  from this paper,  $50^\circ$  and  $60^\circ$  from Barcons et al. (2007) and López-Santiago et al. (2007) respectively.

K stars, and four M stars. With a threshold of  $ML=8$  we expect around 27 spurious detections (see Section 7.3.1) in the hard band. We have computed sensitivity maps, effective areas and  $\log N(>S) - \log S$  curves also for  $ML > 15$  ( $5\sigma$  detection). Thirteen hard sources identified as AC remain at this ML threshold. At this ML cutoff level the expected number of spurious detection in our survey is about one and with an identification probability above 90%, the number of false identifications is expected to be less than five (2% of 228). This is not enough to explain the 13 hard active coronae. We conclude that there is indeed a significant population of hard X-ray emitting active coronae.

#### 7.3.4. Dependence of $\log N(>S) - \log S$ curves on Galactic latitude

As mentioned above, the surface density ( $\log N(>S) - \log S$ ) of soft X-ray emitting stars varies with Galactic latitude. We compared our results with those found by Barcons et al. (2007) and by López-Santiago et al. (2007) based on XMM-Newton observations of high Galactic latitude fields, with mean Galactic latitudes of  $\sim 50^\circ$  and  $\sim 60^\circ$  respectively. We found that the number of sources per square degree varies steeply with Galactic latitude (see Fig. 17), increasing by an order of magnitude from  $b = 60^\circ$  at  $b = 0^\circ$  for fluxes above  $\sim 2 \times 10^{-13} \text{ erg cm}^{-2}\text{s}^{-1}$ .

We fitted these  $\log N(>S) - \log S$  curves with a power-law function of the type  $N(> S) = KS^{-\alpha}$  using a maximum likelihood technique (Crawford et al. 1970; Murdoch et al. 1973). We obtained a maximum likelihood for the following slopes of the curves:

$$\begin{aligned} b \sim 0^\circ, \quad \alpha &= 1.05 \pm 0.25 \\ b \sim 15^\circ, \quad \alpha &= 0.76 \pm 0.21 \\ b \sim 50^\circ, \quad \alpha &= 0.65 \pm 0.16 \end{aligned} \quad (2)$$

A Kolmogorov-Smirnov test (KS-test) allowed us to validate the power-law model. Due to the low number of sources in the highest Galactic latitude  $\log N(>S) - \log S$  curve ( $b = 60^\circ$ ) we only performed a fit to the other three curves. We restricted to fluxes in the range  $10^{-14} - 2 \times 10^{-13} \text{ erg cm}^{-2}\text{s}^{-1}$ . The slope of the

<sup>15</sup> To compare with other publications, we applied a correction factor to convert fluxes from one band to another using PIMMS.

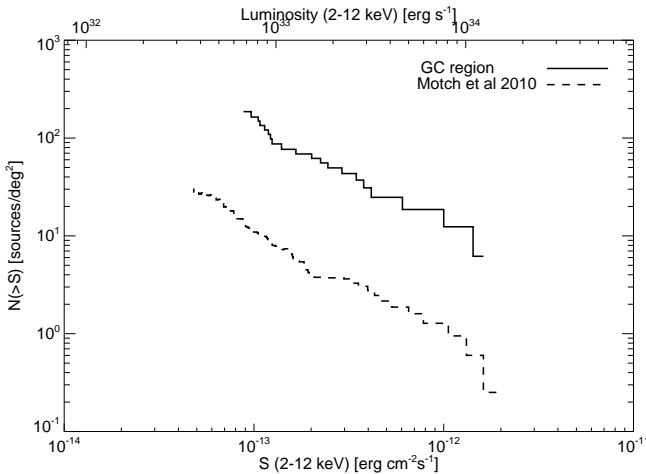


**Fig. 18.**  $\log N(>S)$  –  $\log S$  curves in the Galactic Centre region for the hard band (2–12 keV) corrected from the extragalactic contribution and compared with the results from Motch et al. (2010) based on the XGPS sample from Hands et al. (2004) at  $l \sim 20^\circ$ .

power-law varies with Galactic latitude, effect that is observed in X-ray models of the Galaxy (Guillout et al. 1996), and which is due to the scale height of stars and the relative contribution of the different populations. At low Galactic latitudes, looking directly to the Galactic Plane, the number of stars steadily increases with decreasing limiting fluxes. On the contrary, at high Galactic latitudes, the number of sources is truncated due to the finite scale-height of stars. Young stars have smaller scale-height than old stars, therefore at low Galactic latitudes we are dominated by the young population over the whole range of observed fluxes, while at high Galactic latitudes we are dominated by young stars at high fluxes ( $\geq 10^{-13}$  erg s $^{-1}$  in the 0.5–2 keV band) and by old stars at fainter fluxes (Guillout et al. 1996). Hence, the variation of the  $\log N(>S)$  –  $\log S$  with Galactic latitude reflects an age-scale height dependence.

### 7.3.5. The Galactic Centre region

We clearly detect an excess of hard sources compared to the expected extragalactic contribution (see Section 7.3.3), the excess mainly coming from the Galactic Centre region (field GC2 in Table 1). We subtracted the extragalactic contribution from Mateos et al. (2008) from the total  $\log N(>S)$  –  $\log S$  and compared our results with those from Motch et al. (2010) based on the XGPS sample from Hands et al. (2004) at ( $l \sim 20^\circ$ ,  $b = 0^\circ$ ). We found that the Galactic surface density of hard sources in the Galactic Centre region ( $l = 0.9^\circ$ ,  $b = 0^\circ$ ) is larger than at ( $l = 20^\circ$ ,  $b = 0^\circ$ ) by approximately a factor of ten, reaching a density of about 100 sources/deg $^2$  at a flux of  $\sim 10^{-13}$  erg cm $^{-2}$ s $^{-1}$  (see Fig. 18), but lower than at the Galactic Centre (Muno et al. 2003). This is consistent with the results from Muno et al. (2009) based on Chandra observations in the  $3^\circ$  around Sgr A\*, and with the results from Hong et al. (2009) also based on Chandra observations in the Galactic Bulge.

The increase of hard sources towards the Galactic Centre region might be associated with the Galactic Centre itself. If so, assuming a distance to the Galactic Centre of 8 kpc, the obtained range of luminosities is  $10^{33} - 10^{34}$  erg s $^{-1}$ . It has been proposed

that this concentration of sources is mainly due to an old population of CVs and a minor contribution of a young population of HMXBs at low mass transfer (Muno et al. 2003; Laycock et al. 2005).

## 8. Discussion and Conclusions

We carried out optical spectroscopic follow-up observations of X-ray sources detected in 26 fields by XMM-Newton, at low and intermediate Galactic latitudes, distributed over a broad range in Galactic longitudes and covering a total area of 4 deg $^2$ . Our X-ray survey has a limiting X-ray flux of about  $2 \times 10^{-15}$  erg cm $^{-2}$ s $^{-1}$  and  $1 \times 10^{-14}$  erg cm $^{-2}$ s $^{-1}$  in the 0.5–2 keV and in the 2–12 keV energy bands respectively. A total of 1319 sources have an entry in the 2XMMi-DR3 catalogue. We cross-matched these X-ray sources with the SDSS-DR7, the GSC 2.3, the USNO-B1.0 and the 2MASS catalogues, finding matches for about 50% of the sources. Twenty per cent of the matches are above a 90% identification probability in at least one of the catalogues. At this threshold the number of spurious associations is expected to be less than 2%, and the survey is about 50% complete. Using our follow-up optical spectroscopic observations in combination with cross-correlation with a large range of archival catalogues we classified 316 X-ray sources. The XMM-Newton SSC survey of the Galactic Plane constitutes the largest sample of Galactic spectroscopically identified X-ray sources in this range of X-ray flux and Galactic latitudes.

In the soft band (0.5–2 keV), the majority of the sources are positively identified as stars with spectral types in the range A–M. The number of detected X-ray emitting active corona increases with decreasing effective temperatures and presents an excess of G–K stars. Such a repartition in spectral types is similar to that observed in magnitude and X-ray flux limited samples extracted from the ROSAT all-sky survey at a factor 10 brighter X-ray flux (Motch et al. 1997). Making use of infrared colours we classify 23 stars as evolved giant candidates, being most of them K stars, and representing 18.4 % of the sources with 2MASS counterpart and with individual probability higher than 90%. Since giant stars are not expected to be strong X-ray emitters (Maggio et al. 1990), to maintain their X-ray luminosities with age the most likely scenario is that these stars are RS CVn, i.e. synchronised evolved binaries, where the rotation of stars has not spun-down with age.

A handful of likely pre main sequence stars, T Tauri and Herbig Ae objects are also identified spectroscopically. One of the T Tauri candidates appears far away from any known star forming region.

The measured stellar F<sub>x</sub>/F<sub>v</sub>, X-ray and infrared colours are consistent with expected values for young (100 Myr) to intermediate age (600 Myr) active coronae with a small contribution of BY Dra and RS CVn like binaries. We find that the number of stars per square degree ( $\log N(>S)$  –  $\log S$ ) depends on the Galactic latitude, steadily increasing by one order of magnitude from  $b \sim 60^\circ$  to  $b = 0^\circ$ . X-ray stellar population modelling shows that this increase is due to a combination of age-X-ray luminosity and age-scale height dependencies (Guillout et al. 1996). Since we detect and identify active coronae up to about distances of 1 kpc, we can clearly witness the effect caused by the higher concentration of young and X-ray luminous stars at low Galactic latitudes.

The overall distribution of X-ray detected stellar coronae in spectral types, X-ray spectra, flux and Galactic latitude contains important imprinted information on the local density, star formation rate of up to 2Gyr old stars and on the evolution with

age of the X-ray luminosity, X-ray temperature and of the scale height. In a second paper, we will use X-ray stellar population modelling to constrain these stellar population parameters.

In the hard band (2–12 keV), most of the sources are consistent with an extragalactic nature. We identify, however, a genuine Galactic population of hard sources which accounts for 11% of the detected hard sources. Among identified hard X-ray sources are some of the X-ray stars exhibiting the highest X-ray temperatures and therefore the highest X-ray luminosities. A small fraction of CVs also contributes to the galactic hard X-ray population. We report the discovery of four new  $\gamma$ -Cas analogs which assuming a typical X-ray temperature above  $\sim 7$  keV, are conspicuous hard X-ray sources with (0.2–12 keV) X-ray luminosities of a few  $10^{32}$  erg s $^{-1}$ . The equivalent widths of their H $\alpha$  emission line also spans a small range ( $\sim 30$  Å), typical of these objects. One of the candidates is a very faint  $R \sim 22$  highly reddened object. Although the number of  $\gamma$ -Cas objects still remains small, they appear to dominate by number the population of X-ray bright massive stars detected in the Galaxy. The mechanism giving rise to the X-ray emission of  $\gamma$ -Cas analogs remains unknown. Interestingly, one of the candidates found in our survey is the brightest star (star 9) in the NGC 6649 cluster and a blue straggler (Marco et al. 2007).

After removing the expected extragalactic contribution, we find that the population of Galactic hard sources, increases by a factor of ten from  $l = 20^\circ$  to  $l = 0.9^\circ$ , reaching a surface density of about 100 sources deg $^{-2}$  at a flux of  $\sim 1.3 \times 10^{-13}$  erg cm $^{-2}$ s $^{-1}$ , i.e. 10 $^{33}$  erg s $^{-1}$  at a distance of 8 kpc. We emphasize, however, that, at the exception of one of the  $\gamma$ -Cas analog candidate, 2XMM J180816.6-191939 which has an estimated distance of 6–7 kpc, all other identified hard X-ray sources, stars and CVs are within a range of 1 or 2 kpc. It is therefore unclear whether the local population we identify in this work is truly representative of the nature of the sources detected towards the Galactic Centre regions.

**Acknowledgements.** The XMM-Newton SSC acknowledges sustained financial support from CNES (France) and from Deutches Zentrum für Luft und Raumfahrt (Germany) DLR, under grant numbers FKZ 50 OX 0201 and 50 OX 0801. This research has made use of the SIMBAD database, operated at CDS, Strasbourg, France. This publication makes use of data products from the Two Micron All Sky Survey, which is a joint project of the University of Massachusetts and the Infrared Processing and Analysis Center/California Institute of Technology, funded by the National Aeronautics and Space Administration and the National Science Foundation. This research has made use of the USNO Image and Catalogue Archive operated by the United States Naval Observatory, Flagstaff Station (<http://www.nofs.navy.mil/data/fchpix/>). The Guide Star Catalogue-II is a joint project of the Space Telescope Science Institute and the Osservatorio Astronomico di Torino. Space Telescope Science Institute is operated by the Association of Universities for Research in Astronomy, for the National Aeronautics and Space Administration under contract NAS5-26555. The participation of the Osservatorio Astronomico di Torino is supported by the Italian Council for Research in Astronomy. Additional support is provided by European Southern Observatory, Space Telescope European Coordinating Facility, the International GEMINI project and the European Space Agency Astrophysics Division. Funding for the SDSS and SDSS-II has been provided by the Alfred P. Sloan Foundation, the Participating Institutions, the National Science Foundation, the U.S. Department of Energy, the National Aeronautics and Space Administration, the Japanese Monbukagakusho, the Max Planck Society, and the Higher Education Funding Council for England. The SDSS Web Site is <http://www.sdss.org/>. This publication makes use of data products from the Wide-field Infrared Survey Explorer, which is a joint project of the University of California, Los Angeles, and the Jet Propulsion Laboratory/California Institute of Technology, funded by the National Aeronautics and Space Administration.

## References

- Abazajian, K. N., Adelman-McCarthy, J. K., Agüeros, M. A., et al. 2009, ApJS, 182, 543
- Appenzeller, I. & Mundt, R. 1989, A&A Rev., 1, 291
- Barbera, M., Micela, G., Sciortino, S., Harnden, Jr., F. R., & Rosner, R. 1993, ApJ, 414, 846
- Barcons, X., Carrera, F. J., Ceballos, M. T., et al. 2007, A&A, 476, 1191
- Barcons, X., Carrera, F. J., Watson, M. G., et al. 2002, A&A, 382, 522
- Barrado y Navascués, D. & Martín, E. L. 2003, AJ, 126, 2997
- Bertout, C. 1989, ARA&A, 27, 351
- Bertout, C. & Genova, F. 2006, A&A, 460, 499
- Bessell, M. S. & Brett, J. M. 1988, PASP, 100, 1134
- Campana, S., Moretti, A., Lazzati, D., & Tagliaferri, G. 2001, ApJ, 560, L19
- Carpenter, J. M. 2001, AJ, 121, 2851
- Carrera, F. J., Ebrero, J., Mateos, S., et al. 2007, A&A, 469, 27
- Castelli, F. & Kurucz, R. L. 2004, ArXiv Astrophysics e-prints
- Cohen, D. H. 2000, in Astronomical Society of the Pacific Conference Series, Vol. 214, IAU Colloq. 175: The Be Phenomenon in Early-Type Stars, ed. M. A. Smith, H. F. Henrichs, & J. Fabregat, 156
- Cohen, D. H., Cassinelli, J. P., & Macfarlane, J. J. 1997, ApJ, 487, 867
- Covey, K. R., Agüeros, M. A., Green, P. J., et al. 2008, ApJS, 178, 339
- Covey, K. R., Ivezić, Ž., Schlegel, D., et al. 2007, AJ, 134, 2398
- Crawford, D. F., Jauncey, D. L., & Murdoch, H. S. 1970, ApJ, 162, 405
- Cutri, R. M., Skrutskie, M. F., van Dyk, S., et al. 2003, 2MASS All Sky Catalog of point sources., ed. Cutri, R. M., Skrutskie, M. F., van Dyk, S., Beichman, C. A., Carpenter, J. M., Chester, T., Cambresy, L., Evans, T., Fowler, J., Gizis, J., Howard, E., Huchra, J., Jarrett, T., Kopan, E. L., Kirkpatrick, J. D., Light, R. M., Marsh, K. A., McCallon, H., Schneider, S., Stiening, R., Sykes, M., Weinberg, M., Wheaton, W. A., Wheelock, S., & Zacarias, N.
- Cutri, R. M., Wright, E. L., Conrow, T., et al. 2012, Explanatory Supplement to the WISE All-Sky Data Release Products, Tech. rep.
- De Rosa, R. J., Bulger, J., Patience, J., et al. 2011, MNRAS, 415, 854
- Della Ceca, R., Maccacaro, T., Caccianiga, A., et al. 2004, A&A, 428, 383
- Dempsey, R. C., Linsky, J. L., Fleming, T. A., & Schmitt, J. H. M. M. 1997, ApJ, 478, 358
- Dempsey, R. C., Linsky, J. L., Schmitt, J. H. M. M., & Fleming, T. A. 1993, ApJ, 413, 333
- den Herder, J. W., Brinkman, A. C., Kahn, S. M., et al. 2001, A&A, 365, L7
- Ebisawa, K., Maeda, Y., Kaneda, H., & Yamauchi, S. 2001, Science, 293, 1633
- Ebisawa, K., Tsujimoto, M., Paizis, A., et al. 2005, ApJ, 635, 214
- Fang, M., van Boekel, R., Wang, W., et al. 2009, A&A, 504, 461
- Favata, F., Sciortino, S., Rosner, R., & Vaiana, G. S. 1988, ApJ, 324, 1010
- Feigelson, E. D. 1996, ApJ, 468, 306
- Fleming, T. A., Gioia, I. M., & Maccacaro, T. 1989, ApJ, 340, 1011
- Frasca, A., Guillout, P., Marilli, E., et al. 2006, A&A, 454, 301
- Gagné, M., Fehon, G., Savoy, M. R., et al. 2011, ApJS, 194, 5
- Gänsicke, B. T., Dillon, M., Southworth, J., et al. 2009, MNRAS, 397, 2170
- Giacconi, R., Branduardi, G., Briel, U., et al. 1979, ApJ, 230, 540
- Gilfanov, M. 2004, MNRAS, 349, 146
- Grimm, H.-J., Gilfanov, M., & Sunyaev, R. 2002, A&A, 391, 923
- Grindlay, J. E., Hong, J., Zhao, P., et al. 2005, ApJ, 635, 920
- Güdel, M. & Nazé, Y. 2009, A&A Rev., 17, 309
- Guedel, M., Guinan, E. F., & Skinner, S. L. 1997, ApJ, 483, 947
- Guillout, P., Frasca, A., Klutsch, A., Marilli, E., & Montes, D. 2010, A&A, 520, A94
- Guillout, P., Haywood, M., Motch, C., & Robin, A. C. 1996, A&A, 316, 89
- Guillout, P., Schmitt, J. H. M. M., Egret, D., et al. 1999, A&A, 351, 1003
- Guillout, P., Sterzik, M. F., Schmitt, J. H. M. M., Motch, C., & Neuhaeuser, R. 1998, A&A, 337, 113
- Hands, A. D. P., Warwick, R. S., Watson, M. G., & Helfand, D. J. 2004, MNRAS, 351, 31
- Hasinger, G., Burg, R., Giacconi, R., et al. 1998, A&A, 329, 482
- Herbig, G. H. 1960, ApJS, 4, 337
- Hernández, J., Calvet, N., Hartmann, L., et al. 2005, AJ, 129, 856
- Hertz, P. & Grindlay, J. E. 1984, ApJ, 278, 137
- Hong, J. 2012, MNRAS, 427, 1633
- Hong, J., van den Berg, M., Grindlay, J. E., Servillat, M., & Zhao, P. 2012, ApJ, 746, 165
- Hong, J. S., van den Berg, M., Grindlay, J. E., & Laycock, S. 2009, ApJ, 706, 223
- Jackson, A. P., Davis, T. A., & Wheatley, P. J. 2012, MNRAS, 422, 2024
- Jacoby, G. H., Hunter, D. A., & Christian, C. A. 1984, ApJS, 56, 257
- Jansen, F., Lumb, D., Altieri, B., et al. 2001, A&A, 365, L1
- Joy, A. H. 1945, ApJ, 102, 168
- Kahabka, P., Haberl, F., Payne, J. L., & Filipović, M. D. 2006, A&A, 458, 285
- Kawaler, S. D. 1988, ApJ, 333, 236
- Koenig, X., Grindlay, J. E., van den Berg, M., et al. 2008, ApJ, 685, 463
- Kogure, T. 2009, in Astronomical Society of the Pacific Conference Series, Vol. 404, The Eighth Pacific Rim Conference on Stellar Astrophysics: A Tribute to Kam-Ching Leung, ed. S. J. Murphy & M. S. Bessell, 212
- Lasker, B. M., Lattanzi, M. G., McLean, B. J., et al. 2008, AJ, 136, 735

- Laycock, S., Grindlay, J., van den Berg, M., et al. 2005, ApJ, 634, L53  
 Le Borgne, J.-F., Bruzual, G., Pelló, R., et al. 2003, A&A, 402, 433  
 Lopes de Oliveira, R. & Motch, C. 2011, ApJ, 731, L6  
 Lopes de Oliveira, R., Motch, C., Smith, M. A., Negueruela, I., & Torrejón, J. M. 2007, A&A, 474, 983  
 Lopes de Oliveira, R., Smith, M. A., & Motch, C. 2010, A&A, 512, A22  
 López-Santiago, J., Micela, G., Sciortino, S., et al. 2007, A&A, 463, 165  
 Maccacaro, T., Gioia, I. M., Wolter, A., Zamorani, G., & Stocke, J. T. 1988, ApJ, 326, 680  
 Maggio, A., Vaiana, G. S., Haisch, B. M., et al. 1990, ApJ, 348, 253  
 Malfait, K., Bogaert, E., & Waelkens, C. 1998, A&A, 331, 211  
 Marco, A., Negueruela, I., & Motch, C. 2007, in Astronomical Society of the Pacific Conference Series, Vol. 367, Massive Stars in Interactive Binaries, ed. N. St.-Louis & A. F. J. Moffat, 645  
 Marshall, D. J., Robin, A. C., Reylé, C., Schultheis, M., & Picaud, S. 2006, A&A, 453, 635  
 Mateos, S., Warwick, R. S., Carrera, F. J., et al. 2008, A&A, 492, 51  
 Mathis, J. S. 1990, ARA&A, 28, 37  
 Matt, S. P., MacGregor, K. B., Pinsonneault, M. H., & Greene, T. P. 2012, ApJ, 754, L26  
 Meeus, G., Waelkens, C., & Malfait, K. 1998, A&A, 329, 131  
 Meeus, G., Waters, L. B. F. M., Bouwman, J., et al. 2001, A&A, 365, 476  
 Meyer, M. R., Calvet, N., & Hillenbrand, L. A. 1997, AJ, 114, 288  
 Micela, G., Sciortino, S., Kashyap, V., Harnden, Jr., F. R., & Rosner, R. 1996, ApJS, 102, 75  
 Micela, G., Sciortino, S., Vaiana, G. S., et al. 1988, ApJ, 325, 798  
 Michel, L., Herent, O., Motch, C., Pye, J., & Watson, M. G. 2004, in Astronomical Society of the Pacific Conference Series, Vol. 314, Astronomical Data Analysis Software and Systems (ADASS) XIII, ed. F. Ochsenbein, M. G. Allen, & D. Egret, 570  
 Monet, D. G., Levine, S. E., Canzian, B., et al. 2003, AJ, 125, 984  
 Morley, J. E., Briggs, K. R., Pye, J. P., et al. 2001, MNRAS, 326, 1161  
 Motch, C. 2006, in ESA Special Publication, Vol. 604, The X-ray Universe 2005, ed. A. Wilson, 383  
 Motch, C., Guillout, P., Haberl, F., et al. 1997, A&A, 318, 111  
 Motch, C., Herent, O., & Guillout, P. 2003, Astronomische Nachrichten, 324, 61  
 Motch, C., Lopes de Oliveira, R., Negueruela, I., Haberl, F., & Janot-Pacheco, E. 2007, in Astronomical Society of the Pacific Conference Series, Vol. 361, Active OB-Stars: Laboratories for Stellare and Circumstellar Physics, ed. A. T. Okazaki, S. P. Owocki, & S. Stefl, 117  
 Motch, C. & Pakull, M. W. 2012, Mem. Soc. Astron. Italiana, 83, 415  
 Motch, C., Warwick, R., Cropper, M. S., et al. 2010, A&A, 523, A92  
 Munoz, M. P., Baganoff, F. K., Bautz, M. W., et al. 2003, ApJ, 589, 225  
 Munoz, M. P., Bauer, F. E., Baganoff, F. K., et al. 2009, ApJS, 181, 110  
 Murdoch, H. S., Crawford, D. F., & Jauncey, D. L. 1973, ApJ, 183, 1  
 Okazaki, A. T. & Negueruela, I. 2001, in Astronomical Society of the Pacific Conference Series, Vol. 234, X-ray Astronomy 2000, ed. R. Giacconi, S. Serio, & L. Stella, 281  
 Pallavicini, R., Golub, L., Rosner, R., et al. 1981, ApJ, 248, 279  
 Patterson, J. 1984, ApJS, 54, 443  
 Pfahl, E., Rappaport, S., & Podsiadlowski, P. 2002, ApJ, 571, L37  
 Pickles, A. J. 1998, PASP, 110, 863  
 Pineau, F.-X., Derriere, S., Michel, L., & Motch, C. 2008, in Astronomical Society of the Pacific Conference Series, Vol. 394, Astronomical Data Analysis Software and Systems XVII, ed. R. W. Argyle, P. S. Bunclark, & J. R. Lewis, 369  
 Pineau, F.-X., Derriere, S., Michel, L., & Motch, C. 2010, in Astronomical Society of the Pacific Conference Series, Vol. 434, Astronomical Data Analysis Software and Systems XIX, ed. Y. Mizumoto, K.-I. Morita, & M. Ohishi, 369  
 Pineau, F.-X., Motch, C., Carrera, F., et al. 2011, A&A, 527, A126  
 Pires, A. M., Motch, C., & Janot-Pacheco, E. 2009, A&A, 504, 185  
 Predehl, P. & Schmitt, J. H. M. M. 1995, A&A, 293, 889  
 Pretorius, M. L. & Knigge, C. 2012, MNRAS, 419, 1442  
 Raguzova, N. V. 2001, A&A, 367, 848  
 Raharto, M., Hamajima, K., Ichikawa, T., Ishida, K., & Hidayat, B. 1984, Annals of the Tokyo Astronomical Observatory, 19, 469  
 Reig, P. 2011, Ap&SS, 332, 1  
 Ritter, H. & Kolb, U. 2003, A&A, 404, 301  
 Savage, B. D. & Mathis, J. S. 1979, ARA&A, 17, 73  
 Sazonov, S., Revnivtsev, M., Gilfanov, M., Churazov, E., & Sunyaev, R. 2006, A&A, 450, 117  
 Schlegel, D. J., Finkbeiner, D. P., & Davis, M. 1998, ApJ, 500, 525  
 Schmitt, J. H. M. M. & Liefke, C. 2004, A&A, 417, 651  
 Schrijver, C. J. 1987, A&A, 172, 111  
 Sciortino, S., Favata, F., & Micela, G. 1995, A&A, 296, 370  
 Sidoli, L., Mereghetti, S., Favata, F., Oosterbroek, T., & Parmar, A. N. 2006, A&A, 456, 287  
 Siess, L., Dufour, E., & Forestini, M. 2000, A&A, 358, 593  
 Skinner, S. L., Zhekov, S. A., Güdel, M., Schmutz, W., & Sokal, K. R. 2010, AJ, 139, 825  
 Stelzer, B., Micela, G., Hamaguchi, K., & Schmitt, J. H. M. M. 2006, A&A, 457, 223  
 Stern, R. A., Schmitt, J. H. M. M., & Kahabka, P. T. 1995, ApJ, 448, 683  
 Strüder, L., Briel, U., Dennerl, K., et al. 2001, A&A, 365, L18  
 Sturm, R., Haberl, F., Pietsch, W., et al. 2012, A&A, 537, A76  
 Sugizaki, M., Mitsuda, K., Kaneda, H., et al. 2001, ApJS, 134, 77  
 Tanaka, Y., Inoue, H., & Holt, S. S. 1994, PASJ, 46, L37  
 Tauris, T. M. & van den Heuvel, E. P. J. 2006, Formation and evolution of compact stellar X-ray sources, ed. W. H. G. Lewin & M. van der Klis, 623–665  
 Trümper, J. 1982, Advances in Space Research, 2, 241  
 Turner, D. G. 1981, AJ, 86, 231  
 Turner, M. J. L., Abbey, A., Arnaud, M., et al. 2001, A&A, 365, L27  
 van den Berg, M., Penner, K., Hong, J., et al. 2012, ApJ, 748, 31  
 Walker, A. R. & Laney, C. D. 1987, MNRAS, 224, 61  
 Walter, R., Courvoisier, T. J.-L., Foschini, L., et al. 2004, in ESA Special Publication, Vol. 552, 5th INTEGRAL Workshop on the INTEGRAL Universe, ed. V. Schoenfeld, G. Lichten, & C. Winkler, 417–422  
 Warner, B. 1995, Cataclysmic Variable Stars, ed. C. Cambridge Univ. Press, 1–100  
 Warwick, R. S., Pérez-Ramírez, D., & Byckling, K. 2011, MNRAS, 413, 595  
 Watson, M. G., Auguères, J.-L., Ballet, J., et al. 2001, A&A, 365, L51  
 Watson, M. G., Schröder, A. C., Fyfe, D., et al. 2009, A&A, 493, 339  
 Weisskopf, M. C., Brinkman, B., Canizares, C., et al. 2002, PASP, 114, 1  
 Willems, B. & Kolb, U. 2003, MNRAS, 343, 949  
 Wright, N. J., Drake, J. J., & Civano, F. 2010, ApJ, 725, 480  
 Zickgraf, F.-J., Krautter, J., Reffert, S., et al. 2005, A&A, 433, 151  
 Zinnecker, H. & Preibisch, T. 1994, A&A, 292, 152

**Table 8.** X-ray parameters for detected sources in field 3C449

2XMM Name	$r_{90}$ [""]	$\text{pn\_B1}^*$ [cts $\text{ks}^{-1}$ ]	$\text{pn\_B2}^{**}$ [cts $\text{ks}^{-1}$ ]	2MASS Name	$d_{x-o}$ [""]	$P_{id}$	kmag	GSC Name	$d_{x-o}$ [""]	$P_{id}$	V	USNO Name	$d_{x-o}$ [""]	$P_{id}$	R	Class <sup>†</sup>	SpT <sup>‡</sup>
J223010.5+391803	2.37							N2XK037841	5.4	0.07	1293-0507754	5.5	0.27	19.71			
J223016.2+392502	0.58	$30.0 \pm 2.3$	$3.0 \pm 1.2$	22301621+3925017	0.7	0.51	11.59	N2YH001089	0.3	1.00	14.34	1294-0502068	0.2	1.00	14.37	Star	M2Ve <sup>sp</sup>
J223021.2+392253	1.01	$6.6 \pm 1.1$	$1.2 \pm 0.8$	22302116+3922519	1.3	0.98	12.64	N2XM009117	1.3	0.98		1293-0507828	1.3	0.98	15.29	Star	K7Ve <sup>sp</sup>
J223032.9+392555	1.70	$4.4 \pm 1.2$	$0.9 \pm 1.1$	22303305+3925546	2.1	0.84	14.65	N2XM010425	2.1	0.91		1294-0502199	1.9	0.94	15.73	Star	
J223036.1+392139	0.44	$58.6 \pm 2.5$	$0.5 \pm 0.4$	22303611+3921392	0.7	1.00	8.10	N2XM008981	0.6	0.50	9.27	1293-0507963	0.6	1.00	8.99	Star	F8III <sup>s</sup>
J223039.3+391940	1.83	$2.0 \pm 0.6$	$0.7 \pm 0.5$					N2XN036915	3.9	0.30		1293-0507995	3.8	0.50	19.37		
J223041.5+391733	3.19	$6.3 \pm 1.3$	$1.8 \pm 1.1$												EG	Gal <sup>s</sup>	
J223043.7+392257	1.27	$2.4 \pm 0.6$		22304371+3922579	0.2	1.00	7.68	N2XM001445	0.1	1.00	10.40	1293-0508029	0.1	1.00	9.71	Star	K1III <sup>sp</sup>
J223050.8+393323	2.08	$2.6 \pm 0.9$	$2.1 \pm 1.5$					N2YH001423	4.3	0.26		1295-0508481	3.9	0.53	19.64		
J223057.6+392143	1.79	$0.3 \pm 0.4$	$0.1 \pm 0.2$					N2XM030986	3.1	0.30		1293-0508125	3.3	0.44	19.70		
J223102.1+391838	0.53	$19.3 \pm 1.4$	$1.4 \pm 0.5$	22310213+3918391	0.5	1.00	12.14	N2XN025009	0.5	1.00		1293-0508160	0.5	1.00	15.09	Star	M0Ve <sup>sp</sup>
J223122.8+390914	1.93	$3.4 \pm 1.1$	$0.3 \pm 0.8$	22312286+3909137	0.7	0.99	10.92	N2XN000071	0.8	0.99	13.35	1291-0499913	0.6	0.99	12.99	TTS	K0Ve <sup>sp</sup>
J223123.5+393558	1.96	$10.7 \pm 1.8$	$3.9 \pm 1.4$												EG	AGN <sup>sp</sup>	
J223125.0+391914	0.57	$10.8 \pm 1.1$	$4.9 \pm 0.7$					N2XM007512	0.3	0.98		1293-0508332	0.2	0.98	18.90		
J223128.5+391051	1.42	$6.9 \pm 2.4$	$3.2 \pm 1.9$	22312847+3910520	1.3	0.93	14.76	N2XN024216	1.0	0.95		1291-0499944	1.4	0.94	16.54	Star	K4V <sup>sp</sup>
J223132.5+392458	1.99	$3.1 \pm 0.8$	$0.8 \pm 0.5$	22313239+3924583	1.8	0.93	14.20	N2XM009995	1.7	0.96		1294-0502686	1.7	0.96	14.99	Star	G0V <sup>sp</sup>
J223133.0+391419	1.35	$3.2 \pm 0.8$	$0.4 \pm 0.4$	22313317+3914201	1.7	1.00	9.28	N2XN000041	1.6	1.00	11.52	1292-0502438	1.6	1.00	10.46	Star	K1V <sup>sp</sup>
J223140.5+391539	1.24	$3.0 \pm 0.7$	$0.4 \pm 0.4$					N2XN024784	2.6	0.62		1292-0502476	1.0	0.90	19.51		
J223150.1+392521	1.06	$7.5 \pm 1.2$	$1.8 \pm 0.9$	22315026+3925219	0.9	1.00	11.99	N2XM001392	1.0	1.00	13.59	1294-0502796	1.0	1.00	13.67	Star	K0V <sup>sp</sup>
J223200.3+393127	1.36	$10.9 \pm 2.9$	$1.0 \pm 2.0$					N2XM012497	1.3	0.84		1295-0508917	1.7	0.81	19.73	Star	G2V <sup>sp</sup>
J223204.0+391435	1.85	$1.4 \pm 0.6$	$1.0 \pm 0.6$												EG	AGN <sup>sp</sup>	
J223204.0+392611	1.42	$5.0 \pm 1.0$	$0.4 \pm 0.6$	22320392+3926125	1.5	0.99	12.14	N2XM001365	1.6	0.99	13.28	1294-0502893	1.6	0.99	12.84	Star	G0V <sup>sp</sup>
J223204.3+390922	1.48							N2XN024017	4.8	0.04		1291-0500156	5.1	0.04	19.11		
J223218.1+393006	1.63	$5.6 \pm 1.3$	$2.6 \pm 1.5$					N2XM011980	2.0	0.77		1295-0509013	1.7	0.79	19.70		
J223221.1+393013	1.58	$6.4 \pm 1.4$	$3.4 \pm 1.7$					N2XM012033	3.0	0.57		1295-0509027	3.1	0.59	19.42		
J223227.3+391355	0.75	$45.4 \pm 3.3$	$19.4 \pm 3.0$					N2XM005797	2.4	0.36		1292-0502768	2.2	0.47	18.29	EG	
J223238.4+392409	2.61	$3.3 \pm 1.1$	$1.3 \pm 1.0$					N2XM031494	2.5	0.35		1294-0503147	3.8	0.39	19.34		

**Notes.** \* Count rate in the energy band 0.5–2.5 keV. \*\* Count rate in the energy band 2–12 keV. <sup>†</sup> Class stands for the type of source. Classification can be *Star* for active coronae, *EG* for extragalactic sources, *CV* for cataclysmic variables, *TTS* for T Tauri stars, or *HMXB* for high mass X-ray binaries. The luminosity class corresponds to that derived in Section 6.1. <sup>‡</sup> Spectral type including information on how the source was identified, <sup>sp</sup> stands for spectroscopic identified sources, <sup>s</sup> for objects with SIMBAD identification, and <sup>im</sup> for sources found to be extended in the optical images.

**Table 9.** X-ray parameters for detected sources in field 3C436

2XMM Name	$r_{90}$ [""]	$pn_{\text{B1}}^*$ [cts $\text{ks}^{-1}$ ]	$pn_{\text{B2}}^{**}$ [cts $\text{ks}^{-1}$ ]	2MASS Name	$d_{x-o}$ [""]	$P_{id}$	kmag	GSC Name	$d_{x-o}$ [""]	$P_{id}$	V	USNO Name	$d_{x-o}$ [""]	$P_{id}$	R	Class <sup>†</sup>	SpT <sup>‡</sup>
J214327.0+281603	1.59	1.5±0.5	1.9±0.9	21432699+2815580	5.2	0.12	16.08	N305023834	1.7	0.76		1182-0630006	2.0	0.45			
J214332.8+281213	0.75	7.8±0.8	1.3±0.6	21433285+2812134	0.6	0.99	13.77	N305022044	1.1	0.98	17.19	1182-0630057	0.8	0.98	15.85	Star	K6Ve <sup>sp</sup>
J214337.8+280537	1.21	2.1±0.5	0.6±0.5					N305028465	1.8	0.71		1180-0668164	1.0	0.87	20.10		
J214350.1+275822	1.47	1.5±0.6	2.4±1.1					N305016221	0.6	0.87		1179-0686320	2.6	0.46	19.37		
J214354.7+281022	0.86	3.7±0.5	0.1±0.2	21435472+2810236	1.4	0.95	13.98	N305021207	1.7	0.94	16.91	1181-0656366	1.6	0.93	15.90	Star	K2V <sup>sp</sup>
J214357.2+281957	1.27	2.1±0.7	0.8±0.7					N305043888	0.6	0.82		1183-0599981	0.4	0.85	20.56		
J214400.7+281126	0.48	17.0±0.9	3.4±0.5					N305021689	0.9	0.95	18.51	1181-0656437	0.5	0.98	18.59	EG	AGN <sup>sp</sup>
J214400.8+280609	0.52	11.9±0.8	3.7±0.6					N305019344	0.8	0.96		1181-0656435	1.1	0.90	19.93		
J214406.1+275958	0.68	10.1±1.1	4.3±0.9					N305016825	0.8	0.94		1179-0686476	0.8	0.94	19.64		
J214412.0+281722	0.56	14.4±1.1	4.7±0.8					N305024541	0.8	0.96		1182-0630418	0.8	0.95	19.37		
J214412.7+275954	1.62	2.4±0.6	0.1±0.3					N305016816	1.7	0.77		1179-0686527	2.0	0.78	20.60		
J214414.6+280535	1.69	0.4±0.2	1.5±0.4	21441483+2805354	2.3	0.86	14.70	N305019137	2.4	0.96	16.69	1180-0668510	2.4	0.98	13.74		
J214421.1+280831	0.50	10.9±0.8	2.2±0.4					N305020333	1.8	0.38		1181-0656642	1.6	0.54	18.44		
J214423.6+280320	0.99	3.8±0.6		21442364+2803205	0.4	1.00	12.94	N305018152	0.6	0.97	18.08	1180-0668591	0.5	0.97	17.09	Star	M5Ve <sup>sp</sup>
J214425.0+275821	0.98	4.4±0.8	5.4±1.3					N305016199	1.2	0.94	18.70	1179-0686636	0.8	0.96	18.71		
J214427.1+282346	1.54	4.2±0.9	1.0±1.1	21442714+2823461	0.7	0.98	13.05	N305040365	4.9	0.98		1183-0600218	1.0	0.91	15.08	Star	K7Ve <sup>sp</sup>
J214427.6+282313	1.49	5.2±1.0	3.4±1.2					N305036627	4.8	0.02	18.70	1183-0600226	0.7	0.79			
J214427.7+281153	1.44	1.7±0.4		21442773+2811529	0.9	0.97	13.87	N305021908	0.7	0.91	18.59	1181-0656708	0.7	0.91	18.41		
J214428.0+281846	1.39	2.7±0.6	0.3±0.5	21442813+2818457	0.9	0.97	13.93	N305025270	1.2	0.93	17.71	1183-0600230	1.3	0.96	16.20		
J214434.3+282306	1.44	7.6±1.2	2.7±1.4					N305036605	2.7	0.49		1183-0600289	2.1	0.46	19.58		
J214436.2+280811	1.24	0.8±0.4	1.4±0.5									1181-0656777	4.3	0.32	19.45		
J214439.6+281405	0.49	19.8±1.2	10.6±1.1					N305022954	0.2	0.97		1182-0630685	0.5	0.96	20.08		
J214440.8+275942	0.76							N305016757	1.1	0.96		1179-0686754	0.7	0.98	19.81		
J214459.7+280717	0.80	14.2±1.2	0.8±0.6	21445977+2807167	0.3	1.00	12.28	N305000004	0.1	1.00	13.90	1181-0656966	0.3	1.00	13.79	Star	F7V <sup>sp</sup>
J214504.1+281639	1.49	4.5±0.9	0.7±0.8					N305024225	0.3	0.89		1182-0630904	0.4	0.71	20.07		
J214506.7+280303	2.16							N305018079	1.7	0.82		1180-0668938	1.2	0.85	18.85		
J214512.0+281614	1.15	11.3±1.4	6.8±1.8					N305024004	1.6	0.81		1182-0630968	1.4	0.84	19.94		
J214517.9+281108	2.25	3.8±0.9	1.2±0.9	21451751+2811128	6.9	0.15	14.96	N305021627	7.3	0.02		1181-0657111	7.2	0.09	18.96		

**Table 10.** X-ray parameters for detected sources in field AXJ2019+112

2XMM Name	$r_{90}$ [""]	$\text{pn\_B1}^*$ [cts $\text{ks}^{-1}$ ]	$\text{pn\_B2}^{**}$ [cts $\text{ks}^{-1}$ ]	2MASS Name	$d_{x-o}$ [""]	$P_{id}$	kmag	GSC Name	$d_{x-o}$ [""]	$P_{id}$	V	USNO Name	$d_{x-o}$ [""]	$P_{id}$	R	Class <sup>†</sup>	SpT <sup>‡</sup>
J201848.3+112104	2.05	2.5±0.8	2.4±1.0					N1YB031812	3.1	0.27		1013-0571884	3.5	0.26	20.10		
J201900.0+113335	1.86	3.1±0.8	0.0±0.5	20190010+1133350	1.1	0.73	15.48	N1YB038048	1.2	0.78	18.94	1015-0585360	0.8	0.77	18.68		
J201900.1+113507	1.12	30.7±2.4	2.9±1.1	20190019+1135077	0.6	1.00	10.50	N1YB000545	0.5	1.00	11.59	1015-0585363	0.5	1.00	10.81	Star G3V <sup>sp</sup>	
J201905.9+112833	1.58	2.0±0.8	1.6±0.7	20190591+1128371	3.3	0.34	13.84	N1YB035790	3.3	0.62	15.47	1014-0582124	3.3	0.56	15.03	Star G2V <sup>sp</sup>	
J201908.8+113542	1.58	5.4±1.1		20190893+1135426	0.8	1.00	9.09	N1YB000540	0.8	1.00	10.40	1015-0585506	0.8	1.00	10.01	Star F5V <sup>s</sup>	
J201909.4+113936	1.77		1.4±1.7	20190953+1139308	5.7	0.03	15.46	N1YB040486	5.9	0.02	18.89	1016-0593168	5.6	0.03	17.73		
J201909.7+113146	1.48	4.8±0.9	0.8±0.5	20190991+1131467	2.1	0.82	13.12	N1YB037233	2.3	0.80	15.79	1015-0585519	1.9	0.83	15.57	Star K2V <sup>sp</sup>	
J201918.0+112713	1.31	3.7±0.7	3.9±0.8												EG	QSO <sup>s</sup>	
J201921.6+112354	1.14	11.8±1.2	2.6±0.7	20192160+1123543	0.7	0.99	11.91	N1YB033420	0.5	0.99	14.33	1013-0572442	0.3	1.00	14.13	Star K0V <sup>sp</sup>	
J201923.3+114051	1.94	6.0±1.7	3.7±1.7	20192355+1140507	3.8	0.12	15.84	N1YB040987	4.0	0.09	18.59	1016-0593424	3.6	0.29	17.60		
J201928.8+112852	2.30	2.9±0.7		20192896+1128529	1.4	0.70	15.68	N1YB049561	1.4								
J201928.9+112930	1.09	15.0±1.4	0.7±0.6	20192899+1129299	0.9	0.97	13.32	N1YB036175	1.0	0.89	18.19	1014-0582534	0.7	0.94	17.08	Star M5Ve <sup>sp</sup>	
J201930.2+112449	1.15	14.5±1.4	4.0±0.9									1014-0582553	2.0	0.31	17.03		
J201931.2+112900	1.55	3.1±0.7	1.0±0.6	20193141+1128599	2.0	0.69	14.78	N1YB035965	2.2	0.70	18.51	1014-0582566	1.8	0.75	17.10		
J201942.5+111611	1.54	4.3±1.2	2.8±1.8	20194258+1116117	0.2	0.97	12.91	N1YB028900	0.1	0.92	16.54	1012-0569389	0.3	0.96	15.84		
J201942.8+114031	1.62	11.5±2.2	5.0±1.8	20194280+1140312	0.6	0.76	16.75	N1YB040859	0.1	0.83	19.15	1016-0593741	0.4	0.77	18.97		
J201944.5+113101	1.64	4.4±1.0	1.5±0.9					N1YB036856	1.7	0.62		1015-0586123	1.3	0.70	19.40		
J201946.7+113454	4.52	4.6±1.3	1.5±1.0					N1YB038700	12.9	0.03		1015-0586149	10.8	0.04	18.33		
J201953.9+113800	1.27	26.2±3.0	4.4±2.3	20195398+1138002	0.7	0.99	11.30	N1YB000529	0.8	0.99	13.18	1016-0593928	0.8	0.99	12.79	Star K0V <sup>sp</sup>	
J201959.1+113336	2.65	0.6±2.0		20195923+1133349	1.8	0.76	13.74	N1YB038025	1.8	0.62		1015-0586359	1.4	0.65	17.43		
J202000.8+112506	1.40	7.8±1.5	8.2±2.1	20200090+1125041	2.1	0.37	15.54	N1YB033993	1.9	0.56	18.80	1014-0582998	1.5	0.73	18.05		
J202005.9+113645	2.30	6.9±1.9	2.0±1.7					N1YB039414	1.3	0.75	18.92	1016-0594132	1.5	0.54			
J202008.6+112118	2.20	3.5±1.4	3.9±2.2					N1YB031980	3.4	0.25	18.73	1013-0573179	3.4	0.26	18.17		

**Table 11.** X-ray parameters for detected sources in field G21.5-09 offset 2

2XMM Name	$r_{90}$ [""]	$\text{pn\_B1}^*$ [cts ks $^{-1}$ ]	$\text{pn\_B2}^{**}$ [cts ks $^{-1}$ ]	2MASS Name	$d_{x-o}$ [""]	$P_{id}$	kmag	GSC Name	$d_{x-o}$ [""]	$P_{id}$	V	USNO Name	$d_{x-o}$ [""]	$P_{id}$	R	Class $^{\dagger}$	SpT $^{\ddagger}$
J183211.2-103442	1.09	4.1 $\pm$ 0.8	6.3 $\pm$ 1.4	18321132-1034443	1.5	0.63	14.40	S9MZ012436	1.2	0.89		0794-0408906	0.9	0.56			
J183218.1-102743	1.57	4.2 $\pm$ 0.9	1.3 $\pm$ 0.8	18321809-1027440	1.3	0.73	12.37	S9MZ016477	1.8	0.85		0795-0410775	1.4	0.87	16.92		
J183220.7-103509	0.54	10.0 $\pm$ 1.6	447.5 $\pm$ 8.4													EG	HII $^s$
J183223.1-104349	0.90	8.4 $\pm$ 1.1	1.9 $\pm$ 1.1	18322304-1043495	1.5	0.40	13.60	S9MX019635	1.6	0.71		0792-0410638	1.3	0.77	19.87	Star	M2V $^{sp}$
J183226.4-103848	1.59	1.8 $\pm$ 1.3	0.9 $\pm$ 1.8	18322648-1038460	2.2	0.92	9.84										
J183228.1-102709	0.80	10.6 $\pm$ 1.2	4.5 $\pm$ 1.1	18322816-1027103	0.7	0.89	12.22	S9MZ016804	0.7	0.91		0795-0410993	1.0	0.87	18.70	Star	M4V $^{sp}$
J183231.4-103323	1.31	1.9 $\pm$ 0.5	0.5 $\pm$ 0.4	18323149-1033227	1.2	0.89	12.78	S9MZ013113	1.0	0.96	17.52	0794-0409293	1.3	0.92	16.91		
J183235.8-103206	1.90	1.0 $\pm$ 0.4	1.9 $\pm$ 0.6	18323597-1032058	1.6	0.87	11.91										
J183238.4-104908	1.15	4.8 $\pm$ 1.0	12.8 $\pm$ 2.2	18323848-1049084	0.4	0.77	13.43	S9MX057000	0.6	0.86		0791-0409361	0.3	0.78	18.96		
J183238.8-103458	1.02	1.6 $\pm$ 0.5	1.9 $\pm$ 0.6	18323890-1034577	1.1	0.98	10.70	S9MZ012261	0.8	0.98		0794-0409419	1.3	0.95	16.37	Star	K0III $^{sp}$
J183239.1-103126	1.42	1.9 $\pm$ 0.4	1.3 $\pm$ 0.5	18323920-1031260	0.9	0.99	9.82	S9MZ014213	0.4	0.99	15.79	0794-0409425	1.2	0.99	14.66	Star	K0III $^{sp}$
J183240.8-103945	1.87	0.4 $\pm$ 0.3	1.6 $\pm$ 0.6	18324068-1039496	4.0		14.70										
J183247.5-103038	1.08	2.3 $\pm$ 0.5	0.9 $\pm$ 0.4	18324750-1030383	0.3	0.99	11.30	S9MZ014672	0.5	0.99	17.27	0794-0409556	0.1	0.99	16.20		
J183248.3-103951	1.47	0.2 $\pm$ 0.2	1.3 $\pm$ 0.5	18324846-1039505	1.9	0.70	11.79										
J183258.0-104032	1.73	1.2 $\pm$ 0.4	1.0 $\pm$ 0.4														
J183301.5-103527	1.46	0.6 $\pm$ 0.4	1.8 $\pm$ 0.7	18330130-1035282	4.5	0.36	13.38										
J183303.0-104214	1.21	10.3 $\pm$ 1.9	5.5 $\pm$ 2.6					S9MX059820	1.3	1.00						Star	K4V $^{sp}$
J183305.9-103721	1.18	1.3 $\pm$ 0.4	0.8 $\pm$ 0.4	18330602-1037215	0.6	0.93	12.59	S9MX020860	0.3	0.98	17.48	0793-0410616	0.6	0.98	16.04	Star	G4V $^{sp}$
J183308.9-103508	1.76	0.0 $\pm$ 0.2	0.2 $\pm$ 0.3	18330879-1035075	2.5	0.33	13.11										
J183315.7-102936	0.71	5.0 $\pm$ 0.8	7.9 $\pm$ 1.1	18331569-1029372	0.8	0.96	11.55	S9MX021773	1.2	0.77		0795-0411976	0.5	0.95	17.49		
J183327.7-103523	0.43	35.7 $\pm$ 1.9	57.8 $\pm$ 2.7	18332777-1035243	0.7	1.00	8.27	S9MX000062	0.8	1.00	11.96	0794-0410181	0.4	1.00	11.48	HMXB	Be/X $^{sp}$
J183331.8-104028	1.12	3.3 $\pm$ 0.7	0.0 $\pm$ 0.4	18333177-1040288	0.8	0.99	10.51	S9MX020331	1.2	1.00	14.56	0793-0411091	0.7	1.00	14.04	Star	M2V $^{sp}$

**Table 12.** X-ray parameters for detected sources in field GC2

2XMM Name	$r_{90}$ ["]	$\text{pn\_B1}^*$ [cts $\text{ks}^{-1}$ ]	$\text{pn\_B2}^{**}$ [cts $\text{ks}^{-1}$ ]	2MASS Name	$d_{x-o}$ ["]	$P_{id}$	kmag	GSC Name	$d_{x-o}$ ["]	$P_{id}$	V	USNO Name	$d_{x-o}$ ["]	$P_{id}$	R	Class <sup>†</sup>	SpT <sup>‡</sup>
J174623.1-281156	1.94			17462327-2811532	3.3	0.86	10.90	S8DY022573	0.3	0.94	17.24	0618-0681779	0.7	0.94	16.20	Star	K2V <i>sp</i>
J174626.8-280413	1.34			17462682-2804152	1.3	0.98	10.48	S8DY029594	1.2	0.99	14.80	0619-0716672	1.5	0.97	14.29		
J174631.2-281028	0.85	$13.5 \pm 1.7$	$4.9 \pm 1.6$	17463125-2810287	0.6	1.00	8.53	S8DY024069	0.6	1.00	13.48	0618-0681890	0.5	1.00	12.70	Star	K1III <i>sp</i>
J174641.4-280811	1.89	$0.3 \pm 0.5$	$4.8 \pm 1.4$	17464164-2808110	2.5	0.19	11.37										
J174645.2-281547	0.58			17464524-2815476	0.2	1.00	7.18										
J174652.2-280909	1.79	$0.4 \pm 0.5$	$6.2 \pm 1.6$	17465241-2809149	5.9	0.02	11.78	S8DY025135	5.1	0.04	17.25	0618-0682213	4.6	0.31	16.32	Star	F9V <i>sp</i>
J174653.1-280203	1.53			17465284-2802027	3.8	0.26	12.39										
J174654.6-281658	0.62	$20.6 \pm 2.0$	$12.7 \pm 2.1$	17465462-2816580	0.6	1.00	11.08	S8DY016860	0.9	0.99	15.09	0617-0636761	0.6	1.00	14.30	Star	G0V <i>sp</i>
J174658.8-281423	2.38			17465885-2814264	2.9	0.06	13.35	S8DY019754	3.4	0.17		0617-0636840	7.5	0.30	14.90		
J174705.3-280859	0.38	$127.8 \pm 3.7$	$18.1 \pm 1.6$	17470538-2808594	0.5	1.00	7.48	S8DY000193	0.4	1.00	9.48	0618-0682463	0.4	1.00	9.05	Star	F3III <i>s</i>
J174707.8-280123	1.74	$3.5 \pm 0.9$	$0.6 \pm 0.8$	17470800-2801225	2.8	0.84	10.39	S8DY031922	2.6	0.96	13.55	0619-0717446	2.4	0.67	13.07	Star	K3V <i>sp</i>
J174714.8-280613	0.87	$5.0 \pm 0.8$	$2.4 \pm 0.8$	17471488-2806136	0.8	0.99	11.36	S8DY027712	0.4	1.00	15.38	0618-0682654	0.7	0.99	14.58	Star	G7V <i>sp</i>
J174715.1-281744	1.93	$1.3 \pm 0.6$	$2.9 \pm 1.2$	17471541-2817459	3.2	0.21	11.89										
J174717.7-275838	1.33	$2.9 \pm 0.9$	$0.6 \pm 1.0$	17471770-2758380	0.0	0.98	12.25	S8DY033929	0.3	0.99	15.76	0620-0729320	0.4	0.99	15.40	Star	K1III <i>sp</i>
J174717.8-281027	0.75	$0.3 \pm 0.3$	$15.3 \pm 1.6$	17471785-2810256	1.9	0.09	12.30										
J174718.0-281735	1.85	$2.2 \pm 0.8$	$2.0 \pm 0.9$	17471815-2817349	0.9	0.94	12.22										
J174720.5-281323	1.86	$0.2 \pm 0.3$	$3.5 \pm 1.0$	17472050-2813212	2.8	0.41	11.16										
J174726.5-281702	2.08	$3.0 \pm 0.9$	$0.4 \pm 0.8$	17472662-2817027	0.4	0.91	13.51	S8DY016600	0.3	0.95	17.35	0617-0637328	0.4	0.95	16.35	Star	M1Ve <i>sp</i>
J174728.0-280421	1.58	$0.8 \pm 0.5$	$2.6 \pm 0.9$	17472808-2804227	1.0	0.92	12.06	S8DY047798	1.2	0.81		0619-0718002	1.0	0.85	17.60	Star	F: <i>sp</i>
J174729.8-281305	1.27	$4.1 \pm 0.9$	$0.8 \pm 0.6$	17472986-2813061	0.6	0.92	13.90	S8DY021179	0.4	0.98	16.46	0617-0637389	0.5	0.98	15.80	Star	G9V <i>sp</i>
J174730.8-281347	0.86	$7.1 \pm 1.0$		17473086-2813480	0.7	0.96	11.41	S8DY020377	0.6	0.97	17.42	0617-0637407	0.5	0.98	16.47	Star	M5V <i>sp</i>
J174732.7-282104	1.45	$4.2 \pm 1.3$		17473283-2821046	0.8	0.98	12.48	S8DY011343	0.6	1.00	14.82	0616-0602189	1.2	0.99	14.17		
J174733.5-281839	1.79	$3.5 \pm 1.1$	$1.5 \pm 1.5$	17473359-2818406	1.1	0.98	11.49	S8DY014563	1.1	1.00	13.47	0616-0602196	1.4	1.00	13.21		
J174735.5-282012	1.82	$4.1 \pm 1.1$	$0.8 \pm 0.9$	17473564-2820116	1.8	0.80	12.09	S8DY012417	1.9	0.82	16.94	0616-0602229	2.0	0.42		Star	G <i>s</i>
J174736.7-281445	1.95	$2.8 \pm 0.8$	$0.5 \pm 0.6$	17473672-2814458	0.8	0.98	11.22	S8DY019308	1.0	1.00	14.16	0617-0637522	0.9	1.00	13.79	Star	F9V <i>sp</i>
J174745.9-280732	1.63	$2.6 \pm 0.8$	$1.6 \pm 0.9$	17474629-2807356	5.4		12.45										
J174746.3-280655	2.11	$0.5 \pm 0.4$	$5.5 \pm 1.4$	17474628-2806569	1.4	0.76	11.22										
J174751.9-280248	1.39	$0.6 \pm 1.3$	$1.1 \pm 2.5$	17475200-2802476	1.1	0.71	12.62										
J174756.1-280508	1.10	$6.8 \pm 1.3$	$4.2 \pm 1.2$	17475617-2805084	0.7	0.94	12.55				0619-0718676	1.0	0.75	19.07			
J174801.8-281710	1.05	$4.5 \pm 1.3$	$2.2 \pm 2.1$	17480185-2817106	0.6	1.00	11.52	S8DY016392	1.2	0.97	16.48	0617-0637905	1.7	0.86	15.10	Star	M4Ve <i>sp</i>
J174810.7-281831	2.09	$6.2 \pm 1.6$	$0.6 \pm 1.0$	17481080-2818312	1.2	1.00	7.54	S8DY000265	1.3	1.00	10.73	0616-0602683	1.3	1.00	9.67		
J174819.7-280727	1.99		$15.1 \pm 3.5$	17481973-2807269	0.5	1.00	4.34	S8DY026529	0.9	0.99	16.09	0618-0683828	0.6	1.00	14.22	Star	M6V <i>s</i>

**Table 13.** X-ray parameters for detected sources in field GRB001025

2XMM Name	$r_{90}$ ["]	$pn\_B1^*$ [cts $\text{ks}^{-1}$ ]	$pn\_B2^{**}$ [cts $\text{ks}^{-1}$ ]	2MASS Name	$d_{x-o}$ ["]	$P_{id}$	kmag	GSC Name	$d_{x-o}$ ["]	$P_{id}$	V	USNO Name	$d_{x-o}$ ["]	$P_{id}$	R	Class <sup>†</sup>	SpT <sup>‡</sup>
J083536.8-130647	2.95	$4.5 \pm 1.0$	$0.2 \pm 0.9$					S5WJ005955	5.4	0.17	0768-0209716	7.1	0.29	20.80			
J083538.6-130356	1.60	$5.4 \pm 1.1$	$3.7 \pm 1.6$	08353868-1303546	1.9	0.92	14.47	S5WJ006888	1.5	0.95	0769-0217305	1.7	0.61	16.21			
J083544.1-125744	1.73	$3.3 \pm 0.9$	$0.2 \pm 1.0$	08354410-1257486	4.1	0.61	14.24	S5WI007738	4.1	0.53	0770-0229071	3.9	0.63	17.11			
J083546.3-130912	1.02	$15.6 \pm 2.9$	$9.6 \pm 3.9$					S5WJ005116	0.1	0.97	0768-0209769	0.5	0.97	20.19			
J083555.1-125854	2.10	$3.4 \pm 1.2$	$0.2 \pm 1.1$	08355517-1258535	0.6	0.99	12.18	S5WI000795	0.4	0.99	0770-0229152	0.6	0.99	13.54			
J083603.5-131407	2.00	$1.6 \pm 0.6$	$3.5 \pm 1.4$					S5WJ003325	5.5	0.04	0767-0198711	5.6	0.18	20.00			
J083605.7-125321	1.19	$5.0 \pm 1.0$	$2.2 \pm 1.1$					S5WI009484	0.9	0.95	0771-0239435	0.8	0.96	19.54	EG	$\text{EG } sp$	
J083606.9-125348	0.82	$10.7 \pm 1.3$	$3.9 \pm 1.4$					S5WI009304	1.4	0.82	0771-0239448	1.1	0.92		EG	$\text{EG } sp$	
J083609.1-130455	1.22							S5WI005293	1.0	0.94	0769-0217581	0.6	0.98	20.16			
J083611.3-125840	0.41	$61.8 \pm 2.3$	$22.9 \pm 1.7$					S5WI007472	0.4	0.99	0770-0229320	0.3	1.00	18.37	EG	$\text{EG } sp$	
J083614.8-125724	1.11	$3.6 \pm 0.7$	$1.7 \pm 0.8$					S5WI007877	1.4	0.87	0770-0229371	1.2	0.92	20.21			
J083615.5-130341	1.09	$3.0 \pm 0.5$	$1.5 \pm 0.6$					S5WI005740	1.5	0.91	0769-0217644	1.4	0.94	18.16			
J083616.3-130949	0.48	$28.4 \pm 1.5$	$1.9 \pm 0.6$	08361624-1309496	1.2	0.95	12.02	S5WI003854	1.2	0.98	0768-0210033	0.8	0.99	15.51	Star	$\text{Me } sp$	
J083622.8-131502	1.68	$2.5 \pm 0.7$	$1.8 \pm 1.0$	08362279-1315034	1.1	1.00	9.67	S5WI000981	1.0	1.00	11.54	0767-0198871	1.0	1.00	10.95		
J083622.9-130903	0.74	$39.2 \pm 3.3$	$4.9 \pm 2.1$	08362291-1309049	1.4	1.00	6.89	S5WI000926	1.2	0.69	7.99	0768-0210115	1.2	1.00	7.68	Star	F5V s
J083624.2-125919	0.76	$4.1 \pm 0.6$	$1.8 \pm 0.6$					S5WI007225	0.5	0.98	0770-0229459	0.2	0.99	20.23	EG	$\text{EG } sp$	
J083627.8-130200	0.89	$2.4 \pm 0.4$	$1.7 \pm 0.5$					S5WI032790	1.3	0.82					EG	$\text{EG } sp$	
J083631.6-131635	1.54	$2.7 \pm 0.7$	$1.4 \pm 0.9$					S5WI002040	1.9	0.82	0767-0198941	1.6	0.87	18.57			
J083633.5-130033	1.38	$1.0 \pm 0.3$	$0.2 \pm 0.3$					S5WI006798	4.9	0.01	0769-0217812	4.5	0.18	20.23			
J083639.4-125426	1.18	$2.4 \pm 0.6$	$1.0 \pm 0.7$					S5WI009049	0.4	0.96	0770-0229590	1.2	0.90	20.23			
J083645.5-130401	1.24	$0.2 \pm 0.2$	$2.6 \pm 0.5$					S5WI005638	0.9	0.92	0769-0217902	0.8	0.92	18.80			
J083645.6-125242	1.58	$3.1 \pm 0.7$	$1.0 \pm 0.6$								0771-0239798	3.9	0.28	20.23			
J083646.0-130716	1.87	$0.4 \pm 0.3$	$0.2 \pm 0.3$					S5WI004612	6.1	0.02	0768-0210375	6.2	0.12	19.80			
J083646.3-125929	0.82	$4.1 \pm 0.6$	$1.6 \pm 0.5$					S5WI007181	0.5	0.98	0770-0229655	0.6	0.98	19.47			
J083647.1-131652	0.84	$10.2 \pm 1.3$	$3.4 \pm 1.3$								0767-0199056	0.4	0.92		EG	$\text{EG } sp$	
J083648.5-130150	1.05	$1.9 \pm 0.4$	$0.4 \pm 0.3$	08364849-1301508	0.5	0.99	14.01	S5WI006369	0.7	0.97	0769-0217935	0.6	0.97	18.11	Star	$\text{Me } sp$	
J083648.7-125729	1.35	$2.2 \pm 0.5$	$0.3 \pm 0.4$	08364883-1257297	0.6	0.99	13.09	S5WI007875	1.3	0.96	0770-0229672	0.7	0.92	17.20	Star	$\text{Me } sp$	
J083649.7-130931	1.82	$1.1 \pm 0.4$	$0.7 \pm 0.4$					S5WI003939	2.5	0.75	0768-0210423	3.7	0.59	18.60			
J083650.2-131249	1.93	$1.3 \pm 0.5$	$1.2 \pm 0.7$								0767-0199092	2.1	0.65	20.23			
J083700.8-131702	1.61	$4.2 \pm 0.9$	$2.2 \pm 1.3$	08370080-1317036	1.6	0.96	13.53	S5WI001935	1.5	0.97	0767-0199193	1.7	0.95	15.94		F/G sp	
J083702.0-130622	2.53	$0.4 \pm 0.4$	$0.3 \pm 0.5$					S5WI004879	1.5	0.82	0768-0210540	1.2	0.89	20.19			
J083703.1-131439	1.75	$3.1 \pm 0.8$	$0.1 \pm 0.3$					S5WI002500	0.6	0.90	0767-0199211	1.3	0.85	20.23			
J083708.8-130226	0.85	$4.8 \pm 0.8$	$0.7 \pm 0.6$					S5WI006177	0.2	0.96	0769-0218101	0.3	0.97	19.94			
J083715.2-130923	1.00	$3.9 \pm 0.7$	$2.5 \pm 0.8$					S5WI003980	0.4	0.96	0768-0210645	0.5	0.98	20.22			
J083715.5-131036	1.34	$1.9 \pm 0.6$	$1.6 \pm 0.7$					S5WI003619	1.2	0.85	0768-0210648	1.2	0.83	20.19			
J083719.4-125623	1.58							S5WI008287	1.4	0.87	0770-0229939	1.3	0.92	19.88			
J083721.5-125720	0.68	$6.2 \pm 2.9$	$2.5 \pm 4.5$					S5WI007934	0.1	0.99	0770-0229958	0.5	0.98	19.73	EG	$\text{EG } sp$	
J083727.9-130012	1.51							S5WI006959	2.4	0.63	0769-0218296	2.2	0.63	19.98			
J083732.5-130700	1.96			08373236-1307042	4.5	0.16	14.63	S5WI000899	4.2	0.44	0768-0210774	4.1	0.59	14.97			

**Table 14.** X-ray parameters for detected sources in field GROJ1655-40

2XMM Name	$r_{90}$ [""]	$\text{pn\_B1}^*$ [cts $\text{ks}^{-1}$ ]	$\text{pn\_B2}^{**}$ [cts $\text{ks}^{-1}$ ]	2MASS Name	$d_{x-o}$ [""]	$P_{id}$	kmag	GSC Name	$d_{x-o}$ [""]	$P_{id}$	V	USNO Name	$d_{x-o}$ [""]	$P_{id}$	R	Class <sup>†</sup>	SpT <sup>‡</sup>
J165256.2-394813	1.69			16525614-3948111	3.0	0.22	13.45	S8VD122070	4.3	0.19		0501-0492854	3.6	0.26	17.92		
J165301.1-395414	1.62	4.6± 1.0	2.1± 0.8	16530089-3954165	3.3	0.23	12.98	S8VD117711	4.7	0.01		0500-0495133	4.6	0.25	17.26		
J165304.2-395557	1.47	6.9± 1.2	1.2± 0.9									0500-0495183	1.1	0.98	12.12	Star	M2V <sup>sp</sup>
J165306.1-400008	1.67			16530610-4000033	4.9	0.04	13.07	S8VD112419	5.0			0499-0495184	5.0		18.66		
J165310.5-394449	1.13	12.6± 1.4	3.3± 0.9	16531037-3944492	0.9	0.91	11.11	S8VD040934	1.3	0.98	14.46	0502-0490447	0.8	0.98	13.44	Star	K1V <sup>sp</sup>
J165314.3-395805	2.15	1.0± 0.6	0.0± 0.6	16531441-3958024	2.0	0.34	13.44	S8VD114350	1.5	0.49							
J165314.9-395309	1.38	5.9± 0.9	0.2± 0.3	16531480-3953088	0.3	0.88	12.92	S8VD039158	1.1	0.93	16.64	0501-0493194	0.5	0.92	15.88	Star	K4V <sup>sp</sup>
J165315.0-395509	1.84	4.2± 0.8	0.8± 0.7	16531489-3955070	0.9	0.79	13.42	S8VD038485	1.2	0.93	16.18	0500-0495363	1.0	0.90	15.74		
J165334.2-400005	1.49	4.8± 1.0	1.3± 0.7	16533391-4000054	1.6	0.96	9.06	S8VD000430	1.4	1.00	0499-0495689	1.4	1.00	10.47	Star	F5V <sup>s</sup>	
J165342.7-395501	2.45	0.6± 0.4	0.6± 0.5	16534252-3954596	0.9	0.80	12.83	S8VD117190	0.9	0.89	0500-0495910	1.3	0.75	17.42			
J165348.8-395537	1.84	1.0± 0.4	0.5± 0.5	16534902-3955373	2.4	0.85	10.00	S8VD038316	2.2	0.92	14.42	0500-0496017	4.3	0.86			
J165351.4-393658	1.85	9.5± 3.1	2.5± 3.6									0503-0487504	1.5	0.86	15.00		
J165354.2-395918	2.42	2.1± 0.6		16535448-3959229	5.3	0.30	13.28	S8VD142309	4.4	0.14						Star	M <sup>s</sup>
J165358.3-394743	2.06	0.8± 0.4	0.2± 0.4	16535841-3947453	3.4	0.05	13.61	S8VD122478	3.0	0.05						EG	AGN <sup>sp</sup>
J165402.0-394630	1.34	0.6± 0.4	5.5± 0.9	16540206-3946305	0.5	0.91	12.65	S8VD123148	0.6	0.81						Star	K0 <sup>s</sup>
J165402.6-393818	1.71	4.2± 1.1	2.6± 1.1														F3V <sup>sp</sup>
J165407.3-394601	1.43	3.6± 0.7	0.8± 0.5	16540733-3946006	1.0	0.97	10.29	S8VD000325	1.2	1.00	12.03	0502-0491615	0.6	1.00	12.31	Star	
J165407.9-395738	1.65	2.6± 0.9	1.3± 0.9	16540782-3957388	0.7	0.88	12.70	S8VD037531	0.4	0.98	15.40	0500-0496309	1.5	0.87	14.72		
J165410.5-394204	1.34	7.6± 1.1	0.4± 0.5	16541072-3942036	0.8	0.89	12.35	S8VD041287	0.8	0.98	15.42	0502-0491662	1.3	0.89	15.05	Star	K1V <sup>sp</sup>
J165411.4-395236	2.00	1.1± 0.4	0.8± 0.4	16541121-3952363	2.9	0.53	11.46	S8VD039361	2.7	0.59	16.70	0501-0494271	2.6	0.52	16.04		G <sup>s</sup>
J165412.4-395434	1.43	3.6± 0.7		16541228-3954342	0.9	0.78	13.05	S8VD038715	1.2	0.91	16.32	0500-0496380	1.8	0.61	15.61	Star	K0V <sup>sp</sup>
J165418.3-394804	1.81	1.3± 0.5	3.0± 0.8	16541850-3948015	3.0	0.07	15.19	S8VD122289	3.0	0.07							
J165420.0-394751	2.59	0.3± 0.4	0.7± 0.5	16542023-3947493	5.5	0.01	12.78	S8VD040423	5.2	0.28	14.81	0502-0491797	5.5	0.11	14.42		
J165421.3-394635	1.47	3.4± 0.7	1.1± 0.5	16542125-3946353	0.4	0.88	13.47	S8VD040651	0.4	0.97	16.68	0502-0491817	0.7	0.93	15.50	Star	K0V <sup>sp</sup>
J165421.8-395310	1.64	1.7± 0.5	1.2± 0.6	16542169-3953112	1.1	0.79	12.76	S8VD165306	1.5	0.59							
J165423.5-394910	1.70	0.0± 0.2	3.7± 0.8	16542382-3949094	3.5	0.10	14.06										
J165424.0-394225	1.53	1.8± 0.7	3.6± 1.3	16542365-3942276	4.9		14.54										
J165426.3-394455	2.18	0.4± 0.4	1.3± 0.7	16542650-3944546	0.4	0.86	12.40	S8VD124019	0.8	0.65		0502-0491881	0.9	0.73			
J165427.0-395227	1.59	1.7± 0.5	1.3± 0.5	16542692-3952295	1.5	0.56	13.29	S8VD119313	1.4	0.67		0501-0494508	1.4	0.73			
J165428.3-400100	2.01	2.4± 1.3															
J165438.2-400146	1.30	10.9± 1.6	1.9± 0.9	16543820-4001455	0.5	0.92	12.43	S8VD035512	0.8	0.98	15.13	0499-0496973	0.7	0.96	14.74	Star	G7V <sup>sp</sup>
J165440.5-394705	1.41	6.4± 1.0	1.7± 0.8	16544046-3947063	0.4	0.94	11.48	S8VD040569	0.3	0.97	16.23	0502-0492068	0.2	0.94	15.29	Star	G9V <sup>sp</sup>
J165440.5-394910	1.86	2.5± 0.7	0.7± 0.8	16544016-3949089	3.0	0.24	12.31	S8VD040199	2.8	0.82	14.05	0501-0494695	2.7	0.82	14.31	Star	F5V <sup>sp</sup>
J165445.1-400228	2.15	7.6± 1.5	1.3± 1.3	16544553-4002249	5.1	0.40	15.02	S8VD035135	3.3	0.74	15.54	0499-0497102	6.7	0.74	17.34		
J165445.9-394329	2.27	0.9± 0.7		16544561-3943291	4.0	0.81	13.61	S8VD041126	3.9	0.58	17.15	0502-0492136	4.2	0.49	15.29		
J165500.1-394205	2.08	7.8± 1.7	1.2± 1.3	16550028-3942037	2.9	0.91	9.29	S8VD000306	2.9	1.00	9.99	0502-0492305	2.9	1.00	9.84		
J165508.2-395920	2.49	1.2± 0.9	14.8± 3.1	16550799-3959164	4.8	0.02	14.51	S8VD000423	8.1	0.11	12.69	0500-0497258	7.3	0.53			
J165515.6-394544	1.18	45.4± 3.1	11.3± 2.4	16551565-3945449	0.9	0.87	12.25	S8VD040806	1.6	0.93	15.75	0502-0492505	1.9	0.89	14.61	Star	K4V <sup>sp</sup>
J165519.0-395301	2.21	8.9± 1.9		16551890-3953013	1.1	0.91	10.44	S8VD000365	1.2	0.98	12.47	0501-0495240	6.3	0.95	16.32		

**Table 15.** X-ray parameters for detected sources in field HTCas

2XMM Name	$r_{90}$ [""]	$\text{pn\_B1}^*$ [cts $\text{ks}^{-1}$ ]	$\text{pn\_B2}^{**}$ [cts $\text{ks}^{-1}$ ]	2MASS Name	$d_{x-o}$ [""]	$P_{id}$	kmag	GSC Name	$d_{x-o}$ [""]	$P_{id}$	V	USNO Name	$d_{x-o}$ [""]	$P_{id}$	R	Class <sup>†</sup>	SpT <sup>‡</sup>
J010844.0+600542	1.68	6.6± 1.2	1.8± 1.3					NAMD035494	5.8		17.81						
J010930.4+600639	2.09	3.1± 0.6		01093093+6006419	4.0	0.72	11.73	NAMD035847	4.4	0.87	13.33	1501-0041748	4.7	0.65	13.06	Star	F5V <sup>sp</sup>
J010933.5+601619	1.52	6.1± 1.2	0.9± 1.0	01093377+6016205	2.0	0.97	9.77	NAMF000679	1.9	0.99	12.44	1502-0043542	1.9	0.99	11.92	Star	K4V <sup>sp</sup>
J010955.2+601852	2.82			01095635+6018496	8.9	0.02	14.58	NAMF016855	8.7		17.79	1503-0044677	8.5	0.01	17.38		
J010956.8+595336	1.57	4.8± 1.7	1.8± 2.4	01095677+5953369	0.7	0.81	14.83	NAMD046861	0.7	0.60		1498-0040815	1.1	0.56	19.16		
J010959.0+595359	1.99	3.5± 1.0	1.6± 1.5					NAMD028376	4.2			1498-0040840	5.1		18.71	Star	M2V <sup>sp</sup>
J011001.9+601106	1.79	2.8± 0.6	0.1± 0.3	01100226+6011077	2.3	0.83	13.18	NAMD037374	2.3	0.66	18.13	1501-0042040	2.0	0.67	17.43	Star	M4V <sup>sp</sup>
J011008.9+595219	2.70	5.4± 1.3	3.0± 2.0	01100923+5952187	2.2	0.78	13.39	NAMD027075	1.8	0.82	17.15	1498-0040944	1.8	0.80	15.96	Star	M3V <sup>sp</sup>
J011009.1+600051	2.07	2.5± 0.6	1.3± 0.6	01100930+6000495	2.1	0.77	14.01	NAMD032753	2.0	0.75	17.54	1500-0040272	1.6	0.76	16.87		
J011017.6+600917	1.96	2.4± 0.5	1.0± 0.5					NAMD036754	6.4			1501-0042168	6.1		19.03		
J011024.8+601119	1.49	4.1± 0.7	0.3± 0.3	01102501+6011193	0.9	0.80	14.66	NAMD049532	1.3	0.70						Star	M4V <sup>sp</sup>
J011026.4+600352	1.71	2.5± 0.6	0.1± 0.3	01102672+6003513	2.5	0.71	13.48	NAMD034374	2.5	0.73	16.83	1500-0040432	2.2	0.75	16.21		
J011027.4+600039	1.16	20.0± 1.4	1.2± 0.5	01102768+6000390	1.6	0.92	11.53	NAMD032647	1.4	0.97	15.01	1500-0040445	1.2	0.97	14.47	Star	M1V <sup>sp</sup>
J011033.4+595853	1.97			01103408+5958544	4.8	0.14	13.19	NAMD031557	4.7	0.01	18.23	1499-0041427	4.7	0.01	17.75	Star	M4V <sup>sp</sup>
J011038.2+600146	1.27	14.1± 1.5	3.5± 1.1	01103854+6001456	2.7	0.84	10.00	NAMD000514	2.7	0.98	10.47	1500-0040559	2.7	0.99	10.34	Star	A0V <sup>s</sup>
J011056.5+595937	1.99	1.5± 0.7	2.8± 1.1	01105673+5959329	4.7	0.12	15.38	NAMD031903	4.7	0.02		1499-0041674	4.7	0.03	18.90		
J011056.6+600459	2.27	1.5± 0.5	1.5± 0.7	01105749+6004583	6.4	0.04	15.25	NAMD034868	6.5		18.23	1500-0040726	6.4	0.01	17.83		
J011105.0+601551	2.56			01110601+6015506	7.0	0.10	13.98	NAMF014008	6.9	0.04	17.38	1502-0044319	6.8	0.06	16.62		
J011123.3+600258	1.82	2.4± 0.7	1.4± 0.8	01112309+6002581	1.7	0.55	15.47					1500-0040969	2.2	0.37			

**Table 16.** X-ray parameters for detected sources in field LHB-3

2XMM Name	$r_{90}$ [""]	$\text{pn\_B1}^*$ [cts $\text{ks}^{-1}$ ]	$\text{pn\_B2}^{**}$ [cts $\text{ks}^{-1}$ ]	2MASS Name	$d_{x-o}$ [""]	$P_{id}$	kmag	GSC Name	$d_{x-o}$ [""]	$P_{id}$	V	USNO Name	$d_{x-o}$ [""]	$P_{id}$	R	Class <sup>†</sup>	SpT <sup>‡</sup>
J230733.5+613634	1.69			23073340+6136319	2.6	0.95	12.33	N190039257	2.5	0.97	15.37	1516-0352460	2.4	0.96	14.87	Star	K1Ve <sup>sp</sup>
J230804.6+613351	2.03	1.9±0.6		23080441+6133514	1.5	0.93	13.25	N190039027	1.5	0.95	17.30	1515-0347087	1.7	0.93	16.25		
J230817.5+614001	1.45	2.0±0.5	0.1±0.5	23081765+6140032	2.1	0.89	13.63	N193013396	2.4	0.93	16.93	1516-0352782	4.4	0.85	16.68		
J230825.6+613428	1.60	2.0±0.5	0.7±0.5	23082597+6134250	4.4	0.93	13.61	N190039115	1.7	0.96	17.63	1515-0347234	1.2	0.41			
J230837.3+613849	1.70	2.0±0.5	0.3±0.3	23083749+6138518	2.7	0.81	13.88	N190039407	2.7	0.89	17.10	1516-0352929	2.9	0.88	16.48		
J230855.0+613657	1.38			23085515+6136585	0.8	0.90	15.02	N198028365	4.1	0.93	17.00	1516-0353040	1.6	0.63	16.66		
J230911.4+614327	0.40	89.6±3.1	6.4±1.0	23091139+6143277	0.3	1.00	10.70	N19U000026	0.4	1.00	12.72	1517-0359727	0.2	1.00	12.17	Star	G7V <sup>sp</sup>
J230915.4+612704	1.91	1.7±0.6	1.8±1.0	23091486+6127042	4.1	0.73	13.11	N19S027005	4.0	0.16		1514-0344726	4.3	0.22	19.13		
J230918.4+613623	1.86	2.3±0.5		23091838+6136209	2.3	0.89	13.29	N198028341	2.3	0.90	17.18	1516-0353208	2.2	0.89	16.33		
J230920.1+613922	0.85	8.4±1.1	0.2±0.3	23092018+6139228	0.4	1.00	7.90	N19V000125	0.4	1.00	8.06	1516-0353240	0.4	1.00	8.06	Star	A <sup>s</sup>
J230923.2+612553	1.78	2.5±0.8	0.6±0.6	23092313+6125536	0.9	0.98	12.12	N19S026829	0.8	0.99	15.60	1514-0344777	0.9	0.98	15.10	Star	K4Ve <sup>sp</sup>
J230926.8+613550	1.51	1.3±0.4		23092660+6135509	1.7	0.98	12.10	N19S000005	1.4	0.99	14.07	1515-0347656	2.7	0.70	13.87	Star	G3V <sup>sp</sup>
J230933.2+614215	0.52	23.7±1.7	3.3±0.8	23093321+6142154	0.3	1.00	11.83	N19V004359	0.2	1.00	15.78	1517-0359907	0.5	1.00	14.48	Star	M0Ve <sup>sp</sup>
J230934.5+614614	2.00	0.8±0.4	2.3±0.8	23093459+6146178	3.6	0.58	14.16	N19U000756	3.8	0.10		1517-0359921	4.1	0.13	19.14		
J230939.8+613432	1.10	3.7±0.6	0.7±0.4	23093986+6134311	1.8	0.96	12.43	N19S028200	1.7	0.95	16.79	1515-0347770	1.5	0.95	16.08	Star	M0Ve <sup>sp</sup>
J230940.9+613510	1.04	1.7±0.4	1.9±0.5	23094084+6135119	1.6	0.93	13.23	N19S028257	2.2	0.83	17.62	1515-0347778	3.0	0.60	15.85		
J230943.4+614109	0.90	5.8±1.3	0.6±0.9	23094359+6141084	1.4	0.96	13.00	N19V004094	1.5	0.95	17.72	1516-0353465	1.2	0.96	16.25	Star	K7Ve <sup>sp</sup>
J230944.3+613435	1.17	3.3±0.6	0.4±0.3	23094418+6134353	1.0	1.00	10.51	N19S000009	0.7	1.00	13.01	1515-0347822	1.0	1.00	12.82	Star	G0V <sup>sp</sup>
J230955.7+613655	1.27	2.2±0.5	0.1±0.2	23095558+6136543	1.3	0.90	14.51	N19V003013	1.1	0.85		1516-0353561	1.4	0.80	18.81		
J230956.3+614006	1.06	3.9±0.6	1.5±0.4	23095635+6140082	1.3	0.98	12.62	N19V003918	1.5	0.98	15.83	1516-0353567	2.5	0.90	14.76	Star	G0V <sup>sp</sup>
J231001.0+613635	0.51	24.6±1.5	1.4±0.5	23100095+6136340	1.3	0.99	10.35	N19V000145	1.1	1.00	12.23	1516-0353591	1.1	1.00	11.99	Star	F6V <sup>sp</sup>
J231011.6+614904	1.56	5.6±1.1		23101154+6149049	0.8	0.99	11.02	N19U000010	0.8	1.00	12.66	1518-0362824	1.1	1.00	12.67	Star	F5V <sup>sp</sup>
J231012.5+613348	1.81	1.9±0.5	0.5±0.4	23101265+6133500	1.6	0.98	11.94	N19S028151	1.8	0.99	14.37	1515-0348118	1.8	0.99	14.38	Star	G0V <sup>sp</sup>
J231012.7+613239	1.63	1.3±0.5	1.9±0.8	23101298+6132414	2.6	0.89	13.07	N19S027998	2.9	0.49	18.81	1515-0348124	2.8	0.61	17.87		
J231021.4+614503	1.65	2.0±0.6		23102156+6145023	1.9	0.90	13.51	N19U000669	1.5	0.95	17.63	1517-0360246	2.1	0.82		Star	K7Ve <sup>sp</sup>
J231023.5+613515	1.42	2.4±0.6	0.4±0.5	23102343+6135147	1.3	1.00	9.53	N19V000158	1.1	1.00	11.06	1515-0348224	1.1	1.00	10.68	Star	F3V <sup>sp</sup>
J231028.2+614811	1.53	3.8±0.9	0.2±0.8	23102822+6148119	0.6	0.98	13.04	N19U001047	0.5	0.99	17.42	1518-0362905	0.9	0.98	16.68	Star	K1V <sup>sp</sup>
J231032.6+614328	1.25	2.7±0.7	2.9±1.1	23103252+6143300	2.0	0.96	11.98	N19V004808	1.9	0.78	18.75	1517-0360318	2.4	0.67	17.88		
J231036.8+613243	1.36	5.3±0.9	1.3±0.8	23103654+6132424	2.5	0.47	13.14	N19S028042	2.7	0.55	16.71	1515-0348345	1.7	0.28	14.97		
J231100.8+614028	0.91	8.0±1.9	2.8±2.2	23110073+6140272	1.5	0.99	11.61	N19V004104	1.3	0.99	16.41	1516-0353998	1.2	0.98	15.67	Star	M2Ve <sup>sp</sup>

**Table 17.** X-ray parameters for detected sources in field PKS0745-19-offset

2XMM Name	$r_{90}$ [""]	$\text{pn}_B\text{B1}^*$ [cts $\text{ks}^{-1}$ ]	$\text{pn}_B\text{B2}^{**}$ [cts $\text{ks}^{-1}$ ]	2MASS Name	$d_{x-o}$ [""]	$P_{id}$	kmag	GSC Name	$d_{x-o}$ [""]	$P_{id}$	V	USNO Name	$d_{x-o}$ [""]	$P_{id}$	R	Class <sup>†</sup>	SpT <sup>‡</sup>	
J074722.4-190702	1.29	16.5± 1.9	3.2± 1.1	07472249-1907028	0.3	1.00	12.00	S3NV029046	0.2	0.99		0708-0151420	2.7	0.92	13.68	Star	G9V <sup>sp</sup>	
J074734.5-185656	0.79	17.6± 1.6	16.0± 2.0													EG	AGN <sup>sp</sup>	
J074736.0-190554	1.68	2.6± 0.8	4.9± 1.6													EG	Gal <sup>image</sup>	
J074737.6-185944	1.12	4.2± 0.8	2.8± 1.0															
J074739.6-190735	0.88	9.8± 1.3	0.7± 0.6	07473964-1907361	0.3	1.00	12.58	S3NV034178	2.7	0.11		0710-0150157	3.0	0.10	19.60			
J074740.3-190105	1.53	3.5± 0.7	1.9± 0.8	07474053-1901097	5.2	0.14	15.17	S3NV032388	5.4	0.01		0708-0151682	0.6	1.00	14.27	Star	G3V <sup>sp</sup>	
J074742.2-190224	1.44	3.1± 0.8	0.8± 0.8					S3NV032416	1.4	0.68		0709-0152008	1.3	0.71	19.90			
J074742.7-190749	2.04	2.2± 0.9	1.0± 1.1					S3NV028339	6.0	0.01		0708-0151731	6.5	0.01	19.46			
J074743.5-185654	0.58	25.2± 1.7	7.3± 1.4					S3NV036069	0.8	0.89		0710-0150259	1.5	0.64		CV	CV <sup>sp</sup>	
J074752.5-190428	1.50	3.3± 1.2	1.7± 1.3	07475247-1904248	3.3	0.77	13.04	S3NV031046	4.1	0.29		0709-0152175	3.8	0.47	15.27			
J074752.6-185713	1.42	2.0± 0.6	1.5± 0.8	07475277-1857099	4.2	0.16	14.91	S3NV035585	4.4	0.03		0710-0150416	4.0	0.23	17.12			
J074755.5-190647	0.90	9.7± 3.4	4.6± 3.5	07475552-1906480	0.5	0.99	13.11	S3NV029250	0.4	0.99		0708-0151945	0.6	0.98	14.89			
J074757.1-190243	1.25	1.2± 0.4	1.7± 0.5	07475724-1902411	3.2	0.26	15.52	S3NV032226	4.2	0.01		0709-0152254	4.2	0.04	18.22			
J074758.7-190602	0.86	2.9± 0.6	2.1± 0.7												EG	AGN <sup>sp</sup>		
J074802.1-185952	1.57	0.3± 0.3	1.3± 0.5	07480243-1859498	5.1	0.15	14.86	S3NV034214	5.2	0.01		0710-0150592	5.4	0.17				
J074802.3-185820	1.56	3.1± 0.6		07480248-1858198	1.8	0.98	11.94	S3NV000360	2.0	0.99		0710-0150598	2.1	0.98	13.55	Star	F6V <sup>sp</sup>	
J074802.4-185745	1.87	0.1± 0.2	1.8± 0.7					S3NV054772	2.2	0.33					EG	Gal <sup>sp</sup>		
J074802.4-190251	1.06	2.0± 0.4	1.4± 0.5	07480246-1902517	0.9	0.95	15.01	S3NV032109	1.3	0.91		0709-0152357	1.3	0.89	16.68	Star	G4V <sup>sp</sup>	
J074804.6-190814	0.99	1.3± 0.4	2.0± 0.6												EG	AGN <sup>sp</sup>		
J074805.5-190506	0.68	3.6± 0.5	4.1± 0.6												EG	AGN <sup>sp</sup>		
J074806.0-190856	0.59	8.0± 0.9	4.1± 0.7												EG	AGN <sup>sp</sup>		
J074807.2-185640	2.22	1.2± 0.4	0.6± 0.6	07480737-1856385	2.5	0.88	13.60	S3NV036281	2.8	0.86		0710-0150697	3.0	0.84	15.37	Star	G9V <sup>sp</sup>	
J074808.4-190528	1.88	0.5± 0.3	0.8± 0.4	07480860-1905315	3.6	0.27	14.83	S3NV030147	3.2	0.21		0709-0152479	3.5	0.39	18.59			
J074810.6-190417	1.60	0.6± 0.3	0.2± 0.2	07481067-1904122	5.3	0.15	14.53	S3NV031121	5.6	0.01		0709-0152527	5.0	0.09	16.42			
J074814.7-190536	1.18	1.3± 0.3	0.8± 0.3					S3NV030067	0.8	0.74					EG	AGN <sup>sp</sup>		
J074815.4-191415	1.11	3.0± 0.6	3.5± 0.8	07481542-1914175	1.8	0.73	15.52	S3NV022991	1.4	0.82		0707-0152048	1.7	0.67	18.38	Star	K1V <sup>sp</sup>	
J074818.6-191730	0.55	21.2± 1.4	2.9± 0.9	07481863-1917317	1.1	0.98	11.76	S3NV020236	0.9	0.99		0707-0152103	1.2	0.96	14.36	Star	G9V <sup>sp</sup>	
J074820.9-190721	1.52	1.0± 0.3	0.7± 0.3					S3NV028800	3.7	0.33		0708-0152364	2.2	0.41		EG	Gal <sup>image</sup>	
J074821.3-191510	1.17	2.8± 0.5	0.7± 0.5	07482134-1915105	0.0	0.98	13.33	S3NV022264	0.1	0.98		0707-0152155	0.1	0.97	15.12	Star	G1V <sup>sp</sup>	
J074821.9-190255	1.14	1.5± 0.3	1.0± 0.4	07482205-1902536	2.6	0.48	15.04	S3NV032061	2.7	0.35		0709-0152733	2.7	0.47	16.75	Star	M5V <sup>sp</sup>	
J074822.1-190807	1.47	1.0± 0.3	0.3± 0.2	07482218-1908056	3.8	0.85	11.24	S3NV028312	3.6	0.93		0708-0152385	3.3	0.93	13.24	Star	G9V <sup>sp</sup>	
J074823.1-190937	0.52	12.1± 0.8	0.3± 0.3	07482309-1909379	0.6	1.00	12.52	S3NV027003	0.3	1.00		0708-0152415	0.3	1.00	14.15	Star	G9V <sup>sp</sup>	
J074823.3-191408	1.87	1.1± 0.4	1.7± 0.6					S3NV023098	3.3	0.12					EG	AGN <sup>sp</sup>		
J074824.5-190734	0.69	4.7± 0.6	0.8± 0.4	07482459-1907339	0.3	0.99	12.87	S3NV028656	0.3	1.00		0708-0152444	0.4	0.99	14.53	Star	G3V <sup>sp</sup>	
J074825.0-185549	0.88	2.7± 0.6	7.5± 1.2					S3NV036692	2.5	0.10		0710-0151034	0.2	0.89	20.28	EG	AGN <sup>sp</sup>	
J074826.0-191733	0.98	5.6± 0.8	0.0± 0.6	07482598-1917339	1.0	1.00	7.98	S3NV000651	1.0	0.55	9.33	0707-0152239	1.0	1.00	9.10	Star	A4III <sup>s</sup>	
J074826.5-190216	1.25	1.3± 0.3	0.8± 0.3	07482637-1902149	3.0	0.43	14.74	S3NV032619	3.4	0.17		0709-0152805	2.6	0.75	15.45	Star	F7V <sup>sp</sup>	
J074828.7-191245	1.16	1.8± 0.4	0.5± 0.3												EG	Gal <sup>image</sup>		
J074829.0-191641	0.70	9.2± 0.9		07482906-1916413	0.1	1.00	10.23	S3NV000630	0.0	1.00	11.82	0707-0152292	0.0	1.00	11.56	Star	F4V <sup>sp</sup>	
J074829.3-191425	2.01	1.4± 0.4	0.0± 0.2	07482946-1914262	2.4	1.00	8.26	S3NV000593	2.4	1.00	10.80	0707-0152301	2.4	1.00	10.13	Star	G7III <sup>sp</sup>	
J074830.1-190245	1.51	0.9± 0.3	0.8± 0.3	07483023-1902410	4.6	0.20	14.07	S3NV032232	4.6	0.10		0709-0152879	4.4	0.42	15.30	Star	M5V <sup>sp</sup>	
J074832.1-185427	0.57	22.0± 2.1	1.4± 0.8	07483207-1854278	0.5	1.00	11.72	S3NU018280	0.4	1.00		0710-0151161	0.3	1.00	13.62	Star	G2V <sup>sp</sup>	
J074836.0-185324	2.49			07483626-1853267	4.4	0.68	13.74	S3NU018812	4.1	0.77		0711-0152383	5.5	0.69				
J074836.9-191058	1.62	0.9± 0.3	1.2± 0.4	07483695-1910595	1.1	0.81	15.00	S3NV025814	5.1	0.02		0708-0152650	5.0	0.19	15.98			
J074837.8-185837	1.44	0.7± 0.3	0.5± 0.3												0710-0151250	3.9	0.16	17.44
J074839.6-191301	1.38	0.2± 0.3	2.2± 0.5					S3NV053803	1.6	0.57					EG	Gal <sup>image</sup>		
J074841.3-190004	1.78	0.6± 0.3	0.5± 0.4	07484118-1900030	2.6	0.87	13.87	S3NU015531	2.9	0.85		0709-0153068	4.4	0.78				
J074841.5-190427	1.39	0.8± 0.3	0.1± 0.2	07484163-1904293	2.1	0.98	11.54	S3NU000818	2.0	1.00		0709-0153075	1.9	0.84	12.80	Star	F4V <sup>sp</sup>	
J074842.7-190343	1.22	1.6± 0.4	2.8± 0.5	07484262-1903453	3.1	0.21	15.87	S3NU013927	3.0	0.12		0709-0153091	3.2	0.36	18.27			
J074843.8-190653	1.57	1.3± 0.3	0.1± 0.2					S3NU050871	1.5	0.45		0708-0152762	1.6	0.56	20.39			
J074844.0-191029	0.39	0.3± 0.3	0.3± 0.4												Star	K1III <sup>s</sup>		
J074846.8-190338	1.20	1.7± 0.4	1.5± 0.4					S3NU013964	1.1	0.69		0709-0153175	1.4	0.66	19.78	EG	Gal <sup>image</sup>	
J074847.1-190410	0.53	0.5± 0.3	14.0± 0.9	07484710-1904112	0.7	0.97	14.78	S3NU013757	0.8	0.93		0709-0153176	1.7	0.27	17.61	EG	AGN <sup>sp</sup>	
J074849.6-191704	0.79	5.8± 0.8	6.4± 1.2												EG	AGN <sup>sp</sup>		
J074849.7-190900	1.54	0.8± 0.3	0.9± 0.4												EG	AGN <sup>sp</sup>		
J074851.5-190746	1.50	1.2± 0.3	0.2± 0.3	07485130-1907493	4.6	0.97	14.23	S3NU012384	0.6	0.98		0708-0152846	0.5	0.97	14.52	Star	K4V <sup>sp</sup>	
J074852.5-185856	0.86	4.1± 0.7	2.1± 0.6												EG	AGN <sup>sp</sup>		
J074853.7-190127	2.15	1.0± 0.4	0.9± 0.5	07485392-1901245	3.4	0.44	15.18	S3NU014923	3.8	0.12		0709-0153296	3.5	0.35	19.58			
J074854.0-185629	1.79	2.1± 0.6	0.4± 0.4	07485400-1856300	0.6	0.94	13.79	S3NU017179	0.5	0.94		0710-0151522	0.5	0.93	15.36			
J074855.3-185823	0.81	6.5± 0.8	0															

**Table 18.** X-ray parameters for detected sources in field PSRJ0117+5914

2XMM Name	$r_{90}$ [""]	$\text{pn\_B1}^*$ [cts $\text{ks}^{-1}$ ]	$\text{pn\_B2}^{**}$ [cts $\text{ks}^{-1}$ ]	2MASS Name	$d_{x-o}$ [""]	$P_{id}$	kmag	GSC Name	$d_{x-o}$ [""]	$P_{id}$	V	USNO Name	$d_{x-o}$ [""]	$P_{id}$	R	Class <sup>†</sup>	SpT <sup>‡</sup>
J011559.0+590914	1.44	$17.7 \pm 3.5$	$9.9 \pm 4.6$	01155905+5909141	0.2	0.99	9.49	NAMI000071	0.1	1.00	11.41	1491-0041464	0.1	1.00	11.11	HMXB	Be/X <sup>sp</sup>
J011610.8+591341	1.79	$5.2 \pm 1.8$	$9.2 \pm 3.0$	01161131+5913387	4.2	0.55	14.96	NAMI032506	1.1	0.60	1492-0040572	1.2	0.42	17.37			
J011637.5+591434	3.08	$2.9 \pm 1.2$	$1.2 \pm 1.5$	01163885+5914375	10.3		15.03	NAMI033223	10.6	0.24	1492-0040833	2.6	0.25	19.23			
J011655.4+591807	1.64	$7.4 \pm 1.6$	$1.5 \pm 0.9$	01165553+5918054	2.5	0.86	12.29	NAMK004202	2.5	0.91	14.93	1493-0042033	4.6	0.94	15.91	Star	K4V <sup>sp</sup>
J011705.5+592228	2.22	$1.5 \pm 1.2$	$2.2 \pm 1.7$					NAMK006268	0.6	0.53	18.54	1493-0042154	0.7	0.52	18.66		
J011734.6+591516	1.58	$2.6 \pm 0.9$	$4.3 \pm 1.2$	01173479+5915147	2.0	0.68	14.80	NAMI033702	2.2	0.70	17.49	1492-0041424	1.4	0.81	17.23	Star	F0V <sup>sp</sup>
J011747.5+591836	1.65	$1.7 \pm 0.8$	$3.8 \pm 1.2$	01174685+5918373	5.0	0.03	15.54	NAMI035913	5.0	0.01	17.32	1493-0042571	5.2	0.01	16.97		
J011749.3+591235	1.42	$6.0 \pm 1.2$	$1.6 \pm 0.7$	01174933+5912341	1.6	0.92	12.14	NAMI031660	1.6	0.97	14.38	1492-0041539	3.8	0.89	14.15	Star	F7V <sup>sp</sup>
J011750.6+592032	1.79	$10.4 \pm 4.2$	$0.2 \pm 2.5$					NAMK005215	3.0	0.18	1493-0042609	2.7	0.31	19.06			
J011754.2+591001	1.47	$9.9 \pm 1.7$	$3.2 \pm 1.2$	01175433+5909598	1.5	0.95	11.45								Star	K1V <sup>sp</sup>	
J011757.0+591149	1.21	$21.9 \pm 2.3$	$0.9 \pm 0.7$	01175713+5911480	1.9	0.93	11.74	NAMI000044	1.8	0.98	13.55	1491-0042638	1.5	0.98	13.35	Star	G7V <sup>sp</sup>
J011757.3+590835	1.78	$3.8 \pm 1.2$	$0.4 \pm 0.6$	01175724+5908338	1.3	0.61	15.59	NAMI049432	0.9	0.50							
J011801.6+591420	1.73	$4.1 \pm 1.9$	$4.6 \pm 2.3$	01180198+5914176	3.5	0.70	13.06	NAMI032938	3.7	0.63	16.30	1492-0041699	3.3	0.70	15.92		
J011801.9+591757	2.18	$1.8 \pm 0.8$	$2.6 \pm 1.1$	01180162+5917587	2.9	0.34	16.55	NAMI035516	3.1	0.53	18.03	1492-0041691	3.5	0.46	17.74		
J011804.5+592442	2.13	$3.0 \pm 1.3$	$4.8 \pm 2.1$	01180421+5924383	5.3	0.76	15.02	NAMK007593	1.9	0.67		1494-0043767	1.2	0.50	17.37		
J011806.9+592641	1.33	$15.9 \pm 2.9$	$29.4 \pm 4.8$									1494-0043783	2.6	0.38	18.67	Star	A3V <sup>sp</sup>
J011820.1+592010	1.36	$11.3 \pm 2.1$	$11.9 \pm 2.5$	01182060+5920083	4.4		15.87	NAMI036823	4.2			1493-0042884	4.3		19.07		
J011836.8+591849	1.07	$40.4 \pm 3.6$	$32.0 \pm 3.6$	01183707+5918487	2.1	0.62	15.10	NAMI036019	1.9	0.61		1493-0043028	1.8	0.65	18.80		
J011842.9+591555	1.97	$4.8 \pm 1.5$	$0.8 \pm 0.9$	01184299+5915543	1.3	0.78	14.39	NAMI034108	1.4	0.75	17.88	1492-0042114	1.1	0.74	17.06		
J011849.0+591510	1.87	$2.3 \pm 1.0$	$3.5 \pm 1.5$					NAMI033543	2.9	0.35	18.60	1492-0042172	2.7	0.36	18.59		
J011916.5+591037	2.02	$9.3 \pm 3.9$	$2.5 \pm 3.4$					NAMI030086	1.7	0.31		1491-0043444	1.4	0.39	19.14		

**Table 19.** X-ray parameters for detected sources in field Ridge 1

2XMM Name	$r_{90}$ [""]	$\text{pn\_B1}^*$ [cts $\text{ks}^{-1}$ ]	$\text{pn\_B2}^{**}$ [cts $\text{ks}^{-1}$ ]	2MASS Name	$d_{x-o}$ [""]	$P_{id}$	kmag	GSC Name	$d_{x-o}$ [""]	$P_{id}$	V	USNO Name	$d_{x-o}$ [""]	$P_{id}$	R	Class <sup>†</sup>	SpT <sup>‡</sup>
J185059.1+001650	1.62	$1.4 \pm 2.1$	18505896+0016476	4.6	13.91	N1NL009316	5.6			0902-0383927	4.4	0.02	18.21				
J185110.4+000815	1.37	$5.0 \pm 0.7$	$0.2 \pm 0.3$	18511045+0008152	0.3	0.98	11.03	N1NL000215	0.5	1.00	13.25	0901-0383704	0.5	1.00	12.99	Star	K1V <sup>sp</sup>
J185114.3-000004	1.07	$1.3 \pm 0.7$	$40.3 \pm 2.7$	18511447-0000036	1.5	0.64	11.80										
J185116.3+000515	1.77	$0.1 \pm 0.2$	$2.5 \pm 0.7$	18511640+0005138	2.0	0.58	12.40	N1NL024991	2.2	0.69	0900-0386154	2.2	0.70	17.28			
J185124.0-000349	2.51			18512423-0003435	6.3	0.37	12.19	S9LE138888	8.5	0.34	18.97	0899-0386249	1.3	0.26	18.15		
J185124.5+000430	1.63	$0.5 \pm 0.3$	$2.5 \pm 0.6$	18512445+0004337	3.8	0.36	10.30	N1NL023734	4.6			0900-0386440	4.3		18.71		
J185125.1+000742	1.11	$9.7 \pm 0.8$	$0.4 \pm 0.3$	18512525+0007422	2.3	0.69	8.73	N1NL000216	1.5	1.00	11.18	0901-0384185	1.5	1.00	10.80	Star	F4V <sup>sp</sup>
J185135.3+000928	1.17	$9.7 \pm 1.7$	$0.7 \pm 1.0$	18513544+0009288	1.1	1.00	8.93	N1NL000209	1.1	1.00	10.29	0901-0384552	1.1	1.00	9.83	Star	G2V <sup>sp</sup>
J185137.1+000936	1.99	$1.4 \pm 1.1$	$2.2 \pm 1.3$	18513704+0009407	4.6	0.08	11.96	N1NL032411	4.3	0.01	0901-0384607	5.2		18.28			
J185137.3-000330	1.46			18513733-0003314	0.8	0.91	11.05	S9LE139786	1.8	0.49		0899-0386994	1.5	0.92	15.04		
J185139.1+001635	1.08	$16.6 \pm 1.2$	$13.0 \pm 1.3$	18513925+0016350	2.2	0.92	8.37	N1NL009237	2.1	0.51	14.41	0902-0384825	1.8	0.98	13.51	Star	K5III <sup>sp</sup>
J185139.9+001308	1.12	$9.6 \pm 0.8$	$0.2 \pm 0.3$	18514005+0013084	2.2	0.95	9.22	N1NL000198	2.2	1.00	10.46	0902-0384844	2.1	1.00	10.10	Star	F4V <sup>sp</sup>
J185140.8+000557	1.62	$1.1 \pm 0.3$	$0.8 \pm 0.4$	18514092+0005574	0.5	0.82	12.12	N1NL026277	0.9	0.62		0900-0387044	0.5	0.70	17.73		
J185142.0+000021	1.54	$2.6 \pm 0.6$	$0.6 \pm 0.4$	18514181+0000226	3.6	0.34	12.30	N1NL015808	2.6	0.51	19.05	0900-0387085	2.5	0.54	18.42		
J185147.2+000924	1.46											0901-0384884	2.7	0.56	18.64		
J185147.6+000733	1.34	$0.5 \pm 0.3$	$3.3 \pm 0.5$	18514778+0007335	1.8	1.00	5.94	N1NL005952	1.8	0.62	17.40	0901-0384899	1.9	0.89	15.40	Star	M5V+ <sup>sp</sup>
J185147.8+000130	1.51	$2.2 \pm 0.5$	$2.1 \pm 0.7$	18514792+0001304	1.5	0.76	12.01	N1NL017920	2.1	0.60		0900-0387281	1.7	0.69	16.77		
J185152.6+001927	1.72	$2.0 \pm 0.6$	$2.1 \pm 1.0$	18515276+0019273	2.4	0.79	10.79	N1NL009914	2.4	0.74	18.68	0903-0382702	2.5	0.72	16.97		
J185207.7+000609	1.95	$2.1 \pm 0.5$	$0.3 \pm 0.4$	18520785+0006100	1.5	0.97	10.42	N1NL000222	1.5	1.00	12.46	0901-0385400	1.3	1.00	12.43	Star	F9V <sup>sp</sup>
J185208.3+001507	1.69	$0.4 \pm 0.9$	$2.4 \pm 2.3$	18520846+0015048	3.2	0.40	11.67	N1NL000188	3.2	0.94	13.88	0902-0385423	3.2	0.94	13.50	Star	K1V <sup>sp</sup>
J185209.9+001207	1.50	$0.5 \pm 0.7$	$3.4 \pm 1.3$	18521006+0012073	2.4	0.91	7.85	N1NL035928	2.0	0.46		0902-0385469	1.9	0.58	17.53		
J185222.3+001127	2.64	$0.2 \pm 0.3$	$0.6 \pm 0.5$	18522230+0011266	1.2	0.29	11.88	N1NL035142	6.5	0.05		0901-0385782	6.5	0.04	16.17		
J185226.9+000353	2.20	$2.6 \pm 0.8$	$1.7 \pm 1.0$	18522711+0003543	2.7	0.39	12.16					0900-0389003	0.7	0.07	21.00		
J185233.2+000638	1.19	$16.8 \pm 1.6$	$13.1 \pm 1.9$	18523311+0006362	3.0		13.94	N1NL027810	2.5	0.19	18.48	0901-0386136	2.8	0.41	16.42		
J185242.0+000715	2.95	$3.6 \pm 0.9$		18524201+0007205	5.3	0.88	10.26	N1NL000455	3.4	0.99	11.91	0901-0386495	3.4	0.99	11.28	Star	K0V <sup>sp</sup>

**Table 20.** X-ray parameters for detected sources in field Ridge 2

2XMM Name	$r_{90}$ [""]	$\text{pn\_B1}^*$ [cts $\text{ks}^{-1}$ ]	$\text{pn\_B2}^{**}$ [cts $\text{ks}^{-1}$ ]	2MASS Name	$d_{x-o}$ [""]	$P_{id}$	kmag	GSC Name	$d_{x-o}$ [""]	$P_{id}$	V	USNO Name	$d_{x-o}$ [""]	$P_{id}$	R	Class <sup>†</sup>	SpT <sup>‡</sup>
J184343.2+005330	0.79	11.3±1.4	2.3±1.2	18434320+0053294	0.8	0.99	11.82	N1R4029991	0.9	1.00	16.35	0908-0372937	0.6	1.00	15.25	Star	M0Ve <sup>sp</sup>
J184351.8+004857	1.80	0.9±0.6	1.2±1.0	18435188+0048571	0.7	0.92	13.77	N1R4026955	0.4	0.99	18.54	0908-0373050	0.4	0.98	17.16	Star	M5Ve <sup>sp</sup>
J184353.9+005016	1.67	0.9±0.4	1.8±0.8	18435398+0050137	3.0	0.31	13.88	N1R4060211	2.6								
J184401.2+005455	1.21	2.8±0.6	0.8±0.4	18440115+0054556	0.9	0.98	11.91	N1R4030948	0.8	1.00	17.36	0909-0376768	1.0	0.98	16.03	TTS	K7Ve <sup>sp</sup>
J184409.8+004736	1.35	3.9±0.9	1.2±0.9	18440983+0047354	0.6	0.97	12.46	N1R4026033	0.6	1.00	17.52	0907-0376900	0.3	1.00	15.72	Star	M0Ve <sup>sp</sup>
J184412.9+010106	1.59	1.8±0.4	0.2±0.3	18441291+0101068	0.1	1.00	9.39	N1R4000082	0.0	1.00	10.98	0910-0375578	0.0	1.00	10.49	Star	A9V <sup>sp</sup>
J184413.9+010026	1.38	0.8±0.3	1.0±0.4	18441389+0100268	0.5	1.00	6.42	N1R4034849	0.3	1.00	17.37	0910-0375599	0.7	0.99	15.51	Star	M5III <sup>sp</sup>
J184421.9+005333	1.09	2.3±0.5	0.1±0.2	18442195+0053342	0.7	1.00	9.35	N1R4000100	0.6	1.00	10.68	0908-0373556	0.6	1.00	10.28	Star	F3V <sup>sp</sup>
J184429.7+010546	1.28	3.2±0.8	0.5±0.7	18442956+0105465	2.8	0.89	13.03	N1R4038341	1.4	1.00	15.89	0910-0375912	1.6	0.99	14.89	Star	M2Ve <sup>sp</sup>
J184431.3+005542	2.80	0.2±0.2	0.7±0.4	18443159+0055453	4.7	0.29	13.89	N1R4064783	8.9	0.31		0909-0377245	4.9	0.72	17.71		
J184436.8+010242	1.33	1.8±0.5	0.3±0.4	18443698+0102420	1.6	0.74	12.75	N1R4036267	2.9	0.13		0910-0376036	1.5	0.79	18.25		
J184437.3+010959	1.27	7.1±1.2	1.1±0.9	18443741+0109595	0.5	0.99	11.16	N1R4000062	0.6	1.00	13.14	0911-0377504	0.7	1.00	12.65	Star	G2V <sup>sp</sup>
J184439.9+005709	1.03	1.9±0.5	2.0±0.6	18443986+0057088	1.2	0.86	12.67	N1R4032511	1.0	0.93		0909-0377370	1.0	0.92	18.32		
J184440.4+004904	0.92	7.5±1.0	0.4±0.4	18444046+0049048	0.9	1.00	10.44	N1R4000113	0.8	1.00	12.26	0908-0373785	0.8	1.00	11.71	Star	F7V <sup>sp</sup>
J184443.4+005908	2.08	1.8±0.5	0.8±0.5	18444347+0059054	3.2	0.20	12.81	N1R4033886	3.0	0.82	17.62	0909-0377420	2.8	0.79	16.29		
J184444.3+005123	0.97	7.1±0.9	0.0±0.5	18444442+0051232	1.3	0.89	12.56	N1R4028572	1.2	0.99	17.48	0908-0373846	1.0	1.00	15.96	Star	M5Ve <sup>sp</sup>
J184447.7+011131	0.68	71.1±4.1	5.3±1.9	18444773+0111320	0.5	1.00	10.49	N1R4000056	0.8	1.00	12.13	0911-0377699	1.7	1.00	11.33	Star	K2V <sup>sp</sup>
J184450.8+005242	1.70	1.8±0.5		18445096+0052394	3.2	0.59	11.33	N1R4029440	1.5	0.99	17.46	0908-0373969	1.8	0.52		Star	M2Ve <sup>sp</sup>
J184500.5+005330	2.39	3.5±0.8	1.4±0.9	18450047+0053340	3.8	0.60	13.21	N1R4030009	2.9	0.88	18.17	0908-0374143	1.9	0.70	16.35		
J184509.3+005012	1.57	3.7±1.0	3.0±1.3	18450929+0050109	1.7	0.99	8.79	N1NK046109	1.6	0.99	16.40	0908-0374277	1.8	0.99	14.88		
J184510.3+004826	1.72	5.2±1.1		18451046+0048275	2.2	0.99	9.47	N1NK000048	2.2	1.00	10.97	0908-0374297	2.2	1.00	10.67	Star	F7V <sup>s</sup>

**Table 21.** X-ray parameters for detected sources in field Ridge 3

2XMM Name	$r_{90}$ [""]	pn-B1* [cts $\text{ks}^{-1}$ ]	pn-B2** [cts $\text{ks}^{-1}$ ]	2MASS Name	$d_{x-o}$ [""]	$P_{id}$	kmag	GSC Name	$d_{x-o}$ [""]	$P_{id}$	V	USNO Name	$d_{x-o}$ [""]	$P_{id}$	R	Class <sup>†</sup>	Spt <sup>‡</sup>
J182650.4-112632	1.96	$2.5 \pm 1.2$	$3.6 \pm 1.7$	18265065-1126375	5.9	12.83	S9JO083709	3.3	0.08							HeAe	A0V <sup>sp</sup>
J182658.4-113258	1.59	$2.9 \pm 1.1$	$2.4 \pm 1.2$	18265832-1132585	1.5	0.96	9.80	S9JO000207	1.3	0.99	0784-0427781	5.0	0.99		Star	G9 <sup>s</sup>	
J182703.7-113713	0.92	$13.8 \pm 2.4$	$8.1 \pm 2.2$	18270375-1137135	0.1	0.95	11.68	S9JO041110	1.7	0.90	0783-0443340	1.7	0.89	15.69			
J182706.3-112436	0.94	$0.2 \pm 0.5$	$22.7 \pm 3.1$	18270617-1124385	2.8		13.27	S9MW001589	2.8	0.20	0785-0414570	2.8	0.25	16.79			
J182711.5-113256	1.91	$0.9 \pm 0.7$	$4.2 \pm 1.5$	18271134-1132578	3.5	0.04	14.49	S9JO044929	3.6	0.27	0784-0428047	3.4	0.42	18.16			
J182711.9-112805	1.58	$0.6 \pm 0.6$	$2.7 \pm 1.1$	18271176-1128058	3.4	0.11	12.76	S9JO050244	2.8	0.51	0785-0414707	2.9	0.48	17.90			
J182714.7-111814	1.49	$4.8 \pm 1.7$	$5.6 \pm 2.0$				S9MW008373	2.5	0.33	0786-0413390	4.7	0.04	20.04	Star	M6V <sup>sp</sup>		
J182718.0-112823	1.42	$2.6 \pm 0.8$	$2.5 \pm 1.0$	18271806-1128261	3.0	0.81	11.60	S9JO049977	1.3	0.92	0785-0414827	1.2	0.92	15.92	Star	F8V <sup>sp</sup>	
J182726.8-112040	1.23	$8.3 \pm 1.8$	$3.4 \pm 1.6$	18272674-1120398	1.1	0.92	11.52	S9MW005936	1.3	0.99	0786-0413664	1.1	0.99	14.39	Star	G2V <sup>sp</sup>	
J182728.5-113741	1.04	$11.3 \pm 2.0$	$2.0 \pm 1.1$	18272856-1137400	1.6	0.91	11.02	S9JO000332	3.0	0.90	0783-0443878	2.7	0.86	13.51	Star	G3V <sup>sp</sup>	
J182730.5-113512	1.92	$4.8 \pm 1.2$	$1.6 \pm 1.0$	18273027-1135116	4.2	0.79	10.56	S9JO000268	4.4	0.98	0784-0428420	6.2	0.97		Star	A2V <sup>sp</sup>	
J182732.2-113357	0.82	$4.6 \pm 1.1$	$12.3 \pm 1.9$	18273223-1133571	0.5	0.99	9.88	S9JO076856	0.4	0.93	0784-0428444	0.9	0.93	17.72			
J182734.2-112303	1.39	$5.0 \pm 1.3$	$1.0 \pm 1.3$	18273432-1123045	1.5	0.57	13.35	S9MW042864	1.4	0.55	0786-0413863	5.2	0.05	18.86	Star	M5V <sup>sp</sup>	
J182736.5-113751	1.65	$2.8 \pm 1.1$	$0.5 \pm 0.9$	18273637-1137497	3.0	0.51	13.34	S9JO040369	5.4	0.88	0783-0444064	5.2	0.89	17.41			
J182740.3-113953	0.73	$36.9 \pm 3.7$	$2.8 \pm 1.8$	18274040-1139532	0.7	0.95	10.03	S9JO038707	1.2	0.84					Star	M5V <sup>sp</sup>	
J182741.2-112716	1.13	$6.9 \pm 1.3$	$1.8 \pm 0.9$	18274138-1127132	3.2	0.95	11.97	S9JO051242	1.5	0.97	0785-0415307	1.4	0.97	15.24	Star	K0V <sup>sp</sup>	
J182744.6-113957	1.37	$11.9 \pm 2.2$	$0.3 \pm 0.7$	18274465-1139576	0.3	1.00	8.78	S9JO000395	0.4	1.00	0783-0444254	0.6	1.00	11.31	Star	G8III <sup>sp</sup>	
J182749.2-112137	1.64	$6.0 \pm 1.7$	$1.1 \pm 1.2$	18274911-1121402	3.4	0.77	11.24	S9MW004873	1.9	0.57	0786-0414235	1.8	0.62	17.71	Star	M4V <sup>sp</sup>	
J182749.5-113725	1.24	$5.0 \pm 1.4$	$8.1 \pm 2.3$	18274944-1137264	1.6	0.80	10.97	S9JO040657	1.4	0.71	0783-0444363	1.2	0.77	18.35			
J182819.0-113021	2.03	$5.9 \pm 1.9$	$1.0 \pm 1.1$	18281911-1130202	2.0	0.76	10.32	S9JO079893	5.0	0.01							
J182824.8-112719	1.98	$2.4 \pm 2.0$	$14.2 \pm 4.2$	18282509-1127191	3.7	0.20	11.35	S9JO050970	5.6	0.14	0785-0416368	4.3	0.24	16.93			

**Table 22.** X-ray parameters for detected sources in field Ridge 4

2XMM Name	$r_{90}$ [""]	$\text{pn\_B1}^*$ [cts $\text{ks}^{-1}$ ]	$\text{pn\_B2}^{**}$ [cts $\text{ks}^{-1}$ ]	2MASS Name	$d_{x-o}$ [""]	$P_{id}$	kmag	GSC Name	$d_{x-o}$ [""]	$P_{id}$	V	USNO Name	$d_{x-o}$ [""]	$P_{id}$	R	Class <sup>†</sup>	SpT <sup>‡</sup>
J182811.6-110436	1.47	$3.5 \pm 1.2$	$7.7 \pm 1.9$													Star	M2V <sup>s</sup>
J182813.6-110112	1.65	$1.6 \pm 1.1$	$11.9 \pm 2.8$	18281374-1101113	1.8	0.53	11.47	S9MW014554	1.5	0.62	0788-0410068	1.6	0.63	18.48			
J182816.1-111127	1.85	$2.9 \pm 1.0$		18281645-1111277	3.9	0.29	12.77	S9MW047577	3.7	0.04	0787-0411021	3.6	0.09	18.43			
J182819.8-111756	2.02	$4.5 \pm 2.0$	$7.7 \pm 2.9$	18281958-1117529	5.1	0.22	10.52	S9MW022732	1.6	0.94	0790-0407829	1.7	0.92	15.36			
J182822.9-105955	2.24	$0.2 \pm 0.7$	$12.0 \pm 3.3$	18282307-1059563	1.5	0.82	11.07										
J182827.5-111749	1.25	$4.5 \pm 1.9$	$49.2 \pm 6.7$	18282760-1117485	2.0	0.09	11.95										
J182832.1-112009	2.31			18283173-1120066	6.4	0.27	10.59	S9MW006275	5.6	0.21	0786-0415215	3.1	0.48	18.23			
J182845.5-111710	1.03	$287.8 \pm 12.9$	$25.8 \pm 5.3$	18284546-1117112	1.2	0.98	8.96	S9MW000461	0.6	1.00	0787-0411608	1.2	1.00	11.77	Star	M1e <sup>s</sup>	

**Table 23.** X-ray parameters for detected sources in field Saturn

2XMM Name	$r_{90}$ [""]	$\text{pn\_B1}^*$ [cts $\text{ks}^{-1}$ ]	$\text{pn\_B2}^{**}$ [cts $\text{ks}^{-1}$ ]	2MASS Name	$d_{x-o}$ [""]	$P_{id}$	kmag	GSC Name	$d_{x-o}$ [""]	$P_{id}$	V	USNO Name	$d_{x-o}$ [""]	$P_{id}$	R	Class <sup>†</sup>	SpT <sup>‡</sup>
J055449.8+221341	1.56	$2.9 \pm 0.7$	$0.4 \pm 0.5$	05544979+2213421	1.3	1.00	11.52	NA68000286	1.4	1.00	13.42	1122-0115462	1.6	1.00	12.69	Star	G0V <i>sp</i>
J055452.2+220557	0.73	$5.1 \pm 0.9$	$9.7 \pm 1.5$	05545226+2205570	1.0	0.98	14.23	NA68004885	1.1	0.92		1120-0103285	1.3	0.63	18.90		
J055458.2+221758	1.88	$1.9 \pm 0.7$	$2.4 \pm 1.0$	05545839+2217598	2.0	0.44	15.44	NA68011496	1.7	0.89	18.51	1123-0112485	2.0	0.88	17.29		
J055504.8+220617	1.22	$2.8 \pm 0.6$	$0.1 \pm 0.4$	05550465+2206156	2.8	0.42	14.13	NA68005051	2.6	0.17		1121-0112930	2.7	0.25	18.11		
J055512.1+220523	1.82	$1.1 \pm 0.4$	$0.4 \pm 0.4$	05551224+2205240	1.1	1.00	11.26	NA68004633	1.2	0.98	16.04	1120-0103505	1.2	0.96	14.62		
J055513.6+215601	1.58	$3.7 \pm 0.9$	$0.8 \pm 1.3$	05551351+2156008	1.9	1.00	8.16	NA68000511	1.8	1.00	10.75	1119-0101543	1.8	1.00	10.00	Star	K2III <i>sp</i>
J055514.2+221849	1.65	$2.3 \pm 0.7$	$0.3 \pm 0.6$	05551422+2218487	0.5	0.97	13.90	NA68012008	0.5	0.92	18.90	1123-0112707	0.1	0.91	17.92		
J055518.4+215539	0.54	$46.6 \pm 3.3$	$0.5 \pm 1.2$	05551838+2155386	0.8	1.00	10.02	NA68032153	0.6	1.00	14.76	1119-0101592	1.3	0.75	14.08	Star	M4Ve <i>sp</i>
J055526.1+221248	1.93	$1.5 \pm 0.4$		05552636+2212497	2.9	0.87	13.47	NA68008500	3.0	0.89	16.53	1122-0115847	3.0	0.88	15.36		
J055530.7+221724	1.95	$0.3 \pm 0.4$	$2.6 \pm 0.8$	05553085+2217235	2.1	0.92	13.56	NA68011155	3.1	0.91	15.18	1122-0115910	2.6	0.59	14.09		
J055533.5+221507	1.40	$2.1 \pm 0.5$	$0.7 \pm 0.4$	05553345+2215064	2.2	0.86	13.64	NA68009771	2.0	0.93	16.93	1122-0115958	2.2	0.87	15.55		
J055536.2+220504	1.50	$1.0 \pm 0.3$	$0.6 \pm 0.3$	05553616+2205052	1.0	0.96	14.04	NA68004474	0.8	0.97	17.49	1120-0103782	1.3	0.96	16.28		
J055544.8+221028	1.13	$1.5 \pm 0.4$	$0.6 \pm 0.3$	05554484+2210289	0.7	0.92	15.60	NA68007224	0.7	0.85		1121-0113406	0.6	0.83	19.10		
J055551.2+220714	1.25	$1.1 \pm 0.3$	$1.7 \pm 0.5$	05555106+2207119	3.3	0.98	13.83	NA68000376	0.2	1.00	14.16	1121-0113474	0.3	1.00	13.42	Star	A2V <i>sp</i>
J055553.9+220033	0.86	$8.3 \pm 1.0$	$0.4 \pm 0.4$	05555404+2200330	0.8	1.00	11.12	NA68000457	0.8	1.00	14.17	1120-0103973	0.9	1.00	13.11	Star	G9V <i>sp</i>
J055605.7+221727	2.19	$2.0 \pm 0.7$	$0.2 \pm 0.5$	05560562+2217303	3.6	0.65	14.41	NA68011225	3.7	0.51	17.87	1122-0116389	3.9	0.51	16.88		
J055617.5+221352	2.12	$1.3 \pm 0.6$		05561773+2213516	3.2	0.74	14.47	NA68009082	3.4	0.70	17.78	1122-0116544	3.0	0.75	16.82		
J055619.7+221115	0.70	$15.4 \pm 1.5$	$0.3 \pm 0.5$	05561977+2211157	0.4	1.00	10.79	NA68007675	1.0	1.00	15.70	1121-0113833	0.7	0.98	14.23	Star	M5Ve <i>sp</i>

**Table 24.** X-ray parameters for detected sources in field WR110

**Table 25.** X-ray parameters for detected sources in field Z And

2XMM Name	$r_{90}$ [""]	$pn\_B1^*$ [cts $\text{ks}^{-1}$ ]	$pn\_B2^{**}$ [cts $\text{ks}^{-1}$ ]	2MASS Name	$d_{x-o}$ [""]	$P_{id}$	kmag	GSC Name	$d_{x-o}$ [""]	$P_{id}$	V	USNO Name	$d_{x-o}$ [""]	$P_{id}$	R	Class <sup>†</sup>	SpT <sup>‡</sup>
J233223.2+485251	2.75	$3.4 \pm 1.1$	$0.1 \pm 1.3$					N16Z023098	4.1	0.28		1388-0496401	3.9	0.47	19.15		
J233229.3+484757	1.95	$3.3 \pm 0.9$	$1.9 \pm 0.9$					N16Z020914	4.1	0.28		1387-0498129	3.8	0.52	18.02		
J233245.9+484354	1.06	$7.0 \pm 1.2$		23324587+4843533	1.3	1.00	10.50	N16Z000014	1.3	1.00	13.32	1387-0498227	1.3	1.00	12.37	Star K0V <sup>sp</sup>	
J233247.1+484326	1.83	$2.7 \pm 0.8$	$0.5 \pm 0.7$	23324713+4843247	1.8	1.00	10.63	N16Z000019	1.7	1.00	12.16	1387-0498236	1.3	1.00	11.44		
J233254.5+484831	0.61	$24.9 \pm 1.7$	$10.6 \pm 1.4$	2332545+4848309	0.3	0.99	14.70	N16Z021191	0.5	0.98	18.64	1388-0496609	0.3	0.99	17.35	EG EG <sup>sp</sup>	
J233309.4+484933	1.82	$0.7 \pm 0.4$	$1.5 \pm 0.6$					N16Z021729	6.2	0.01	18.90						
J233315.1+485635	1.45	$2.0 \pm 0.7$	$0.2 \pm 0.6$	23331494+4856350	1.8	1.00	7.98	N16Z000541	2.0	0.60	9.13	1389-0500243	2.0	1.00	8.83	Star F8III <sup>s</sup>	
J233315.9+484651	0.81	$5.2 \pm 0.8$	$0.1 \pm 0.3$	23331597+4846505	0.8	1.00	12.62	N16Z020379	0.8	0.98	17.78	1387-0498432	0.6	0.98	16.96	Star M4V <sup>sp</sup>	
J233317.0+484138	1.78	$1.9 \pm 0.6$	$1.3 \pm 0.6$					N16Z017706	1.2	0.80		1386-0498636	1.5	0.79	19.06		
J233324.8+485804	1.91	$2.9 \pm 1.0$	$0.2 \pm 0.7$	23332495+4858048	1.1	0.92	13.47	N16Z025328	1.1	0.89	17.88	1389-0500345	1.3	0.85	16.84	Star M2V <sup>sp</sup>	
J233329.1+485728	1.79	$2.2 \pm 0.8$	$0.8 \pm 1.0$	23332918+4857261	2.6	0.65	15.01	N16Z025047	2.5	0.60		1389-0500379	2.3	0.56	16.72		
J233335.1+485424	0.85	$6.3 \pm 1.0$	$2.0 \pm 0.8$					N16Z023816	1.6	0.67		1389-0500419	1.0	0.87	19.35		
J233340.9+485715	0.78	$18.3 \pm 1.9$	$2.0 \pm 1.1$	23334111+4857164	1.5	0.99	11.51	N16Z025017	1.6	0.98	14.67	1389-0500476	1.6	0.97	14.03	Star K0V <sup>sp</sup>	
J233349.7+484142	2.25	$1.2 \pm 0.5$	$0.5 \pm 0.5$									1386-0498858	7.0	0.23	18.21		
J233349.9+483651	1.55	$4.1 \pm 1.0$	$1.9 \pm 1.4$	23334989+4836502	1.4	1.00	9.38	N16Z000079	1.7	1.00	11.77	1386-0498849	1.7	1.00	11.19	Star K3V <sup>sp</sup>	
J233359.8+485253	1.12	$2.0 \pm 0.7$	$2.2 \pm 0.8$					N16Z023126	1.5	0.64		1388-0497068	1.6	0.73	19.36		
J233401.3+484811	0.84	$7.5 \pm 1.0$	$0.8 \pm 0.6$	23340142+4848111	1.2	1.00	11.99	N16Z021069	1.2	0.99	14.87	1388-0497082	1.0	0.99	14.18	Star G5V <sup>sp</sup>	
J233402.8+485110	0.67	$326.4 \pm 7.4$	$153.9 \pm 6.0$												EG ClGal <sup>s</sup>		
J233404.9+485720	1.09	$8.2 \pm 1.4$	$1.5 \pm 1.0$	23340500+4857208	0.3	1.00	12.11	N16Z025026	0.4	1.00	14.59	1389-0500672	0.4	0.99	14.25	Star K0V <sup>sp</sup>	
J233412.0+484338	1.98	$1.6 \pm 0.6$	$0.8 \pm 0.7$					N16Z018779	6.7	0.01	19.27	1387-0498827	7.3	0.10	19.28		
J233412.4+483833	0.91	$11.2 \pm 1.7$	$0.1 \pm 0.6$	23341251+4838333	1.0	0.99	12.60	N16Z015905	1.0	0.99	14.55	1386-0499016	1.0	0.99	14.19	Star G0V <sup>sp</sup>	
J233419.3+485114	1.09	$5.7 \pm 0.9$	$0.5 \pm 0.7$	23341929+4851141	0.6	0.99	13.27	N16Z022458	0.4	0.99	15.70	1388-0497231	0.5	0.99	15.30	Star K0V <sup>sp</sup>	
J233420.5+484418	1.28	$2.3 \pm 0.7$	$1.8 \pm 0.9$					N16Z019141	2.0	0.63		1387-0498896	2.5	0.55	19.18		
J233422.4+484520	1.94	$5.3 \pm 2.2$	$0.3 \pm 1.4$	23342256+4845208	1.1	1.00	10.54	N16Z000642	1.1	1.00	11.87	1387-0498910	1.1	1.00	11.32	Star F3V <sup>sp</sup>	
J233428.9+483905	1.37			23342881+4839051	1.6	0.91	14.47	N16Z016219	1.6	0.95	16.37	1386-0499132	1.6	0.96	15.79	Star F6V <sup>sp</sup>	
J233431.4+485519	0.74	$4.8 \pm 1.1$	$10.3 \pm 2.1$	23344381+4841070	2.2	0.95	12.10	N16Z017450	2.3	0.79	18.21	1389-0500877	1.7	0.90	18.93		
J233443.8+484109	1.62							N16Z024658	2.5	0.37		1389-0500968	1.3	0.74	19.34		
J233444.2+485625	1.05	$9.4 \pm 1.6$	$3.7 \pm 1.8$														
J233447.0+485434	1.41	$5.6 \pm 1.2$	$2.6 \pm 1.7$	23344688+4854368	2.8	0.96	11.51	N16Z000567	2.8	0.98	13.41	1389-0500983	3.1	0.95	13.02	Star G1V <sup>sp</sup>	
J233500.4+484601	1.11	$13.8 \pm 2.0$	$0.8 \pm 1.0$	23350049+4846006	1.1	1.00	11.22	N16Z020023	1.1	0.98	1387-0499194	0.9	0.99	15.09	Star M4V <sup>sp</sup>		
J233509.9+485114	2.24	$3.7 \pm 1.1$	$3.5 \pm 2.3$	23350993+4851114	3.2	1.00	8.36	N16Z022625	4.2	0.70		1388-0497584	3.1	1.00	10.69	Star K2III <sup>sp</sup>	

**Table 26.** X-ray parameters for detected sources in field GRB010220

2XMM Name	$r_{90}$ [""]	$\text{pn\_B1}^*$ [cts $\text{ks}^{-1}$ ]	$\text{pn\_B2}^{**}$ [cts $\text{ks}^{-1}$ ]	2MASS Name	$d_{x-o}$ [""]	$P_{id}$	kmag	GSC Name	$d_{x-o}$ [""]	$P_{id}$	V	USNO Name	$d_{x-o}$ [""]	$P_{id}$	R	Class <sup>†</sup>	SpT <sup>‡</sup>
J023523.0+614950	1.73	$14.6 \pm 2.4$		02352318+6149508	1.3	0.96	11.63	NAWC018003	1.5	0.96	15.49	1518-0076033	1.5	0.95	14.72	Star	M0V <sup>sp</sup>
J023538.4+614542	2.03	$12.0 \pm 1.9$	$0.1 \pm 0.5$	02353855+6145438	1.5	0.97	10.84	NAWC00260	1.4	1.00	11.91	1517-0076673	1.4	1.00	11.22	Star	F5V <sup>sp</sup>
J023542.2+615241	1.88	$7.2 \pm 1.7$	$1.0 \pm 1.7$	02354293+6152437	5.4	0.38	11.59	NAWC020661	5.5	0.43	14.59	1518-0076103	5.5	0.37	14.38	Star	K0V <sup>sp</sup>
J023550.9+614424	1.51	$14.9 \pm 1.9$	$1.7 \pm 1.1$	02355110+6144270	2.9	0.86	11.86	NAWC012302	3.1	0.94	14.82	1517-0076766	3.4	0.81	14.38	Star	K1V <sup>sp</sup>
J023608.0+613451	1.53	$20.9 \pm 2.9$		02360804+6134515	0.4	0.99	12.07	NAWC002906	0.4	1.00	14.50	1515-0079451	0.7	0.99	14.41	Star	K0V <sup>sp</sup>
J023611.4+614047	2.46	$3.3 \pm 1.1$	$1.1 \pm 1.1$	02361162+6140496	2.6	0.68	13.52	NAWC008548	2.6	0.70	17.29	1516-0078393	3.0	0.59	16.31	Star	M1V <sup>sp</sup>
J023639.4+613945	2.23	$3.3 \pm 1.0$	$0.1 \pm 0.5$	02363879+6139491	5.8	0.16	12.78	NAWC007370	5.7	0.09	17.13	1516-0078612	5.9	0.07	15.80	Star	M0V <sup>sp</sup>
J023645.0+613638	1.50	$0.9 \pm 0.7$	$33.1 \pm 3.9$	02364508+6136376	0.8	0.93	14.47	NAWC004176	1.0	0.87		1516-0078665	1.2	0.80	17.74		
J023647.0+613922	1.60	$9.8 \pm 1.6$		02364707+6139227	0.3	1.00	10.57	NAWC000369	0.5	1.00	12.84	1516-0078681	0.5	1.00	12.74	Star	F9V <sup>sp</sup>
J023708.5+615709	2.50	$7.9 \pm 2.1$	$0.6 \pm 1.6$	02370828+6157038	6.2	0.55	15.52	NAWC000927	6.6	0.93	12.90	1519-0073694	6.3	0.66	13.28	Star	F9V <sup>sp</sup>
J023714.7+614540	2.15	$3.7 \pm 0.9$	$0.4 \pm 0.5$	02371514+6145368	4.9	0.99	7.73	NAWC000270	4.7	0.99	10.48	1517-0077442	4.7	0.99	9.71	Star	K2III <sup>sp</sup>
J023719.8+614100	2.45	$2.6 \pm 0.9$	$0.8 \pm 0.8$	02372020+6141040	4.1	0.33	13.79	NAWC008819	4.2	0.10	18.35	1516-0078995	4.2	0.06	17.24	Star	M2V <sup>sp</sup>
J023726.4+614538	2.37	$0.0 \pm 0.2$	$6.2 \pm 1.4$	02372712+6145332	7.1	0.06	14.27	NAWC013396	7.3	0.02	17.36	1517-0077545	6.9	0.08	16.33		
J023748.6+613715	2.23	$4.8 \pm 1.4$	$1.7 \pm 1.3$	02374860+6137161	0.6	0.99	11.96	NAWC004740	0.6	1.00	14.71	1516-0079220	1.1	0.99	14.48	Star	G0V <sup>sp</sup>
J023756.8+615857	3.43	$9.0 \pm 2.9$	$7.0 \pm 4.7$	02375691+6159005	2.9	0.72	12.64	NAWC025258	8.6	0.76	19.00	1519-0074134	8.5	0.70	18.29		
J023757.1+614907	1.81	$5.9 \pm 1.4$	$4.7 \pm 1.7$									1518-0077146	3.9	0.22	19.61		

**Table 27.** X-ray parameters for detected sources in field RXJ0925.7-4758

2XMM Name	$r_{90}$ [""]	$\text{pn\_B1}^*$ [cts $\text{ks}^{-1}$ ]	$\text{pn\_B2}^{**}$ [cts $\text{ks}^{-1}$ ]	2MASS Name	$d_{x-o}$ [""]	$P_{id}$	kmag	GSC Name	$d_{x-o}$ [""]	$P_{id}$	V	USNO Name	$d_{x-o}$ [""]	$P_{id}$	R	Class <sup>†</sup>	SpT <sup>‡</sup>
J092432.8-475917	1.51			09243283-4759163	0.9	0.95	13.49	S5MW007845	0.6	0.90		0420-0186803	0.5	0.93	18.26		
J092439.8-475218	1.49	1.9±0.5	0.1±0.4					S5MW009708	3.7	0.03		0421-0198115	3.4	0.20	16.76		
J092448.1-474928	1.18	2.7±0.5	0.9±0.7	09244827-4749265	2.7	0.51	13.75	S5MW010259	2.6	0.77		0421-0198198	2.7	0.72	16.81	Star	M0V <sup>sp</sup>
J092451.8-475905	0.69	8.5±0.8		09245177-4759045	1.4	1.00	8.14	S5MW000060	1.5	1.00	10.82	0420-0187014	1.5	1.00	10.13	Star	K2V <sup>sp</sup>
J092454.9-475427	1.72	1.3±0.4	0.9±0.4	09245501-4754274	0.6	0.98	12.02	S5MW009194	0.7	0.99		0420-0187059	5.2	0.80	13.09	Star	A9V <sup>sp</sup>
J092458.0-480412	3.64							S5MW006353	7.3	0.05		0419-0178555	7.7	0.27	18.39		
J092500.5-480443	1.24							S5MW006271	0.8	0.96		0419-0178577	0.9	0.96	17.18		
J092500.6-474613	1.12	1.9±0.5	3.9±1.0	09250038-4746125	2.6	0.53	15.16	S5MW010884	3.0	0.05		0422-0215654	2.4	0.43	19.54		
J092506.0-475205	1.41	0.5±0.2	1.5±0.5									0421-0198378	2.0	0.87	19.77		
J092507.7-481018	1.23											0418-0170896	0.4	0.99	15.36		
J092512.5-480832	1.22											0418-0170950	1.2	0.96	17.44		
J092513.6-475152	1.29	1.0±0.3	0.4±0.3	09251379-4751521	1.1	0.96	13.83	S5MW009760	2.3	0.51		0421-0198455	1.4	0.61	18.90		
J092516.4-475422	1.83	1.0±0.3	0.1±0.2	09251653-4754209	1.8	1.00	9.47	S5MW009209	1.6	1.00		0420-0187264	2.2	0.92	17.21		
J092518.2-474727	1.64	1.4±0.4	0.3±0.4	09251826-4747282	0.8	0.95	13.98	S5MW010620	0.9	0.97		0422-0215893	1.1	0.97	16.99	Star	M2V <sup>sp</sup>
J092525.4-480654	1.78							S5MW000109	2.3	1.00		0418-0171071	6.4	0.65	0.00		
J092527.3-474755	0.41	41.0±1.5	6.9±0.8					S5MW010573	1.5	0.97						Star	K4V <sup>sp</sup>
J092527.3-480202	1.19	1.6±0.3	0.1±0.2	09252730-4802027	0.8	1.00	10.07	S5MW000076	0.7	1.00	11.96	0419-0178866	0.7	1.00	11.44		
J092531.1-474851	1.60	1.5±0.4	0.9±0.4	09253133-4748512	1.8	0.97	12.83	S5MW010350	1.7	0.99		0421-0198636	1.8	0.79	15.82	Star	G5V <sup>sp</sup>
J092541.3-474759	1.76							S5MW059247	1.4	0.83		0422-0216190	1.2	0.83	19.34		
J092541.7-475310	1.72	0.9±0.3	0.0±0.1	09254173-4753086	2.3	0.98	11.94	S5MW000037	2.1	1.00		0421-0198735	5.1	1.00	0.00		
J092550.0-480150	0.54	10.1±0.6	0.7±0.2	09254994-4801502	0.8	0.98	13.02	S5MW007085	1.0	0.99		0419-0179060	0.6	0.99	16.93		
J092554.4-475017	1.07							S5MW000031	0.8	1.00	11.31	0421-0198878	0.8	1.00	11.23		
J092555.6-474618	1.48							S5MW000021	2.1	1.00	11.65	0422-0216378	2.1	1.00	11.33		
J092556.2-480932	1.28	1.5±0.4	0.4±0.3	09255625-4809330	0.5	0.98	13.27	S5MW004521	0.5	0.97		0418-0171364	0.5	0.97	17.23	Star	M5V <sup>sp</sup>
J092556.3-480421	0.88	2.8±0.4	2.1±0.3	09255633-4804224	0.6	1.00	10.01	S5MW006316	0.0	1.00		0419-0179120	0.3	1.00	15.11		
J092556.5-475927	1.60	0.2±0.3		09255661-4759287	1.5	0.99	11.36	S5MW007778	1.8	0.99		0420-0187660	2.3	0.98	14.17		
J092559.0-480036	2.26	1.0±0.3		09255917-4800369	1.7	0.74	15.02	S5MW058072	1.5	0.67		0419-0179140	2.2	0.76	20.32		
J092603.1-480610	1.52	1.5±0.3	0.7±0.3	09260337-4806143	4.6	0.43	14.55	S5MW005660	4.5	0.01		0418-0171417	5.0	0.01	19.63		
J092616.4-475149	1.54																
J092616.9-475235	1.84			09261713-4752377	3.1	0.28	15.42	S5MW009530	3.2	0.05		0421-0199110	3.7	0.01	19.57		
J092620.3-475822	0.52	9.6±0.6	0.4±0.2	09262038-4758226	0.2	1.00	12.47	S5MW008063	0.4	1.00		0420-0187910	0.7	1.00	14.86	Star	G9V <sup>sp</sup>
J092620.6-480330	0.55	9.8±0.6	0.6±0.2	09262069-4803306	0.5	1.00	12.60	S5MW006574	0.5	1.00		0419-0179349	0.7	1.00	14.94	Star	G9V <sup>sp</sup>
J092621.7-475504	1.17							S5MW008973	0.2	0.99		0420-0187921	2.5	0.85	17.37		
J092622.6-475551	0.47	17.1±0.8	1.5±0.3	09262272-4755508	0.7	0.99	11.78	S5MW000043	0.8	1.00		0420-0187929	0.9	1.00	13.93	Star	G6V <sup>sp</sup>
J092626.2-475633	1.35	1.5±0.4	0.1±0.3	09262624-4756318	1.2	0.99	11.79	S5MW000046	1.1	1.00		0420-0187971	1.0	1.00	13.70	Star	G6V <sup>sp</sup>
J092640.0-475110	0.97			09264001-4751095	0.8	1.00	11.40	S5MW000034	0.9	1.00		0421-0199313	0.5	1.00	13.33		
J092642.4-480845	1.53			09264247-4808445	1.2	1.00	11.27	S5MW000123	1.1	1.00		0418-0171773	2.5	0.82	12.43		
J092649.7-475855	1.90			09264982-4758531	2.1	0.84	14.04	S5MW007879	2.9	0.51		0420-0188178	2.9	0.52	17.60		

**Table 28.** X-ray parameters for detected sources in field ARLac

2XMM Name	$r_{90}$ [""]	$\text{pn\_B1}^*$ [cts $\text{ks}^{-1}$ ]	$\text{pn\_B2}^{**}$ [cts $\text{ks}^{-1}$ ]	2MASS Name	$d_{x-o}$ [""]	$P_{id}$	kmag	GSC Name	$d_{x-o}$ [""]	$P_{id}$	V	USNO Name	$d_{x-o}$ [""]	$P_{id}$	R	Class <sup>†</sup>	SpT <sup>‡</sup>
J220742.2+455258	2.22			22074198+4552576	2.8	0.82	12.21	N2TW034514	2.6	0.60	17.27	1358-0468831	2.9	0.54	16.61	Star	M4Ve <sup>sp</sup>
J220752.3+454742	1.14							N2TW030293	0.5	0.76		1357-0480103	0.4	0.80	18.97		
J220755.6+454838	1.51							N2TW072280	3.4	0.05	19.54	1358-0469023	4.1	0.02	18.71		
J220802.2+455600	2.21			22080238+4556026	2.1	0.96	10.81	N2TW001240	2.2	0.99	12.63	1359-0465243	2.2	0.96	12.11	Star	G9V <sup>sp</sup>
J220804.8+454140	1.37							N2X4071640	1.1	0.56		1356-0483745	1.9	0.53	19.10		
J220805.6+454805	1.32			22080555+4548054	1.1	0.98	11.71	N2X4056378	0.7	0.98	14.33	1358-0469168	1.1	0.97	14.06	Star	K0Ve <sup>sp</sup>
J220808.7+453929	1.63							N2X4055750	3.2	0.27	18.58	1356-0483804	3.2	0.26	18.14		
J220814.1+454034	1.36			22081450+4540347	3.5	0.11	15.74	N2X4055852	4.0	0.01	18.81	1356-0483885	3.4	0.09	18.34		
J220822.6+454535	1.85			22082281+4545330	3.1	0.53	14.94	N2X4056238	2.9	0.68	17.01	1357-0480507	2.5	0.83	15.43	Star	K0V <sup>sp</sup>
J220833.1+454204	2.59			22083387+4542007	8.3	0.88	14.53	N2X4029403	8.8	0.98	18.16	1357-0480660	6.1	0.94	18.43		
J220836.0+454632	2.37							N2X4071910	7.1	0.04		1357-0480711	5.7	0.02	18.74		
J220837.8+453129	1.23			22083774+4531279	2.3	0.98	10.06	N2X4027141	2.4	0.92	15.11	1355-0486243	2.1	0.92	14.41	Star	M4Ve <sup>sp</sup>
J220842.0+453716	2.96							N2X4028358	5.3	0.08	18.81	1356-0484255	5.4	0.11	19.09		
J220855.0+453448	2.40							N2X4072926	5.4			1355-0486459	2.2	0.37	19.25		
J220856.1+455510	1.76							N2X4031802	1.5	0.50		1359-0465995	0.9	0.45	19.17		
J220912.6+454021	1.47							N2X4028954	4.9		18.54						
J220916.5+453255	2.37			22091597+4532508	7.9		14.63	N2X4027369	7.3	0.01	17.16	1355-0486726	7.7		16.37		
J220924.8+454449	1.88			22092428+4544499	5.9	0.39	13.66	N2X4029911	5.1	0.20	15.74	1357-0481411	3.8	0.11	18.74		
J220929.1+455206	2.26							N2X4031245	0.8	0.49		1358-0470349	1.4	0.39	19.21		
J220932.5+454217	2.81			22093291+4542123	6.5	0.03	15.63	N2X4029287	6.8	0.02	18.33	1357-0481525	6.0	0.06	17.88		
J220932.8+454730	2.04			22093282+4547334	2.7	0.45	15.30	N2X4030439	2.6	0.46	18.36	1357-0481524	2.9	0.41	17.83		
J220942.7+454639	1.80			22094274+4546393	0.7	1.00	9.16	N2X4000715	0.7	1.00	9.73	1357-0481668	0.7	1.00	9.58	Star	A5V <sup>sp</sup>

**Table 29.** X-ray parameters for detected sources in field Geminga

2XMM Name	$r_{90}$ [""]	$pn_{\text{B1}}^*$ [cts ks $^{-1}$ ]	$pn_{\text{B2}}^{**}$ [cts ks $^{-1}$ ]	2MASS Name	$d_{x-o}$ [""]	$P_{id}$	kmag	GSC Name	$d_{x-o}$ [""]	$P_{id}$	V	USNO Name	$d_{x-o}$ [""]	$P_{id}$	R	Class $^{\dagger}$	SpT $^{\ddagger}$
J063259.6+174637	2.25			06325942+1746402	4.9	0.14	15.86	N8L5012571	5.0	0.08	18.10	1077-0136581	5.2	0.08	18.61		
J063307.4+175236	1.96							N8L5015706	1.3	0.62	18.61	1078-0139187	2.0	0.46	18.94		
J063313.4+175432	1.49			06331327+1754321	1.4	1.00	8.65	N8L5000363	1.3	1.00	11.53	1079-0140062	1.3	1.00	10.95	Star	K2V $^{sp}$
J063314.2+173539	1.21			06331408+1735389	2.2	0.35	15.07	N8L5006823	2.3	0.20	17.86					Star	K $^{sp}$
J063317.3+175212	2.40			06331730+1752098	2.4	0.83	13.10	N8L5015536	2.3	0.92	13.92	1078-0139361	2.4	0.93	13.86		
J063318.9+175521	1.27			06331896+1755215	1.2	0.95	11.58	N8L5017134	1.1	0.98	14.31	1079-0140185	2.7	0.96			
J063319.4+175035	1.84			06331927+1750390	4.2	0.26	14.93	N8L5014677	4.3	0.07	18.57	1078-0139386	4.4	0.06	18.88		
J063322.6+173430	1.68			06332285+1734348	4.9	0.09	14.96	N8L5006467	5.7		17.21	1075-0135475	5.3	0.02	18.43		
J063324.0+175307	1.63							N8L5015966	3.9			1078-0139446	3.4	0.04	19.05		
J063324.3+174806	1.85							N8L5013314	3.5	0.07		1078-0139440	5.0	0.43	19.10		
J063330.3+175300	2.31			06333026+1753004	1.0	0.75	14.82	N8L5015828	6.9	0.71		1078-0139517	7.3	0.61	19.23		
J063334.0+175512	1.86			06333392+1755104	3.4	0.53	14.64	N8L5017008	3.3	0.41	17.99	1079-0140436	3.6	0.27	17.71		
J063335.4+173408	1.73			06333529+1734091	2.3	0.83	13.71	N8L5006301	1.8	0.88	17.11	1075-0135634	2.2	0.43	18.08		
J063335.5+173927	1.23			06333542+1739278	1.5	0.98	10.02	N8L5008231	1.5	0.99	13.65	1076-0135209	1.8	0.96	13.09	Star	G6V $^{sp}$
J063339.0+175933	1.30							N8L5019086	1.3	0.80	18.55	1079-0140504	1.9	0.31	18.87		
J063341.8+175408	1.98							N8L5016459	5.0			1079-0140559	5.1	0.06	18.85		
J063342.7+175017	1.73							N8L5014405	4.5	0.01		1078-0139723	4.4	0.12	19.27		
J063344.6+175644	1.28			06334452+1756438	1.6	0.73	15.40	N8L5044039	1.5	0.67		1079-0140604	1.6	0.71	19.24		
J063344.8+174552	2.45							N8L5012036	8.3			1077-0137200	7.2		19.20		
J063347.8+173520	1.97							N8L5006655	5.3	0.01	18.35	1075-0135812	5.6	0.01	19.14		
J063349.2+174732	1.46			06334914+1747311	0.9	1.00	8.94	N8L5000416	0.8	1.00	11.56	1077-0137269	0.8	1.00	11.11	Star	K2V $^{sp}$
J063350.2+173444	1.78			06335008+1734448	1.4	0.90	13.34	N8L5006493	1.2	0.94	15.71	1075-0135849	1.7	0.90	15.48	Star	M2Ve $^{sp}$
J063351.2+173826	1.39			06335106+1738254	3.1	0.20	13.37	N8L5007772	2.8	0.24	17.39				Star	M4Ve $^{sp}$	
J063357.3+174050	1.32							N8L5008976	3.1	0.02	17.74						
J063400.3+173624	1.38							N8L5007043	1.6	0.62		1076-0135568	2.4	0.16	18.89		
J063402.6+175308	1.35			06340266+1753066	1.2	0.94	13.43	N8L5015919	1.0	0.98	15.90	1078-0140019	1.1	0.97	15.69		
J063406.7+175945	1.02			06340671+1759451	0.1	1.00	10.01	N8L5019184	0.3	1.00	14.60	1079-0140931	0.1	0.99	14.08	Star	M4Ve $^{sp}$
J063410.3+174949	1.74			06341057+1749476	4.0	0.33	15.34	N8L5014246	3.6	0.67	16.62	1078-0140135	3.3	0.43	15.83		
J063413.0+175652	2.21			06341318+1756519	2.8	0.45	15.89	N8L5017821	2.5	0.59	17.96	1079-0141016	2.1	0.57	18.37		
J063415.6+174000	2.09			06341534+1739546	7.0		15.67	N8L5008390	6.6	0.46		1076-0135782	7.0	0.89	18.26		
J063419.4+174039	1.64			06341951+1740371	2.8	0.92	11.29	N8L5008865	2.4	0.96	14.40	1076-0135839	2.2	0.94	13.89		
J063419.8+173415	1.84							N8L5006261	2.5	0.34		1075-0136304	3.4	0.25	18.85		
J063425.1+174212	1.09			06342536+1742110	3.1	0.48	10.46	N8L5000446	3.2	0.97	11.11	1077-0137788	3.2	0.99	11.02	Star	A7V $^{sp}$
J063431.2+174645	2.42			06343131+1746406	4.4	0.64	13.24	N8L5012515	4.6	0.74	14.56	1077-0137855	4.6	0.76	14.11		
J063434.2+174728	1.83			06343417+1747276	1.3	0.82	14.20	N8L5012877	1.1	0.81		1077-0137888	1.3	0.67	18.83		
J063437.3+173937	2.69			06343704+1739355	4.7	0.71	12.99	N8L5008207	4.7	0.86	14.08	1076-0136067	5.1	0.79	14.03		
J063446.4+174355	2.50							N8L5010882	5.0	0.09	18.15	1077-0138063	4.8	0.12	18.65		
J063449.3+174355	1.96							N8L5010861	5.0	0.01		1077-0138095	5.5	0.02	19.07		

**Table 30.** X-ray parameters for detected sources in field PSR0656+14

2XMM Name	$r_{90}$ [""]	$\text{pn\_B1}^*$ [cts $\text{ks}^{-1}$ ]	$\text{pn\_B2}^{**}$ [cts $\text{ks}^{-1}$ ]	2MASS Name	$d_{x-o}$ [""]	$P_{id}$	kmag	GSC Name	$d_{x-o}$ [""]	$P_{id}$	V	USNO Name	$d_{x-o}$ [""]	$P_{id}$	R	Class <sup>†</sup>	SpT <sup>‡</sup>
J065909.7+141815	2.79							N8NG016348	6.5	0.06	18.03	1043-0124959	6.1	0.07	17.46		
J065911.5+141114	1.42							N8NG013375	5.0	0.02	15.16	1041-0123358	4.5	0.46	14.34	Star K4Ve <sup>sp</sup>	
J065920.2+140910	2.10			06592030+1409103	1.4	0.93	12.99	N8NG012537	1.5	0.91	14.93	1041-0123456	1.2	0.88	15.12		
J065948.6+141917	1.98							N8NG016828	5.7	0.01	17.98	1043-0125399	5.8	0.02	16.86		
J065950.7+142201	1.92							N8NG018137	0.7	0.64		1043-0125421	1.1	0.67	20.25		
J065956.9+141219	1.56			06595708+1412228	3.8	0.93	10.41	N8NG000520	3.5	0.99	12.04	1042-0123543	3.7	0.92	12.10	Star G9V <sup>sp</sup>	
J065959.2+140319	1.56							N8NG031476	1.2	0.56		1040-0123513	0.6	0.68	20.06	Star G0V <sup>sp</sup>	
J070001.0+141210	2.50			07000164+1412093	7.9	0.01	14.91	N8NG013701	8.3	0.38	18.77	1042-0123602	8.1		18.34		
J070003.9+141047	2.23			07000357+1410476	5.0	0.21	15.35	N8NG013163	4.3	0.40	17.24	1041-0123938	4.6	0.32	16.83		
J070006.2+141315	2.95			07000650+1413133	4.8	0.41	14.87	N8NG032672	8.8	0.49		1042-0123658	8.2	0.33	14.53		
J070008.7+140205	3.39							N8NG031372	9.1	0.35		1040-0123627	9.6		18.59		
J070009.6+142213	1.22			07000973+1422159	3.2	0.18	16.27	N8NG018269	2.8	0.46	17.72	1043-0125642	2.9	0.38	17.14	Star K5V <sup>sp</sup>	
J070015.3+142109	1.37							N8NG033935	1.0	0.69		1043-0125715	0.4	0.72	19.23		
J070019.7+141211	1.32			07001983+1412119	1.4	0.95	13.52	N8NG013730	1.5	0.87	17.54	1042-0123794	1.3	0.85	16.76	Star M0Ve <sup>sp</sup>	
J070020.1+140700	2.60			07002034+1406582	3.3	0.72	13.94	N8NG011674	3.5	0.55	17.35	1041-0124133	3.3	0.52	16.56		
J070026.9+142044	2.03			07002693+1420443	0.6	0.97	11.63	N8NG017571	0.4	0.98	13.95	1043-0125854	0.6	0.97	13.71		
J070029.5+140851	1.54			07002926+1408501	4.6	0.01	15.41	N8NG012365	4.4	0.07	18.15	1041-0124255	4.2	0.14	17.77		
J070032.8+140714	1.48			07003287+1407122	2.0	0.96	11.58	N8NG000600	1.9	0.98	13.16	1041-0124287	1.7	0.97	13.21	Star G0V <sup>sp</sup>	

**Table 31.** X-ray parameters for detected sources in field RX J0002+6246

2XMM Name	$r_{90}$ [""]	pn_B1* [cts $\text{ks}^{-1}$ ]	pn_B2** [cts $\text{ks}^{-1}$ ]	2MASS Name	$d_{x-o}$ [""]	$P_{id}$	kmag	GSC Name	$d_{x-o}$ [""]	$P_{id}$	V	USNO Name	$d_{x-o}$ [""]	$P_{id}$	R	Class†	SpT‡
J000100.9+624803	2.85		00010072+6248002	3.2	0.41	14.43	NAKK099897	3.4	0.13		1527-0000767	5.2	0.15				
J000105.3+624933	3.30		00010531+6249344	0.7	0.77	12.85	NAKK101247	9.4	0.66		1528-0000834	0.4	0.59	16.03			
J000114.0+625231	1.28		00011391+6252302	1.0	1.00	7.94	NAKK000440	0.8	1.00	10.47	1528-0000936	0.8	1.00	9.76			
J000130.0+625236	1.68		00013004+6252367	0.2	0.96	12.33	NAKK038949	0.3	0.97	15.65	1528-0001138	5.4	0.94	17.88	Star	K2V <sup>sp</sup>	
J000132.4+624326	2.60		00013333+6243272	6.2	0.50	11.71	NAKK000650	6.3	0.67	13.47	1527-0001201	6.8	0.50	17.77	Star	F3V <sup>sp</sup>	
J000134.1+625008	1.22						NAKK035163	1.1	0.85	17.82	1528-0001181	0.8	0.88	17.48	CV	CV <sup>sp</sup>	
J000135.8+625723	1.89		00013575+6257262	3.2	0.77	12.97	NAKK045931	3.2	0.72	16.62	1529-0001203	3.4	0.63	15.82			
J000150.5+625749	2.98		00015040+6257460	3.8	0.20	15.32	NAKK046355	4.2	0.09	18.81	1529-0001381	4.0	0.11	18.09			
J000203.2+624436	1.74		00020300+6244377	1.7	0.88	13.02	NAKK027914	1.6	0.92	14.72	1527-0001596	0.9	0.54				
J000203.9+625601	2.68						NAKK043581	5.2	0.05	18.49	1529-0001571	7.8	0.04	19.32			
J000208.3+625347	2.22		00020815+6253486	1.3	0.57	15.23	NAKK126605	1.3			1528-0001589	4.3	0.14				
J000222.1+624510	1.79		00022277+6245112	4.7	0.07	15.22	NAKK028607	4.9	0.05	17.70	1527-0001817	3.7	0.06	18.64			
J000238.7+623357	2.67		00023971+6233599	7.2	0.11	14.61	NAKK087638	7.5	0.01		1525-0002122	7.3	0.02	16.78			
J000245.8+625846	2.33		00024589+6258472	0.8	0.80	13.93	NAKK111713	0.9	0.72		1529-0002088	7.4	0.47	15.40			
J000248.0+625149	1.81		00024843+6251514	3.4	0.95	10.45	NAKK124515	4.1	0.75		1528-0002133	3.3	0.52	15.83	Star	F6V <sup>sp</sup>	
J000248.4+624014	2.72		00024908+6240218	8.7	0.06	14.95	NAKK000736	8.6	0.21	13.14	1526-0002314	8.5	0.10	18.71			
J000257.2+624230	1.90		00025683+6242318	2.9	0.42	14.73	NAKK094747	2.9	0.51	17.15	1527-0002332	6.4	0.34	17.80			
J000257.9+623547	2.47						NAKK088977	5.0	0.01		1525-0002369	4.3	0.11	19.27			
J000309.2+625404	2.20		00030922+6254083	3.6	0.42	14.95	NAKK106321	3.5	0.32	17.51	1529-0002370	3.5	0.28	16.77			
J000317.9+623824	2.39		00031845+6238252	3.2	0.58	13.73	NAKK091105	3.2	0.15		1526-0002787	3.8	0.22	16.85	Star	M5V <sup>sp</sup>	
J000323.6+625418	2.03		00032372+6254192	0.7	0.95	12.50	NAKK126633	6.6	0.96		1529-0002562	1.1	0.62	15.19	Star	K2V <sup>sp</sup>	
J000326.5+625629	1.77		00032679+6256308	1.8	0.76	13.91	NAKK131894	5.7	0.80		1529-0002601	2.2	0.73	16.20			
J000335.7+624736	1.48		00033537+6247384	3.8	0.12	15.34	NAKK099381	3.6	0.08	18.52	1527-0002884	3.7	0.08	17.94			
J000336.0+625156	3.07		00033643+6252057	9.2	0.14	15.43	NAKK103938	3.4	0.19	18.50	1528-0002787	9.5	0.20	19.24			
J000340.4+624745	2.42		00034054+6247469	1.7	0.74	13.80	NAKK09689	0.8	0.86	16.68	1527-0002955	1.2	0.60	15.61			
J000351.7+625449	2.29						NAKK107162	6.2			1529-0002895	7.5		19.42			
J000400.2+625330	1.26		00040061+6253275	4.1		15.45	NAKK105549	4.2			1528-0003134	3.7		18.87			
J000404.5+624326	1.18		00040446+6243254	0.8	0.99	11.32	NAKK095530	0.9	0.98	14.83	1527-0003230	0.5	0.98	14.07	Star	M0V <sup>sp</sup>	
J000405.4+624428	1.91		00040535+6244299	1.2	0.87	13.69	NAKK096482	1.1	0.86	16.84	1527-0003241	1.5	0.84	16.17	Star	G0V <sup>sp</sup>	
J000419.3+625342	2.46		00042000+6253375	6.2	0.48	14.13	NAKK105786	6.2	0.37		1528-0003413	7.1	0.56				

**Table 32.** X-ray parameters for detected sources in field SS Cyg

2XMM Name	$r_{90}$ [""]	pn.B1* [cts $\text{ks}^{-1}$ ]	pn.B2** [cts $\text{ks}^{-1}$ ]	2MASS Name	$d_{x-o}$ [""]	$P_{id}$	kmag	GSC Name	$d_{x-o}$ [""]	$P_{id}$	V	USNO Name	$d_{x-o}$ [""]	$P_{id}$	R	Class <sup>†</sup>	SpT <sup>‡</sup>
J214158.1+432518	2.25			21415811+4325110	7.1	0.68	15.50	N2TU118332	1.7	0.91	16.10	1334-0441110	7.5	0.87	18.03	Star	M4Ve <sup>sp</sup>
J214222.8+432332	1.92			21422285+4323330	0.5	0.97	11.88	N2TU116949	0.6	0.92	16.16	1333-0464128	0.8	0.88	15.90	Star	M2Ve <sup>sp</sup>
J214229.5+432533	2.07			21422942+4325320	2.1	0.96	11.29	N2TU118768	2.0	0.95	14.77	1334-0441611	1.7	0.56	14.23	Star	M0Ve <sup>sp</sup>
J214229.8+434615	2.36							N2U5023566	7.0		18.52	1337-0436148	7.2		18.10		
J214232.5+432722	1.40			21423257+4327228	0.2	0.99	11.48	N2U5002936	0.5	0.99	13.97	1334-0441661	0.6	0.98	13.72	Star	K3Ve <sup>sp</sup>
J214309.4+432335	1.83			21430939+4323345	1.3	0.98	10.75	N2TU000683	1.1	0.99	12.98	1333-0464948	6.1	0.98	17.70		
J214314.4+432352	2.14							N2TU117668	6.2	0.44	18.14	1333-0465038	6.0	0.44	18.48		
J214316.6+433801	2.61			21431647+4337568	5.2	0.10	17.02	N2U5014287	5.2	0.06	18.45	1336-0438409	5.3	0.07	18.50		
J214319.9+433635	1.77			21432012+4336388	4.2	0.93	9.92	N2U5000783	4.2	0.96	11.70	1336-0438459	4.2	0.97	11.57	Star	F7V <sup>sp</sup>
J214320.0+433435	1.22			21432016+4334346	1.2	0.99	10.80				1335-0436830	2.3	0.86	16.38	EG	Gal <sup>s</sup>	
J214326.9+433320	1.61			21432700+4333182	2.5	0.63	11.64	N2U5000808	1.4	1.00	11.70	1335-0436934	3.6	0.81	9.87	EG	Gal <sup>image</sup>
J214344.0+433506	1.76			21434411+4335064	0.4	0.97	11.92	N2U5011105	0.4	0.96	15.00	1335-0437233	0.5	0.94	14.72	Star	K4Ve <sup>sp</sup>
J214345.3+432744	2.26			21434545+4327485	3.9	0.22	15.80	N2U5003467	5.7	0.15	18.66	1334-0442898	5.8	0.12	18.83		

**Table 33.** X-ray parameters for detected sources in field PSRJ2043+2740

2XMM Name	$r_{90}$ [""]	$\text{pn\_B1}^*$ [cts $\text{ks}^{-1}$ ]	$\text{pn\_B2}^{**}$ [cts $\text{ks}^{-1}$ ]	2MASS Name	$d_{x-o}$ [""]	$P_{id}$	kmag	GSC Name	$d_{x-o}$ [""]	$P_{id}$	V	USNO Name	$d_{x-o}$ [""]	$P_{id}$	R	Class <sup>†</sup>	SpT <sup>‡</sup>
J204244.6+274528	1.09			20424479+2745290	2.0	1.00	6.97	N333000391	2.1	0.92	10.48	1177-0649471	2.1	1.00	9.65	Star	K5V <sup>s</sup>
J204245.9+273738	2.58							N333056243	3.9	0.20		1176-0636927	3.4	0.18	19.41		
J204255.9+273628	2.52							N333054632	7.6	0.00		1176-0637156	7.6	0.00	18.49		
J204258.2+274351	1.50			20425847+2743514	2.9	0.76	13.21	N333064028	3.0	0.84		1177-0649784	2.8	0.89	13.69	EG	Gal <sup>s</sup>
J204258.9+273622	1.80			20425922+2736228	3.0	0.84	12.39	N333054712	3.3	0.59		1176-0637225	3.2	0.63	16.35	Star	M5Ve <sup>sp</sup>
J204259.5+274153	2.53			20430004+2741479	8.5	0.60	15.57	N333061372	5.2	0.48		1176-0637235	4.0	0.43	16.44		
J204305.5+274004	2.51							N333059288	0.8	0.32		1176-0637376	0.8	0.34	19.34		
J204307.5+274405	2.72							N333108742	3.9	0.04		1177-0650007	7.2	0.10	19.30		
J204308.7+273225	1.82			20430910+2732287	6.2	0.09	15.33	N333049680	6.3	0.10		1175-0619288	4.7	0.05	16.75		
J204322.5+274506	1.84							N333108998	6.2	0.10		1177-0650344	3.0	0.13	19.32		
J204325.8+273331	2.19			20432529+2733316	7.2	0.00	15.79					1175-0619714	7.0	0.00	19.74		
J204325.8+273721	2.17							N333056066	1.7	0.31		1176-0637852	1.6	0.30	19.45		
J204326.4+272853	1.85							N333044801	5.8	0.00		1174-0630822	5.7	0.00	19.09		
J204326.5+274407	2.05			20432685+2744088	3.9	0.95	10.19	N333141226	4.0	0.60		1177-0650455	4.0	0.98	11.06	Star	G0V <sup>s</sup>
J204326.7+274444	1.20			20432691+2744459	2.3	0.89	12.48	N333065021	3.0	0.91		1177-0650459	3.3	0.69	13.83	Star	F6V <sup>sp</sup>
J204327.0+274307	1.81							N333062974	2.8	0.19		1177-0650468	2.8	0.20	19.35		
J204328.2+274141	1.95			20432821+2741381	3.5	0.31	15.71	N333061271	4.6	0.17		1176-0637893	4.3	0.23	16.91		
J204330.4+273215	2.18			20432998+2732182	7.3	0.03	13.06	N333049631	7.3	0.02		1175-0619821	7.5	0.01	14.78		
J204331.0+274200	1.92							N333061782	5.2	0.00		1177-0650537	5.3	0.00	19.68		
J204336.4+273054	1.69			20433644+2730541	0.1	0.68	15.45	N333047716	0.5	0.69		1175-0619971	3.9	0.63	16.83		
J204337.9+273700	1.65			20433812+2737006	2.1	0.92	12.82	N333055746	2.2	0.94		1176-0638121	6.4	0.87	19.04	Star	G3V <sup>sp</sup>
J204338.1+273423	1.28			20433820+2734233	0.7	0.77	16.13	N333105950	0.6	0.61		1175-0620009	0.6	0.56	19.53		
J204340.5+273513	1.93							N333106236	5.8	0.15		1175-0620059	3.7	0.24	17.68		
J204341.7+273133	1.97							N333139456	2.5	0.27		1175-0620085	3.9	0.37	18.74		
J204342.7+275205	1.04			20434291+2752052	2.4	0.98	9.17	N332000188	2.6	0.97	12.26	1178-0653933	2.6	0.94	11.51	Star	K4Ve <sup>sp</sup>
J204346.4+273334	2.16							N333051568	2.9	0.31		1175-0620190	3.0	0.40	17.58		
J204346.9+273424	2.33			20434708+2734175	6.7	0.01	15.47	N333052707	6.6	0.32		1175-0620198	6.4	0.00	18.23		
J204347.2+273515	1.04			20434731+2735154	1.2	0.80	15.06	N333053493	1.4	0.53		1175-0620205	1.8	0.48	19.08	Star	F6V <sup>sp</sup>
J204349.1+274403	1.80			20434938+2744024	3.0	0.76	13.13	N332013378	3.2	0.85		1177-0650972	3.7	0.79	18.41		
J204351.0+272940	2.51			20435100+2729348	6.0	0.03	15.49	N333046015	5.9	0.04		1174-0631348	5.7	0.06	16.96		
J204353.7+273229	2.26							N333049933	4.5	0.09		1175-0620369	4.1	0.12	17.70		
J204359.5+274227	1.86			20435975+2742248	3.3	0.58	14.18	N332012428	3.2	0.21		1177-0651195	3.4	0.23	18.39		
J204400.5+273243	1.88			20440093+2732440	5.3	0.01	15.13	N333050325	5.6	0.01		1175-0620525	5.5	0.01	17.31		
J204402.5+272911	1.75							N333113398	2.3	0.41		1174-0631595	2.7	0.17	19.52		
J204403.7+273939	2.54			20440366+2739444	5.5	0.14	15.04	N332010986	5.5	0.01		1176-0638711	6.9	0.01	0.00		
J204408.1+274629	3.19							N332014982	9.0	0.00		1177-0651349	9.2	0.00	17.87		
J204410.4+274850	2.08							N332016421	6.1	0.00		1178-0654565	5.9	0.01	18.26		
J204416.5+274735	1.56			20441669+2747361	1.9	1.00	8.96	N332015927	2.0	0.55		1177-0651549	1.9	1.00	9.78	Star	F2V <sup>s</sup>
J204417.1+273613	1.35			20441726+2736119	2.6	0.93	11.65	N332000374	4.2	0.90		1176-0639040	3.9	0.67	0.00	Star	G1V <sup>sp</sup>
J204425.0+274236	2.32							N332012562	8.0	0.00		1177-0651762	7.9	0.00	18.16		
J204428.2+273334	1.91							N332008019	2.7	0.34		1175-0621138	5.9	0.34	19.18		
J204440.2+274231	3.07			20444049+2742309	3.8	0.86	12.28	N332084691	6.7	0.53		1177-0652143	3.8	0.55	16.19	Star	M2Ve <sup>sp</sup>